Technische Universität München
Fakultät für Physik

Dissertation

Quantization and Scattering in the Presence of Singular Attractive Potential Tails

Tim-Oliver Müller

Physik Department
Fachgebiet Theoretische Atomphysik
Prof. Dr. Harald Friedrich

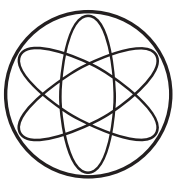

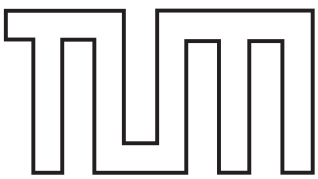

Technische Universität München
Physik Department
Fachgebiet Theoretische Atomphysik

Quantization and Scattering in the Presence of Singular Attractive Potential Tails

Dipl.-Phys. (Univ.) Tim-Oliver Müller

Vollständiger Abdruck der von der Fakultät für Physik der Technischen Universität München zur Erlangung des akademischen Grades eines

Doktors der Naturwissenschaften (Dr. rer. nat.)

genehmigten Dissertation.

Vorsitzender:		Univ.-Prof. Dr. Winfried Petry
Prüfer der Dissertation:	1.	Univ.-Prof. Dr. Harald Friedrich
	2.	Univ.-Prof. Dr. Martin Zacharias

Die Dissertation wurde am 04.12.2012 bei der Technischen Universität München eingereicht und durch die Fakultät für Physik am 17.01.2013 angenommen.

Contents

List of Figures

List of Tables

Chapter 1

Introduction

The fundamental physics of atoms, ions, and molecules is essentially governed by the underlying electrostatic interactions. These are responsible for the existence of stable atoms as well as for the characteristics of quantization and scattering phenomena on microscopic and mesoscopic scales.

Nature's simplest two-body system is constituted by the hydrogen atom, which is a substantial component of macroscopic matter. The quantization of its binding energy was partially described by the empirical Balmer formula [1] already in 1885 and can correctly be derived either from the Bohr model or from quantum mechanics by explicitly solving the Schrödinger equation [2]. The attractive Coulomb potential $-C/r$ is responsible for the binding of the negatively charged electron to the positively charged proton, i.e., the formation of atomic hydrogen. The same concept holds for more complex atoms that consist of a nucleus of charge number Z, with Z electrons attached to it.

Understanding the formation of microscopic matter was promoted significantly by the famous gold foil experiment [3], which was performed by the group of Ernest Rutherford in 1909. They were able to identify the Coulombic force of the atomic nuclei to be responsible for the characteristic deflection pattern of α-particles that are scattered by a thin gold foil. The famous Rutherford cross section for Coulombic scattering can theoretically be reproduced under the assumption of heavy atomic nuclei of charge number Z. The establishment of a rigorous quantum mechanical scattering theory for Coulombic potentials has certainly been pushed by its prominence in atomic physics. The result for the Rutherford cross section was first obtained from classical calculations which accidentally give the same result that is obtained from fully quantum mechanical calculations (see, e.g., Ref. [4]). The transition from a discrete set of bound states to a continuum of scattering states around the dissociation threshold in the presence of an attractive Coulombic potential tail is perfectly described within the framework of *quantum defect theory* [5, 6].

While the long-range Coulomb force governs the interaction between charged particles, the interaction between two compound particles in the absence of net charges is, in general, more complicated. Interatomic potentials have a characteristic long-range behavior that is essentially described by van der Waals or London *dispersion forces* [7, 8] (in case that relativistic retardation effects [9] are not considered). These play a predominant role when the polarizabilities of the interacting partners are large, as is generally the case for atoms or molecules. The long-range interaction energy between atomic partners can in general be given in terms of a multipole expansion [10]. The interaction of the 2^{n_A}-pole moment

of particle A with the 2^{n_B}-pole moment of particle B contributes to the total interaction energy with a term proportional to r^{-n}, with $n = n_A + n_B + 1$ [11]. While this holds true for permanent polarizations, the induced polarizations contribute with a term proportional to r^{-2n}, according to second-order perturbation theory [12].

In contrast to Coulombic tails, these tail potentials do not support any physically meaningful stationary solutions with vanishing flux density by themselves. In order to support an elastic scattering process, the full interaction potential thus needs to deviate from the singular form of its tail at small distances. In the short-range region the interaction potential is repulsive. In contrast to the tail part of the potential, its actual form remains unknown in general. The bound-state spectra of these kinds of interaction potentials also differ strongly from those of potentials with Coulombic tails; potentials that vanish faster than $-1/r^2$ asymptotically do not provide a Rydberg series of infinitly many bound states, but support only a finite number of bound states of which the least bound, in general, has a finite binding energy [4]. The quantization condition is then given by $n_{\mathrm{th}} - n = F(E_n)$, where $F(E)$ is referred to as the *quantization function* [13] and n_{th} is the finite and generally noninteger *threshold quantum number*. The first but deficient approach to the correct form of the quantization function was given by the *near-dissociation expansion* of LeRoy, Bernstein [14] and Stwalley [15].

In recent years, interatomic collisions in the low-energy regime have encountered a sustained interest since their understanding is crucial for the creation and manipulation of ultracold atomic samples that lay the foundation for a multitude of studies reaching from Bose-Einstein condensation [16, 17] to atom lasers [18, 19], quantum simulators [20, 21], and reams of further discoveries and applications such as controlled ultracold chemistry [22, 23]. The physics of a trapped atomic quantum gas is crucially influenced by the fundamental two-body collisions between ground-state atoms in the ultracold regime. These effective interactions are mediated by the scattering length of the interaction potential which is $-C_6/r^6$ at long-range (induced dipole-dipole interaction). Properties of the quantum gas may be manipulated by tuning the scattering length via magnetic or optical Feshbach resonances [24–26].

The development of a rigorous scattering theory for actual short-range potentials (see, e.g., Ref. [27–29]) was promoted by its applicability to scattering processes in nuclear physics. Many concepts of the established theoretical framework for potential scattering have been developed in this context. In 1947, Fermi and Marshall proposed the existence of a *scattering length* to describe interference phenomena of slow neutrons [30] in the limit of low collision energies. Later on, in 1949, Blatt and Jackson as well as Hans Bethe applied the *effective-range theory*, which was originally developed by Julian Schwinger [31], to nuclear scattering processes [32, 33].

Various studies have tried to overcome the difficulties that arise due to the lack of physical reference wave functions for potentials that fall off faster than $1/r^2$ asymptotically and are more singular than $-1/r^2$ at the origin. The first comprehensive study of scattering by a potential from this particular class was given by O'Malley, Spruch and Rosenberg [34, 35], who noticed the breakdown of the effective-range expansion for polarization induced potentials that have attractive tails given by $-C_4/r^4$, and presented a modified expansion with adjusted scattering parameters. For general inverse-power potentials $-C_\alpha/r^\alpha$, with $\alpha > 2$, the leading-order terms of the expansion of the scattering phase shift were predicted by Levy and Keller in 1963 [36]. An exhaustive number of recent studies (see Ref. [37] and

references therein) exists which abuse the term quantum defect theory for their description of collisional and bound-state properties of potentials with tails more singular than $-1/r^2$; the absence of defect-free physics, however, reduces the concept of a quantum defect to absurdity. Nonetheless, their results are scientifically sound and have a wide range of applicability [38, 39].

The present work deals with quantization and scattering in the presence of such long-range interactions that can be described by an attractive tail potential $V_{\text{tail}}(r)$ that falls off faster than $-1/r^2$ in the limit of large distances and is more singular than $-1/r^2$ at the origin. These potential tails occur whenever one of the colliding partners has zero net charge. The topic of this thesis is essentially inspired by an idea that was first formulated by Gribakin and Flambaum [40], who presented a parametrization of the scattering length for potentials with inverse-power tails and suggested the possibility of finding a general parametrization of the scattering phase shift. Against the background of previous works [13, 41–43] that explicitly give correct quantization functions for this certain class of potentials, this work shows, how — in the presence of singular attractive potential tails — the bound-state spectra and the scattering properties are interdependent. A theoretical framework is presented, which unifies previous approaches [13–15, 37, 40–42, 44] to scattering and quantization in the presence of attractive potential tails that are more singular than $-1/r^2$. This is achieved via a strict separation of the effects that are due to the nature of the long-range potential tail $V_{\text{tail}}(r)$ from those effects that are due to the short-range deviations of the full potential from the singular form of its tail.

Structure of the Present Thesis

The present thesis is organized as follows. Chapter 2 gives an overview of the theoretical framework that is used in the present work. The concepts of scattering theory are presented and the cross section for elastic scattering is derived; its connection to the scattering phase shift is established. The WKB approximation is introduced, which provides analytical accessibility of the wave function, whenever the criterion for its applicability is fulfilled. The corresponding semiclassical wave function in the presence of classical turning points is discussed.

In Chapter 3, the main concepts of the present thesis are developed. We identify the tail part of the interaction potential which is subject to the description within the framework of the WKB approximation. A convenient parametrization of the short-range wave function is given, which provides a physically meaningful boundary condition for the singular attractive potential tail that is used as a reference potential in order to reproduce the long-range physics of the full interaction potential.

For energies below the dissociation threshold, the influence of the short-range part of the potential enters the quantization rule via the threshold quantum number n_{th}. The influence of a tail potential that vanishes faster than $-1/r^2$ asymptotically and is more singular than $-1/r^2$ at the origin is expressed in the quantization function. For energies above the dissociation threshold, a parametrization of the s-wave phase shift is presented that depends on the noninteger remainder Δ_{th} of the threshold quantum number n_{th} and the properties of the tail potential. A connection to the properties of quantum reflection is established, so that the scattering phase shift is expressed in terms of the physically tangible properties of the tail potential. Threshold laws are given both for quantization

and elastic scattering.

In Chapter 4, the formalism presented in Chapter 3 is applied to the particular class of inverse-power tail potentials which play a major role in the interaction of atoms and molecules with each other and with ions. An explicit expression for the quantization function is presented for the particular case of a $-1/r^3$ tail potential. The tail functions that enter the formula for the scattering phase shift are derived for the class of inverse-power tails. These are explicitly presented for reference potentials $-1/r^\alpha$ with integer values of α from three to six. The particularities of the threshold laws for elastic s-wave scattering for different values of α are thoroughly discussed; especially for the case of an inverse-cube tail potential, for which a finite scattering length does not exist.

Chapter 5 demonstrates the applicability of the formalism derived in the preceding chapters to specific interaction potentials. The progression of near-threshold bound states of the sodium dimer in particular electronic states is analyzed (Section 5.1) with the help of the quantization function for inverse-cube tails. The advantages over the purely semiclassical LeRoy-Bernstein quantization rule are exposed. Two different types of Lennard-Jones potentials are analyzed with respect to the influence of the inverse-power tail potential on the asymptotics of the wave function. The interdependence of the bound-state spectra and the scattering properties is demonstrated by revealing the parameters that determine the short-range wave function. For the case of an inverse-cube tail potential, the threshold law for elastic scattering is verified. A strict separation of the effects due to the long-range tail of the interaction is also achieved in the presence of a tail potential that is a superposition of a $-1/r^4$ term and a $-1/r^6$ term. For a certain model potential the scattering phase shift is analyzed from this point of view.

Chapter 6 summarizes the methods and results of the present thesis. The prospects of further application are discussed in the context of atomic and molecular physics.

Chapter 2

Theoretical Framework

In this chapter, the general framework for quantization and scattering in the presence of spherically symmetric two-body interaction potentials is presented. A general overview of the concepts of scattering theory including the description of bound states is given. We introduce a modified version of the WKB approximation that provides analytical access to the wave function, which characterizes the corresponding two-body physics.

2.1 Scattering and Quantization

The well-established scattering theory for binary collisions (see, e.g., Refs. [27–29, 45–47]) is presented. Starting from the Hamiltonian of the reduced two-body system, the concept of partial wave analysis is introduced, that provides an explicit method for calculating the cross sections for elastic scattering and offers a simple picture for understanding the existence of a discrete set of normalizable bound states, i.e., quantization.

2.1.1 Schrödinger equation and partial wave analysis

The nonrelativistic time evolution of a quantum state is governed by the *Schrödinger equation* [2], which is

$$i\hbar\frac{\partial}{\partial t}\Psi(\boldsymbol{r},t) = \hat{H}(\boldsymbol{r},t)\Psi(\boldsymbol{r},t) \tag{2.1}$$

in coordinate representation. The Hamiltonian $\hat{H}$ that characterizes the relative motion of a two-particle system with reduced mass μ is given by

$$\hat{H} = \left(-\frac{\hbar^2}{2\mu}\Delta + V(\boldsymbol{r},t)\right), \tag{2.2}$$

where $V(\boldsymbol{r},t)$ is the interaction energy, which depends on the relative position vector $\boldsymbol{r}$ between the two particles, and could in general be time-dependent. For our purposes the interaction potential $V(\boldsymbol{r},t) \equiv V(\boldsymbol{r})$ is assumed not to depend on time, which allows us to use the separation ansatz $\Psi(\boldsymbol{r},t) = \psi(\boldsymbol{r}) \cdot f(t)$ that gives $f(t) = \exp(-iEt/\hbar)$ for the time-dependent part and the *stationary Schrödinger equation*

$$\left(-\frac{\hbar^2}{2\mu}\Delta + V(\boldsymbol{r})\right)\psi(\boldsymbol{r}) = E\,\psi(\boldsymbol{r}) \tag{2.3}$$

for the wave function $\psi(\boldsymbol{r})$ that depends on the spatial coordinates. The energy value E is the eigenvalue of the Hamiltonian (2.2) and therefore the amount of energy that is associated with the relative motion of the two particles.

The explicit time dependence of the Schrödinger equation is thereby eliminated in Eq. (2.3). However, the stationary Schrödinger equation (2.3) is still a partial differential equation including all three spatial coordinates. Finding solutions to this kind of equation is a highly nontrivial problem; but it can, under given circumstances, be further simplified.

For typical interatomic two-body potentials — as considered in this work — the potential energy $V(\boldsymbol{r}) \equiv V(r)$ usually depends only on the internuclear separation $r = |\boldsymbol{r}|$ and not on the orientation of the two colliding particles. In this case the rotational invariance gives rise to further separability of the system. The spherical symmetry naturally leads to the ansatz

$$\psi(\boldsymbol{r}) = \frac{u_l(r)}{r} Y_{l,m}(\theta, \phi)\,, \tag{2.4}$$

where the $Y_{l,m}(\theta, \phi)$ are the spherical harmonics that are the eigenstates of the angular momentum operators $\hat{\boldsymbol{L}}^2$ and L_z to the eigenvalues $l(l+1)\hbar^2$ and $m\hbar$ respectively. With the Laplacian given in spherical coordinates

$$\Delta = \frac{\partial^2}{\partial r^2} + \frac{2}{r}\frac{\partial}{\partial r} - \frac{\hat{\boldsymbol{L}}^2}{r^2\hbar^2} \tag{2.5}$$

we arrive at the *radial Schrödinger equation*

$$\left(-\frac{\hbar^2}{2\mu}\frac{d^2}{dr^2} + \frac{l(l+1)\hbar^2}{2\mu r^2} + V(r)\right) u_l(r) = E\, u_l(r)\,, \tag{2.6}$$

which is an ordinary second-order differential equation for any angular momentum quantum number l. It has the same form as the full stationary Schrödinger equation for a one-dimensional system with the effective potential

$$V_{\text{eff}}(r) = \frac{l(l+1)\hbar^2}{2\mu r^2} + V(r) \tag{2.7}$$

in each partial wave. Equation (2.6) can easily be solved — at least numerically — for a given boundary condition. For a particular potential $V(r)$, the radial Schrödinger equation (2.6) might also be solvable with analytical methods. These cases are, however, very rare.

When the Laplacian (2.5) is applied to the $1/r$ term in the wave function (2.4), an additional term proportional to $\delta(r)/r$ is obtained in the radial Schrödinger equation (2.6), which is in contrast to its one dimensional analog. The existence of that term requires any physically meaningful radial wave function to be zero at the origin.[1] The radial wave function $u_l^{\text{reg}}(r)$ that solves Eq. (2.6) and fulfills

[1] For the cases studied in this work, this discussion is in principle unnecessary for our purposes, since normalizability already requires relation (2.8) to be fulfilled for the solutions of (2.6) in typical interatomic potentials that have a singular repulsive core.

$$\lim_{r\to 0} \frac{u_l^{\mathrm{reg}}(r)}{r} = \mathrm{const}\,, \qquad |\mathrm{const}| < \infty \tag{2.8}$$

is referred to as the *regular solution* to the radial Schrödinger equation (2.6). Solutions to (2.6) other than the regular solution are referred to as *irregular solutions*.

Equation (2.8) fixes the boundary condition on the inner side of the interaction region. Depending on the peculiarities of the interaction potential $V(r)$ and the energy E, these solutions might be subject to further constraints that lead to normalizable solutions only for a discrete set of energies, i.e., quantization.

The interaction energy usually vanishes in the limit of large internuclear separations. In that case the regular solutions for energies above the potential threshold at $E = 0$ form a continuum of states and describe the free-particle motion at large distances. This enables the formulation of a scattering process. Interaction potentials that do not allow for the unambiguous identification of the regular solution (2.8) can neither provide for the existence of a spectrum of normalizable bound states, nor do they support a purely elastic scattering process.

2.1.2 Cross sections and the scattering wave function

The main purpose of scattering theory is the calculation of cross sections that contain all the information relevant for the description of a scattering process.

For a spherically symmetric, local interaction potential that vanishes faster than $1/r^2$ asymptotically, a solution to the stationary Schrödinger equation (2.3) for asymptotically free motion in three spatial dimensions can be chosen to fulfill

$$\psi(\boldsymbol{r}) \overset{r\to\infty}{\sim} e^{ikz} + f(\theta)\frac{e^{ikr}}{r}\,, \tag{2.9}$$

i.e., the wave function can — at large distance from the center of the interaction potential — be split up into an incident plane wave traveling in positive z-direction and an outgoing spherical, *scattered* wave that is modulated by the *scattering amplitude* $f(\theta)$. All information about the scattering process inside of the interaction region is contained in this complex amplitude. In Eq. (2.9) the quantity $k = \sqrt{2\mu E}/\hbar$ is the wave number associated with the asymptotically free motion. Given that the interaction potential is spherically symmetric, the wave function $\psi(\boldsymbol{r})$ obeys a cylindrical symmetry around the incident beam axis and the scattering amplitude $f(\theta)$ defined in Eq. (2.9) depends only on the polar scattering angle θ, rather than on the full solid angle Ω, which additionally contains the azimuth angle.

The outgoing flux passing through a surface segment $d\boldsymbol{A} = r^2 d\Omega\,(\boldsymbol{r}/r)$ that is sufficiently far off the scattering center at the polar angle θ can be determined using only the second term in Eq. (2.9)[2]

$$\boldsymbol{j}_{\mathrm{out}} d\boldsymbol{A} = \frac{\hbar}{2i\mu}\left(\psi^*\nabla\psi - \psi\nabla\psi^*\right) d\boldsymbol{A} = \frac{\hbar k}{\mu}\left|f(\theta)\right|^2 d\Omega\,, \tag{2.10}$$

[2]In fact, interference terms exist. These need to be regarded for the rigorous derivation of the *Optical Theorem* $\sigma = 4\pi/k\ \mathrm{Im}[f(\theta = 0)]$ (see, e.g., Ref. [45]).

while the incident flux density is — considering only the first term in Eq. (2.9) — given by $\hbar k/\mu$. The differential cross section is defined as

$$\frac{d\sigma}{d\Omega} = \frac{\text{scattered flux per unit solid angle}}{\text{incident flux per unit area}} \,. \tag{2.11}$$

For the scattering process that is described by the wave function defined in Eq. (2.9), this yields

$$\frac{d\sigma}{d\Omega} = |f(\theta)|^2 \,. \tag{2.12}$$

To actually determine the scattering amplitude and thereby also the physically relevant cross sections, the scattering wave function can — very similar to Eq. (2.4) of the previous section — be expanded in the complete set of eigenfunctions of the operator $\hat{\boldsymbol{L}}^2$, which are now given by the Legendre polynomials $P_l(\cos\theta)$

$$\psi(\boldsymbol{r}) = \sum_{l=0}^{\infty} B_l \frac{u_l(r)}{r} P_l(\cos\theta) \,, \tag{2.13}$$

with the energy-dependent coefficients B_l chosen such that Eq. (2.9) is fulfilled. Inserting this form into the stationary Schrödinger equation (2.3), multiplying the result with $P_{l'}(\cos\theta)$ and integrating over the polar angle, we find that each of the $u_l(r)$ is required to fulfill the radial Schrödinger equation (2.6) as given in the previous section.

The regular and an irregular solution to the potential-free radial Schrödinger equation

$$\left(-\frac{\hbar^2}{2\mu}\frac{d^2}{dr^2} + \frac{l(l+1)\hbar^2}{2\mu r^2} \right) v_l(r) = E\, v_l(r) \tag{2.14}$$

that describe the free relative motion, are given by

$$v_l^{(\mathrm{s})}(r) = \quad kr\, j_l(kr) \overset{r\to\infty}{\sim} \sin\left(kr - l\pi/2\right) \tag{2.15}$$

and

$$v_l^{(\mathrm{c})}(r) = -kr\, n_l(kr) \overset{r\to\infty}{\sim} \cos\left(kr - l\pi/2\right) \tag{2.16}$$

for each value of l, where the $j_l(x)$ are the spherical Bessel function of l^{th} order and the $n_l(x)$ are the corresponding spherical Neumann functions (see, e.g., Refs. [4, 48]). Therefore, the regular solution to the radial Schrödinger equation with an interaction potential vanishing faster than $1/r^2$ asymptotically can — in the limit of large distances — be written as a linear combination of the two solutions (2.15) and (2.16)

$$u_l^{\mathrm{reg}}(r) \overset{r\to\infty}{\sim} \cos\delta_l\, kr\, j_l(kr) - \sin\delta_l\, kr\, n_l(kr) \,. \tag{2.17}$$

We can choose this specific normalization of the regular solution without any loss of generality, since the coefficients B_l in Eq. (2.13) are still to be determined. In the limit

of even larger distances where the influence of the centrifugal potential is also negligible, the regular solution can — according to Eqs. (2.15) and (2.16) — be written as

$$u_l^{\mathrm{reg}}(r) \overset{r\to\infty}{\sim} \sin\left(kr - l\pi/2 + \delta_l\right) . \tag{2.18}$$

Due to the asymptotic form (2.18) of the regular solution, the quantity δ_l is referred to as the energy-dependent *scattering phase shift* in the l^{th} partial wave.

By comparing the partial wave expansion (2.13) to the scattering wave function (2.9) in an expanded form, i.e., substituting the relations

$$e^{ikz} = \sum_{l=0}^{\infty}(2l+1)i^l j_l(kr)P_l(\cos\theta) \tag{2.19}$$

and

$$f(\theta) = \sum_{l=0}^{\infty} f_l P_l(\cos\theta)\,, \tag{2.20}$$

with the *partial wave amplitudes* f_l, expressions for the corresponding expansion coefficients are found. By comparing only the coefficients of the incoming parts of the wave functions, we obtain

$$B_l = \frac{1}{k}(2l+1)i^l e^{i\delta_l} . \tag{2.21}$$

Using this identity, we find

$$f_l = \frac{1}{2ik}(2l+1)\left(e^{2i\delta_l} - 1\right) = \frac{1}{k}(2l+1)e^{i\delta_l}\sin\delta_l \tag{2.22}$$

for the partial wave amplitudes from comparing only the outgoing parts of the wave function. We can now establish a relation between the scattering amplitude and the partial wave phase shifts just by inserting into Eq. (2.20)

$$f(\theta) = \sum_{l=0}^{\infty}\frac{1}{2ik}(2l+1)\left(e^{2i\delta_l} - 1\right)P_l(\cos\theta)\,, \tag{2.23}$$

which can immediately be used to calculate the differential cross section via relation (2.12). The total energy-dependent cross section can be given by integrating the expression (2.12) over the full solid angle

$$\sigma = \int_0^{2\pi} d\phi \int_0^{\pi} \sin\theta d\theta\, |f(\theta)|^2 = 2\pi \int_0^{\pi} \sin\theta d\theta\, |f(\theta)|^2 . \tag{2.24}$$

With the orthogonality relation of the Legendre polynomials [48], the expression (2.24) can easily be evaluated

$$\sigma = \sum_{l=0}^{\infty}\sigma_l = \frac{4\pi}{k^2}\sum_{l=0}^{\infty}(2l+1)\sin^2\delta_l\,, \tag{2.25}$$

defining the *partial cross sections* $\sigma_l = 4\pi/k^2(2l+1)\sin^2\delta_l$.

In order to obtain all information about the scattering process, it is thus sufficient to determine the phase shift in each partial wave. However, this in principle requires the accurate knowledge of the interaction potential $V(r)$ in all of coordinate space, i.e., both at large and at small distances.

For potentials falling off faster than $1/r^2$ the phase shift vanishes in the limit of large l, when the centrifugal term dominates the effective potential (2.7). This defines a termination criterion for the summation in Eq. (2.25). The number of partial waves contributing to the total cross section increases, the higher the collision energy.

2.2 The WKB approximation

In the present section, we focus on the derivation of the semiclassical wave function in the framework of the Wentzel-Kramers-Brillouin (WKB) approximation [49–51]. This method was originally formulated by Jeffreys [52] as a general approximation for solutions to ordinary second-order differential equations before the Schrödinger equation was originally stated [2]. It offers a convenient parametrization of the exact wave function in regions of coordinate space where the criterion for its applicability is well fulfilled.

2.2.1 The semiclassical wave function

We start from the radial Schrödinger equation (2.6) rewritten as

$$\left(\frac{d^2}{dr^2} + \frac{2\mu}{\hbar^2}\left[E - V_{\text{eff}}(r)\right]\right) u(r) = 0\,. \tag{2.26}$$

For the solutions of this equation, we formulate the ansatz

$$u(r) = \exp\left(\frac{i}{\hbar}S(r)\right)\,, \tag{2.27}$$

which immediately leads to the differential equation

$$S'(r)^2 - i\hbar S''(r) = p(r)^2 \tag{2.28}$$

for the quantity $S(r)$, which has the dimension of an action. The *local classical momentum* $p(r)$ is given by

$$p(r) = \sqrt{2\mu\left[E - V_{\text{eff}}(r)\right]}\,. \tag{2.29}$$

We are not appending the index l to the occurring quantities, but one should keep in mind that the present formalism is valid for both zero and for nonzero angular momentum.

Equation (2.28) is still exact; it can be considered a one-dimensional Hamilton-Jacobi equation [53] for the quantum mechanical action $S(r)$ and could have been an alternative starting point of our considerations.

Expanding the quantum mechanical action in orders of $\hbar/i$

$$S(r) = S_0(r) + \frac{\hbar}{i}S_1(r) + \left(\frac{\hbar}{i}\right)^2 S_2(r) + \cdots \tag{2.30}$$

is particularly convenient in the case that characteristic actions of the system are very large compared to the reduced Planck constant $\hbar$. Inserting this expansion into the Hamilton-Jacobi equation (2.28) yields

$$p(r)^2 - \left(S_0'\right)^2 + i\hbar\left(S_0'' + 2S_0'S_1'\right) + \hbar^2\left(S_1'' + 2S_0'S_2' + \left(S_1'\right)^2\right) + \cdots = 0\,. \tag{2.31}$$

This differential equation can be solved for all orders of $\hbar$ sequentially. For the zeroth-order terms in $\hbar$, we find

$$S_0'(r) = \pm p(r) \quad \Rightarrow \quad S_0(r) = \pm \int p(r)dr\,. \tag{2.32}$$

With this result, the differential equation for the first-order terms in Eq. (2.31) is

$$S_1(r)' = -\frac{S_0''(r)}{2S_0'(r)} = -\frac{p'(r)}{2p(r)}\,. \tag{2.33}$$

The solution for $S_1(r)$ can thus be given by

$$S_1(r) = -\frac{1}{2}\ln p(r)\,. \tag{2.34}$$

While, in principle, more terms of the expansion (2.30) could be taken into account, considering only the contributions $S_0(r)$ and $S_1(r)$ in that expansion yields a very simple form of a possible approximate solution to the radial Schrödinger equation (2.26)

$$u_{\mathrm{WKB}}(r) = \frac{C_1}{\sqrt{p(r)}}\exp\left(\frac{i}{\hbar}\int_{r_0}^{r} p(r')dr'\right) + \frac{C_2}{\sqrt{p(r)}}\exp\left(-\frac{i}{\hbar}\int_{r_0}^{r} p(r')dr'\right)\,. \tag{2.35}$$

The reference point r_0 can, in principle, be chosen at an arbitrary distance. The coefficients C_1, C_2 can be chosen such that the wave function fulfills a desired boundary conditions.

2.2.2 Conditions of validity

While it is obvious, that the WKB wave function will be a good approximation to an exact solution of the radial Schrödinger equation in the *semiclassical limit*, i.e., when $\hbar$ becomes very small compared to the typical actions of the considered system, one rather wants to have a more sophisticated measure of the quality of the WKB approximation. A reliable criterion for the validity of the WKB approximation can be found by comparing the relation

$$u_{\mathrm{WKB}}''(r) + \frac{p(r)^2}{\hbar^2}u_{\mathrm{WKB}}(r) - \left(\frac{3}{4}\frac{p'(r)^2}{p(r)^2} - \frac{p''(r)}{2p(r)}\right)u_{\mathrm{WKB}}(r) = 0 \tag{2.36}$$

obtained by explicit evaluation of the second derivative of the WKB wave function (2.35) to the original Schrödinger equation (2.26). Relation (2.36) resembles the original Schrödinger equation whenever the third term on the left-hand side can be neglected in comparison to the second term; the wave function $u_{\mathrm{WKB}}(r)$ will then be a good approximation to the

exact solution $u(r)$. We define the dimensionless *quantality function* by the ratio of both terms

$$\mathcal{Q}_E(r) = \hbar^2 \left(\frac{3}{4} \frac{p'(r)^2}{p(r)^4} - \frac{p''(r)}{2p(r)^3} \right) . \tag{2.37}$$

Whenever the absolute value of the quantality function (2.37) becomes very small compared to unity

$$|\mathcal{Q}_E(r)| \ll 1 , \tag{2.38}$$

the exact wave function can, with good accuracy, be described by a WKB wave (cf. Ref. [54]). It becomes obvious that the accuracy of the WKB approximation is a local property of the Schrödinger equation. To emphasize that the quantality function also depends on the system's energy, the index E is attached to its primary definition (2.37). In a given potential we can now — depending on the system's energy — identify spatial regions of WKB validity via the criterion (2.38).

2.2.3 Presence of classical turning points

One particular weakness of the WKB approximation is its breakdown in the vicinity of classical turning points. Having a closer look at the WKB wave function (2.35), one finds that the amplitude, which is proportional to the inverse square root of the local classical momentum, diverges at a classical turning point r_{ctp} where $p(r_{\mathrm{ctp}}) = 0$, while the exact wave function just has an inflection point $u''(r_{\mathrm{ctp}}) = 0$ according to Eq. (2.26). The root of the local classical momentum is also reflected by the divergence of the quantality function (2.37) at r_{ctp}. This circumstance complicates the procedure of connecting the wave functions from different spatial regions that are separated by a classical turning point.

One classical turning point and the connection problem

The existence of one classical turning point distinguishes two regions in coordinate space. One is the classically allowed region, where the curvature of the quantum mechanical wave function has a sign opposite to that of the wave function itself, which reflects the fact that $p(r)^2 > 0$, and leads to the typical oscillatory behavior of the wave function. The other is the classically forbidden region, where the wave function's curvature has the same sign as the wave function itself. Therefore, the wave function is required to tend to zero in this region to prevent the probability density from diverging.

Consider two distinct regions of WKB validity separated by a quantal region around one classical turning point. In the classically forbidden region the local classical momentum, as defined in Eq. (2.29), is purely imaginary. Inserting this local classical momentum into the expression (2.35) for the wave function in the classically forbidden region of WKB validity gives

$$u_{\mathrm{WKB}}(r) \propto \frac{1}{\sqrt{|p(r)|}} \exp\left(-\frac{1}{\hbar} \left| \int_{r_{\mathrm{ctp}}}^{r} p(r')dr' \right| \right) , \tag{2.39}$$

which is the real-valued solution that vanishes in the classically forbidden region. Choosing the classical turning point r_{ctp} as point of reference is very convenient in order not to obtain an additional phase factor that is just due to the change of sign of $p^2(r)$.

In the classically allowed region, where the local classical momentum $p(r)$ is real-valued, the two contributions to the WKB wave function in Eq. (2.35) can be identified with inward and outward traveling waves. This identification offers the possibility of describing a reflection process, which is — in this case — characterized by a complex reflection amplitude $\exp(i\phi)$ with an absolute value of unity. The WKB wave function in the classically allowed region, related to the classical turning point, can then be given by the real-valued expression

$$u_{\mathrm{WKB}}(r) \propto \frac{1}{\sqrt{p(r)}} \cos\left(\frac{1}{\hbar}\left|\int_{r_{\mathrm{ctp}}}^{r} p(r')dr'\right| - \frac{\phi}{2}\right) . \tag{2.40}$$

This wave function oscillates with a position-dependent wave number $p(r)/\hbar$. The reflection phase ϕ can be considered to be the phase loss due to the wave function penetrating the classically forbidden region.

Whenever there are two distinct regions of WKB validity separated by a quantal region around one classical turning point, we need to fix the normalization constant $\mathcal{N}$ and the phase ϕ of the WKB wave function (2.40) in the classically allowed region of coordinate space, so that it matches the physical solution of the Schrödinger equation. This is referred to as the *connection problem* and can in general be formulated as

$$\frac{1}{\sqrt{|p(r)|}} \exp\left(-\frac{1}{\hbar}\left|\int_{r_{\mathrm{ctp}}}^{r} p(r')dr'\right|\right) \leftrightarrow \frac{\mathcal{N}}{\sqrt{p(r)}} \cos\left(\frac{1}{\hbar}\left|\int_{r_{\mathrm{ctp}}}^{r} p(r')dr'\right| - \frac{\phi}{2}\right) . \tag{2.41}$$

In early works that deal with the WKB approximation, the connection problem is commonly solved for the particular case of a linear potential. In that case, there are exact solutions to the quasi one-dimensional Schrödinger equation that can be given in terms of Airy functions (cf. Ref. [55]) and the connection problem can be solved by comparing to the exact solution that is proportional to the Airy function Ai and vanishes in the classically forbidden region. This gives

$$\phi \equiv \frac{\pi}{2} \quad \text{and} \quad \mathcal{N} \equiv 2 . \tag{2.42}$$

This is considered to be the semiclassical value for the reflection phase, because it particularly applies when the semiclassical limit is achieved locally, i.e., when there is an interval $\mathcal{I}_{\mathrm{ctp}}$ symmetric around the classical turning point with $|\int_{\mathcal{I}_{\mathrm{ctp}}} p(r)dr| \gg \hbar\pi$, small enough, so that the potential can still be assumed to be linear $V(r) \approx V(r_{\mathrm{ctp}}) + V'(r_{\mathrm{ctp}})(r - r_{\mathrm{ctp}})$ for all $r \in \mathcal{I}_{\mathrm{ctp}}$. This formulation is essentially equivalent to connecting the solutions (2.40) and (2.39) on a path around r_{ctp} in the complex plane [53, 55, 56], which also gives the result of Eq. (2.42).

It is obvious that this condition is by no means well fulfilled in general cases. In general problems we can assume the reflection phase to be a function of the energy $\phi = \phi(E)$. This generalization of the conventional WKB theory has been developed in Refs. [57, 58] and can be adapted for the theoretical treatment of various problems in quantum mechanics (see Ref. [54]).

Two classical turning points and quantization

The appropriate choice of the reflection phase fixes the correct boundary condition for the wave function (2.40) in the classically allowed region of WKB validity. This becomes crucial in case that there are two classical turning points $r_{\mathrm{in}}(E) < r_{\mathrm{out}}(E)$ that separate such a region from two classically forbidden regions at $r < r_{\mathrm{in}}(E)$ and $r > r_{\mathrm{out}}(E)$ respectively. In this constellation we expect a discrete set of physically allowed energies E_n at which the corresponding exact wave functions can appropriately be normalized. The normalizability is ensured when the wave function can be described by the WKB wave function (2.39) in the classically forbidden regions. From this requirement the phase losses $\phi_{\mathrm{in}}(E)$ and $\phi_{\mathrm{out}}(E)$ can be determined by solving the connection problem at both classical turning points. With these phases, the wave function in the classically allowed region of WKB validity can — according to Eq. (2.40) — be given in either of the following two forms

$$u_{\mathrm{in}}(r) \propto \frac{1}{\sqrt{p(r)}} \cos\left(\frac{1}{\hbar}\int_{r_{\mathrm{in}}(E)}^{r} p_E(r')\,dr' - \frac{\phi_{\mathrm{in}}(E)}{2}\right), \tag{2.43}$$

$$u_{\mathrm{out}}(r) \propto \frac{1}{\sqrt{p(r)}} \cos\left(\frac{1}{\hbar}\int_{r}^{r_{\mathrm{out}}(E)} p_E(r')\,dr' - \frac{\phi_{\mathrm{out}}(E)}{2}\right). \tag{2.44}$$

The index E is assigned to the local classical momentum to emphasize its dependence on the energy, according to Eq. (2.29). Equation (2.43) relates the wave function to the inner classical turning point $r_{\mathrm{in}}(E)$, while Eq. (2.44) gives the wave function with reference to the outer classical turning point $r_{\mathrm{out}}(E)$.

In the region of WKB validity, the wave functions (2.43) and (2.44) need to be identical except for a factor of -1, which is essentially equivalent to requiring the arguments of the cosine functions to differ exactly by an integer multiple of π. This leads to the condition

$$\frac{1}{\hbar}\int_{r_{\mathrm{in}}(E_n)}^{r_{\mathrm{out}}(E_n)} p_{E_n}(r)\,dr = n\pi + \frac{\phi_{\mathrm{in}}(E_n)}{2} + \frac{\phi_{\mathrm{out}}(E_n)}{2}, \tag{2.45}$$

which is only fulfilled for a discrete set of energies E_n. This condition for the energy eigenvalues of the hamiltonian can be regarded as a generalized form of the *Bohr-Sommerfeld quantization rule* (cf. Ref. [53]). With the convention chosen in (2.45), the energy of the ground state is referred to as E_0. The existence of an ever so small region of WKB validity characterized by the criterion (2.38) in between the two classical turning points enables the determination of the reflection phases $\phi_{\mathrm{in}}(E)$ and $\phi_{\mathrm{out}}(E)$ [54, 58, 59], with which the quantization condition (2.45) is exact.

Chapter 3

Tail-based formulation of quantization and scattering

A formulation of quantization ($E < 0$) and scattering ($E > 0$) is derived, which is applicable to potentials $V(r)$ that have attractive tails $V_{\text{tail}}(r)$ that vanish to $E = 0$ faster than $1/r^2$ at large distances and are more singular than $-1/r^2$ at short distances. For many physically relevant systems, the tail part of the interaction potential is well-known, while its short-range part remains unknown in general.

The modified WKB approximation is used in order to offer a convenient parametrization of the short-range effects. This parametrization provides a boundary condition for the solutions in the reference potential $V_{\text{tail}}(r)$, reproducing the correct long-range behavior of the corresponding exact solution as obtained with the full interaction potential $V(r)$. For near-threshold energies, both the quantization and the scattering properties can thus be derived solely from the tail potential with only one or few short-range parameters reflecting the deviation of the full potential from the singular form of its tail at short distances.

We particularly focus on the case of s waves, but point out that the framework presented is very general in principle and can be applied to higher partial waves without any major restrictions. Parts of the results presented in this chapter have already been published (Refs. [60, 61]).

3.1 Representation of the regular solution in the short-range region

The regular solution to the radial Schrödinger equation (2.6) in the short-range region of a given potential should be insensitive to the actual position of the dissociation threshold; its appropriate representation is the key to the description of scattering and quantization phenomena on the same footing.

We consider the case of interaction potentials $V(r)$ that have attractive tails $V_{\text{tail}}(r)$ that are more singular than $-1/r^2$ at the origin and vanish faster than $1/r^2$ asymptotically. For a potential that is more singular than $-1/r^2$ at the origin, the WKB approximation becomes increasingly accurate for decreasing r and is actually exact in the limit $r \to 0$ (see, e.g., Refs. [4, 54]). This kind of potential does not provide for the unambiguous identification of a regular solution (2.8) by itself; full interaction potentials are thus assumed

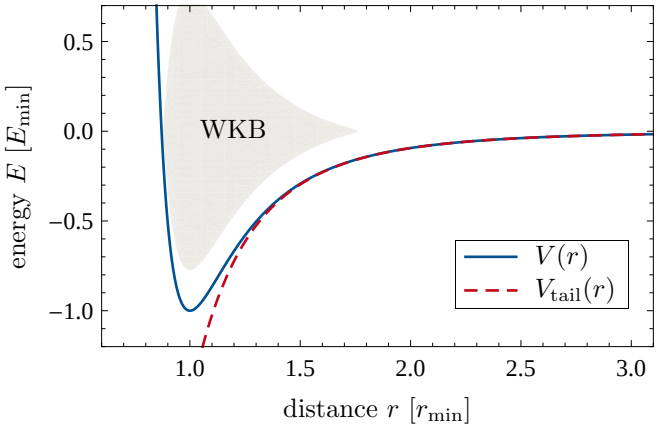

Figure 3.1: Typical form of interaction potentials considered in the present work. The solid line represents the full potential $V(r)$, while the dashed line follows its attractive tail $V_{\text{tail}}(r)$, which vanishes faster than $1/r^2$ at large distances and is more singular than $-1/r^2$ at the origin. The full potential deviates from the singular form of its tail only at short distances. The shaded area indicates the inner region where the WKB approximation is valid. For near-threshold energies this region extends to distances where the full potential is well described by its tail.

to deviate from the singular form of the corresponding singular tail potential $V_{\text{tail}}(r)$ at short distances. In the case that the tail potential $V_{\text{tail}}(r)$ dominates the full interaction potential down to distances that are small compared to its characteristic length scales, the full interaction potential $V(r)$ is deep and a region of WKB validity exists, in which the solutions of the Schrödinger equation can be expressed as real-valued WKB wave functions and the full potential can still safely be approximated by its tail.

Figure 3.1 shows a typical interaction potential that is considered in this work (solid line) together with its tail (dashed line), which fulfills the preconditions for the present treatment, i.e., it vanishes faster than $1/r^2$ asymptotically and it is more singular than $-1/r^2$ at the origin. The shaded area indicates the inner region of WKB validity. For near-threshold energies this region extends to distances where the full potential $V(r)$ is well approximated by its tail $V_{\text{tail}}(r)$.

Based on the recognition of the existence of such a region of WKB validity in deep potentials with tails that are more singular than $-1/r^2$ at the origin, a tail-based parametrization of the regular solution at short distances is derived. In the inner WKB region, the exact regular solution $u_{\text{reg}}(r)$ can be expressed in terms of a conventional WKB wave function with the inner classical turning point $r_{\text{in}}(E)$ as point of reference [cf. Eq. (2.43)]

$$u_{\text{reg}}(r) \propto \frac{1}{\sqrt{p_E(r)}} \cos\left(\frac{1}{\hbar}\int_{r_{\text{in}}(E)}^{r} p_E(r')dr' - \frac{\phi_{\text{in}}}{2}\right) . \tag{3.1}$$

The inner reflection phase ϕ_{in} is in general not a constant but depends on the energy (see Section 2.2). In the short-range region where expression (3.1) is valid, it contains no information about the existence of a potential threshold and is thus valid for both positive and negative energies, without any restrictions.

Relating the WKB representation (3.1) of the exact wave function to a reference point r_E in the outer tail region of the potential, the regular solution can, in the inner region of WKB validity, be given as

$$u_{\rm reg}(r) \propto \frac{1}{\sqrt{p_E(r)}} \sin\left(\frac{1}{\hbar}\int_{r_E}^{r} p_E(r')dr' - \phi_{\rm sr}\right) . \tag{3.2}$$

The reference point r_E can, in general, be chosen to be energy-dependent. Since the present expression (3.2) just paraphrases Eq. (3.1), it also is insensitive to the actual position of the threshold energy.

The short-range phase $\phi_{\rm sr}$ in (3.2) accounts for the shift of the reference point and contains all the influence of the short-range part of the potential. In order to relate this phase to a physically meaningful quantity that is intuitively accessible, we compare the arguments of the sine and cosine functions in Eqs. (3.2) and (3.1), which gives

$$\phi_{\rm sr} = \frac{\phi_{\rm in}(E)}{2} - \frac{\pi}{2} - \frac{1}{\hbar}\int_{r_{\rm in}(E)}^{r_E} p_E(r)dr\,. \tag{3.3}$$

To compensate for the phase accumulated by shifting the reference point from the inner short-range region to the outer tail region of the potential, we make use of the generalized Bohr-Sommerfeld quantization rule (2.45) exactly at threshold ($E = 0$)

$$\frac{1}{\hbar}\int_{r_{\rm in}(0)}^{\infty} p_0(r)dr = n_{\rm th}\pi + \frac{\phi_{\rm in}(0)}{2} + \frac{\phi_{\rm out}(0)}{2}\,, \tag{3.4}$$

where $\phi_{\rm out}(0)$ is the threshold value of the outer reflection phase [54]. The threshold form (3.4) of the modified Bohr-Sommerfeld quantization rule (2.45) introduces the *threshold quantum number* $n_{\rm th}$, which is, by definition, a quantity that reflects the full potential. It is the hypothetical quantum number at $E = 0$ and is therefore not necessarily an integer. However, its integer part $\lfloor n_{\rm th} \rfloor$ coincides with the quantum number of the least bound state in the potential well. The introduction of the threshold quantum number dates back to the works of LeRoy, Bernstein [14] and Stwalley [15] in 1970.

Having defined the threshold quantum number $n_{\rm th}$ via relation (3.4), we can give the short-range phase in the form

$$\begin{aligned}\phi_{\rm sr} = &-n_{\rm th}\pi - \frac{\phi_{\rm out}(0)}{2} - \frac{\pi}{2} + \frac{\phi_{\rm in}(E) - \phi_{\rm in}(0)}{2} \\ &+\frac{1}{\hbar}\left(\int_{r_E}^{\infty} p_0(r)dr + \int_{r_{\rm in}(0)}^{r_E} p_0(r)dr - \int_{r_{\rm in}(E)}^{r_E} p_E(r)dr\right) .\end{aligned} \tag{3.5}$$

Obviously, the difference $\phi_{\rm in}(E) - \phi_{\rm in}(0)$ is a smooth function of energy vanishing at threshold. The three integrals in Eq. (3.5) can be approximated — up to a small correction of the order E — by replacing the full potential $V(r)$ by its tail $V_{\rm tail}(r)$

$$\frac{1}{\hbar}\int_{r_E}^{\infty} p_0^{\rm tail}(r)dr - \frac{1}{\hbar}\int_{0}^{r_E} \left[p_E^{\rm tail}(r) - p_0^{\rm tail}(r)\right] dr\,, \tag{3.6}$$

where $p_E^{\text{tail}}(r)$ is the local classical momentum (2.29) obtained with $V_{\text{tail}}(r)$ alone. Thus,

$$\begin{aligned}\phi_{\text{sr}} = &- n_{\text{th}}\pi - \frac{\phi_{\text{out}}(0)}{2} - \frac{\pi}{2} + \frac{1}{\hbar}\int_{r_E}^{\infty} p_0^{\text{tail}}(r)dr \\ &- \frac{1}{\hbar}\int_0^{r_E}\left[p_E^{\text{tail}}(r) - p_0^{\text{tail}}(r)\right]dr + \mathcal{O}(E)\,. \end{aligned} \tag{3.7}$$

With the substitution $V(r) \to V_{\text{tail}}(r)$ the exact regular solution in the short-range region (3.2) is solely related to the tail potential and can be written as

$$u_{\text{reg}}(r) \propto \frac{1}{\sqrt{p_E^{\text{tail}}(r)}} \sin\left(\frac{1}{\hbar}\int_{r_E}^{r} p_E^{\text{tail}}(r')dr' - \xi_{\text{t}} + \left[\Delta_{\text{th}} + \gamma(E)\right]\pi\right)\,, \tag{3.8}$$

where the threshold quantum number n_{th} has been replaced by its *remainder* $\Delta_{\text{th}} = n_{\text{th}} - \lfloor n_{\text{th}} \rfloor$. The additional energy-dependent phase ξ_{t} can easily be calculated from the potential tail alone

$$\begin{aligned}\xi_{\text{t}} = &- \frac{\phi_{\text{out}}(0)}{2} - \frac{\pi}{2} + \frac{1}{\hbar}\int_{r_E}^{\infty} p_0^{\text{tail}}(r)dr \\ &+ \frac{1}{\hbar}\int_0^{r_E}\left[p_0^{\text{tail}}(r) - p_E^{\text{tail}}(r)\right]dr\,. \end{aligned} \tag{3.9}$$

For reasons of convenience, the reference point r_E is chosen to be defined by $V_{\text{tail}}(r_E) = -|E|$ so that it only depends on the absolute value of the energy ($r_E = r_{-E}$) and coincides with the classical tuning point for small negative energies. With this choice, the integrals in Eq. (3.9) take finite values for each energy.

Short-range effects are parametrized via $\Delta_{\text{th}} + \gamma(E)$; they enter the tail-based representation (3.8) of the regular solution only via the remainder Δ_{th} that is a property of the full potential at the dissociation threshold and a small short-range correction

$$\gamma(E) = \gamma_{\text{sr}} E + \mathcal{O}(E^2)\,, \tag{3.10}$$

which is a smooth and small function of the energy accounting for the higher-order terms in Eq. (3.7). For near-threshold energies, it can well be approximated by its first-order term $\gamma_{\text{sr}}E$, or might even be completely negligible. The representation (3.8) is valid for the energy range, for which the full potential $V(r)$ is well approximated by its tail $V_{\text{tail}}(r)$ down to the energy-dependent distance r_E, that, by construction, includes the threshold energy ($E = 0$). Deviations at higher energies can be absorbed in the higher-order terms of the short range correction $\gamma(E)$.

Figure 3.2 illustrates the exact regular solution (dashed line) in a given potential at an arbitrary near-threshold energy together with its WKB representation (3.1) (dotted line), which diverges at the inner classical turning point, and the tail-based representation (3.8) (solid line). With the correct choice of Δ_{th}, all three wave functions are identical in the inner region (shaded area) where both the WKB approximation is valid and the potential essentially equals its tail.

The representation (3.8) of the regular solution is very convenient, since it permits the formulation of a boundary condition in the limit $r \to 0$ for a solution in the reference

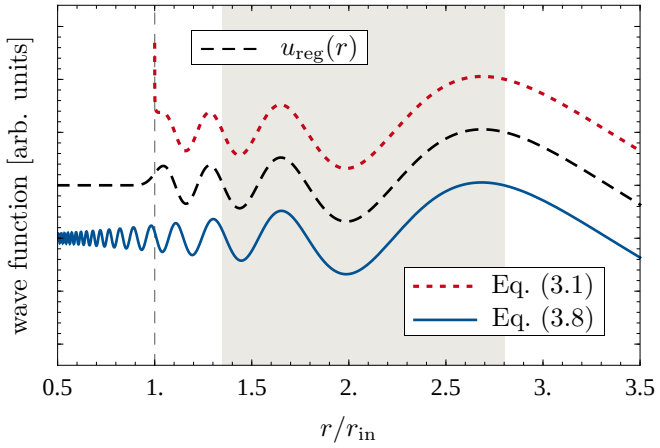

Figure 3.2: Different representations of the regular solution at an arbitrary near-threshold energy in the short-range region of a potential that fulfills the required preconditions of the present treatment. The dashed line shows the exact form of the regular solution. In the shaded area that represents the region where both the WKB approximation is valid and the full potential is well described by its tail, it is essentially equal to both the WKB wave with the full potential (dotted line) as given by Eq. (3.1) and the tail-based form of Eq. (3.8) depicted by the solid line.

potential $V_{\mathrm{tail}}(r)$ that exactly resembles the regular solution as obtained with the full interaction potential $V(r)$ in the inner region of WKB validity and at all distances beyond.

For a known interaction potential $V(r)$, the actual value of the threshold quantum number n_{th} and its remainder Δ_{th} may be estimated, according to Eq. (3.4), by explicitly evaluating the outer reflection phase $\phi_{\mathrm{out}}(0)$ with the tail potential only [see Eq. (3.12) below] and assuming the inner reflection phase to be $\phi_{\mathrm{in}}(0) \approx \pi/2$ which is the semiclassical convention (2.42) and is appropriate for a deep potential well with a steep repulsive core (cf. Section 2.2.3).

3.2 Formulation for bound states

Interaction potentials with attractive tails that fall off faster than $-1/r^2$ support at most a finite number of bound states [4]. This is in contrast to the situation in the presence of truly long-range potential tails, such as for Coulombic tails, where there are countably infinitely many bound states that form a Rydberg series converging to the threshold energy. For the potential tails considered in the present work, a different type of quantization condition applies, which is derived in the following. It is shown how, in the presence of a singular attractive potential tail, its influence on the bound-state spectrum is separated from short-range effects.

3.2.1 Quantization function

Below the dissociation threshold ($E < 0$), all physically relevant wave functions are square integrable bound states. To ensure normalizability, we pick the solutions of the radial Schrödinger equation (2.6) that vanish exponentially in the outer asymptotic region as reference. Since the tail of the interaction potential is assumed to vanish faster than $1/r^2$

asymptotically, these solutions fulfill the bound-state boundary condition

$$u^{(-)}(r) \overset{r\to\infty}{\sim} \exp(-\kappa r)\,, \tag{3.11}$$

where $\kappa = \sqrt{-2\mu E}/\hbar$ is the asymptotic inverse penetration depth into the outer classically forbidden region at energies below the dissociation threshold ($E = 0$). In the inner region of the tail potential, these solutions (3.11) can, for any energy below the dissociation threshold, accurately be represented by WKB waves

$$u^{(-)}(r) \overset{r\to 0}{\propto} \frac{1}{\sqrt{p_E^{\mathrm{tail}}(r)}} \cos\left(\frac{1}{\hbar}\int_r^{r_E} p_E^{\mathrm{tail}}(r')dr' - \frac{\phi_{\mathrm{out}}(E)}{2}\right)\,, \tag{3.12}$$

where r_E is, according to its definition, just the outer classical turning point and $\phi_{\mathrm{out}}(E)$ is the corresponding energy-dependent outer reflection phase [cf. Eq. (2.40)].

In order to reproduce the correct bound-state energies of the full potential by using solutions of the Schrödinger equation including only the potential tail, the asymptotically vanishing solution (3.11) is matched to the tail-based regular solution (3.8) that, for near-threshold energies, resembles the exact regular solution with the full potential in the inner tail-region of WKB validity. The corresponding matching condition requires the sine in (3.8) and the cosine in (3.12) to be identical up to a factor of -1. This is fulfilled whenever

$$n_{\mathrm{th}}\pi + \gamma(E) - \xi_{\mathrm{t}} - \frac{\phi_{\mathrm{out}}(E)}{2} - \frac{\pi}{2} \overset{!}{=} n\pi\,, \tag{3.13}$$

where n is an integer. Rephrasing this condition for the corresponding energy eigenvalue E_n yields

$$n_{\mathrm{th}} - n = F(E_n)\,, \tag{3.14}$$

which defines the *quantization function* $F(E)$ that — together with the threshold quantum number n_{th} — describes the bound-state energies in a given potential well. This quantization function can — for potentials with singular tails — naturally be split up

$$F(E) = F_{\mathrm{tail}}(E) + F_{\mathrm{sr}}(E) \tag{3.15}$$

into its tail part $F_{\mathrm{tail}}(E)$ which can, with the explicit form (3.9) of the phase ξ_{t}, be given as

$$F_{\mathrm{tail}}(E) = \frac{S_{\mathrm{tail}}(0) - S_{\mathrm{tail}}(E)}{\pi\hbar} - \frac{\phi_{\mathrm{out}}(0) - \phi_{\mathrm{out}}(E)}{2\pi}\,, \tag{3.16}$$

and its short-range part $F_{\mathrm{sr}}(E) = -\gamma(E)$, that reflects all approximations that have been made in the derivation of the short-range solution (3.8). The short-range part $F_{\mathrm{sr}}(E)$

of the quantization function is thus determined by short-range effects only. The action integrals in Eq. (3.16) correspond to the actions for classical motion in the tail potential

$$S_{\mathrm{tail}}(E) = \int_0^{r_E} p_E^{\mathrm{tail}}(r) dr \,. \tag{3.17}$$

Due to the distinct singularity of the potential tail at the origin, both action integrals in Eq. (3.16) diverge, but their difference remains finite [cf. Eq. (3.9)].

If we had assumed the outer reflection phase to be independent of the energy, we would have arrived at a purely semiclassical quantization function

$$F_{\mathrm{tail}}^{\mathrm{NDE}}(E) = \frac{1}{\pi\hbar} \left[S_{\mathrm{tail}}(0) - S_{\mathrm{tail}}(E) \right] , \tag{3.18}$$

which is equivalent to the well-established *near-dissociation expansion* of LeRoy, Bernstein [14] and Stwalley [15]. In contrast to the exact formulation (3.16), the LeRoy-Bernstein quantization function (3.18) obscures the anticlassical nature of near-threshold properties for potentials with attractive tails falling off faster than $-1/r^2$ [4].

3.2.2 Limiting expansions

In order to yield the correct quantization function (3.16), the purely semiclassical LeRoy-Bernstein quantization function (3.18) needs to be provided with an additional term that contains the outer reflection phase ϕ_{out} [cf. Eq. (3.16)]. This outer reflection phase is, as discussed in Section 2.2.3, energy-dependent in general; it is expected to deviate all the more from its semiclassical value of $\pi/2$ the closer the energy is to the dissociation threshold, which is the anticlassical limit for potentials that vanish faster than $-1/r^2$ [4].

Low binding energies

The low-energy behavior of the outer reflection phase can be deduced from the behavior at zero energy of the solutions in the potential tail. Two linearly independent zero-energy solutions $w_0(r)$, $w_1(r)$ of the radial Schrödinger equation with the tail potential alone behave as

$$w_0(r) \overset{r\to\infty}{\sim} 1 \quad \text{and} \quad w_1(r) \overset{r\to\infty}{\sim} r \tag{3.19}$$

in the outer asymptotic region[1]. These wave functions can, in the limit of small distances, be accurately represented by WKB waves. These are given by

$$w_{0,1}(r) \overset{r\to 0}{\sim} \frac{D_{0,1}}{\sqrt{p_0^{\mathrm{tail}}(r)}} \cos\left(\frac{1}{\hbar} \int_r^\infty p_0^{\mathrm{tail}}(r') dr' - \frac{\phi_{0,1}}{2} \right) . \tag{3.20}$$

In the limit of low binding energies ($\kappa \to 0$) the solution $u^{(-)}(r)$ that fulfills the bound-state boundary condition (3.11) can, up to the order of the energy, be given by the linear combination of the zero-energy solutions defined by Eq. (3.19)

$$u^{(-)}(r) \overset{\kappa r\to 0}{\sim} w_0(r) - \kappa w_1(r) \overset{r\to\infty}{\sim} 1 - \kappa r \,. \tag{3.21}$$

[1] In fact, the solution $w_1(r)$ that asymptotically behaves as r exists only for potentials that vanish faster than $-1/r^3$ asymptotically. However, the following procedure's range of applicability contains the inverse-cube ($-1/r^3$) reference potential as a limiting case.

Comparing this form of the solution to expression (3.12) in the inner region of the potential tail using (3.20) gives

$$\frac{\phi_{\text{out}}(E)}{2} \overset{\kappa\to 0}{\sim} -\frac{S_{\text{tail}}(0)-S_{\text{tail}}(E)}{\hbar}+\frac{\pi}{2} - \arctan\left(\frac{D_0\cos(\phi_0/2)-\kappa D_1\cos(\phi_1/2)}{D_0\sin(\phi_0/2)-\kappa D_1\sin(\phi_1/2)}\right)+\mathcal{O}(\kappa^2)\,. \tag{3.22}$$

This expression is only correct up to the order κ. The expansion of $\phi_{\text{out}}(E)$ up to this order yields

$$\frac{\phi_{\text{out}}(E)}{2} \overset{\kappa\to 0}{\sim} \frac{\phi_0}{2}-\frac{S_{\text{tail}}(0)-S_{\text{tail}}(E)}{\hbar}+b\kappa+\mathcal{O}(\kappa^2)\,. \tag{3.23}$$

The coefficient of the term of order κ in Eq. (3.23) is a length that will, in the following, be referred to as the *threshold length* b. It is explicitly given by

$$b=\frac{D_1}{D_0}\sin\left(\frac{\phi_0-\phi_1}{2}\right)\,. \tag{3.24}$$

From a more sophisticated effective-range expansion, which is demonstrated in Refs. [13, 43], the term of the order of κ^2 could be deduced from these solutions for potential tails falling off faster than $-1/r^3$.

From the low-energy expansion (3.23) of the outer reflection phase, we can give a universal expression for the quantization function (3.15) at low energies

$$F(E) \overset{\kappa\to 0}{\sim} \frac{b\kappa}{\pi}+\mathcal{O}(\kappa^2)\,, \tag{3.25}$$

which is valid for all potentials with attractive tails that vanish faster than $-1/r^2$ asymptotically [54]. Note, that, in the limit of low energies, the terms including the action integrals both at zero and at finite energy in Eqs. (3.16) and (3.23) cancel exactly. These terms are typically of lower order in the energy than the inverse penetration depth $\kappa=\sqrt{-2\mu E}/\hbar$.

High binding energies

At large negative energies, the outer reflection phase $\phi_{\text{out}}(E)$ tends to $\pi/2$, which is its semiclassical value (2.42). For high binding energies, the conditions for semiclassical behavior are well fulfilled, since the interaction potential is very steep in the vicinity of the outer classical turning point (cf. Section 2.2.3). Assuming the semiclassical value of $\pi/2$, we can give the high-energy expansion of the tail part of the quantization function as

$$F_{\text{tail}}(E) \overset{\kappa\to\infty}{\sim} F_{\text{tail}}^{\text{NDE}}(E)-\frac{\phi_0}{2\pi}+\frac{1}{4}\,, \tag{3.26}$$

which differs from the LeRoy-Bernstein function (3.18) only by a constant offset. Therefore, the shortcomings of the purely semiclassical quantization rule are not revealed, unless bound states with very low binding energies are concerned. This is thoroughly discussed

in Section 5.1.2. However, one should keep in mind that the short-range part $F_{\mathrm{sr}}(E)$ of the quantization function (3.15) is probably not negligible at energies far from threshold.

An asymptotic expansion of the outer reflection phase at high energies can be obtained by taking higher-order corrections to the WKB wave function into account [13, 43]. This procedure can be very useful when the explicit shape of the quantization function is to be determined via an interpolation scheme, as done in Section 4.2.2.

3.3 Formulation for scattering states

In this section, an expression is derived for the scattering phase shift, which characterizes the long-range behavior of the continuum states at $E > 0$. This expression is based on the solutions in the reference potential $V_{\mathrm{tail}}(r)$ and accounts for effects that are due to the deviation of the full potential $V(r)$ from the singular form of its tail at short distances via the short-range parametrization $\Delta_{\mathrm{th}} + \gamma(E)$ [cf. Eq. (3.8)]. A relation to the properties of quantum reflection is explicitly derived, in order to show how the scattering phase shift is influenced by the tangible physical properties of the tail potential.

3.3.1 Parametrization of the scattering phase shift

For potentials vanishing faster than $1/r^2$ at large distances, there are two fundamental, linearly independent solutions $u^{(\mathrm{s})}(r)$ and $u^{(\mathrm{c})}(r)$ of the radial Schrödinger equation (2.26) that behave asymptotically as

$$u^{(\mathrm{s})}(r) \overset{r\to\infty}{\sim} \sin(kr) \;, \quad u^{(\mathrm{c})}(r) \overset{r\to\infty}{\sim} \cos(kr) \;. \tag{3.27}$$

The regular solution of the full potential $V(r)$ can — in the limit of large distances — be written as a superposition of these two fundamental solutions

$$u_{\mathrm{reg}}(r) \propto \cos(\delta_0)\, u^{(\mathrm{s})}(r) + \sin(\delta_0)\, u^{(\mathrm{c})}(r) \,, \tag{3.28}$$

which defines the s-wave phase shift δ_0 for scattering states.

Considering only the attractive tail potential $V_{\mathrm{tail}}(r)$, which is more singular than $-1/r^2$ at the origin, the fundamental solutions $u^{(\mathrm{s})}(r)$ and $u^{(\mathrm{c})}(r)$, which are defined by the boundary conditions (3.27), can — in the limit of small distances — accurately be represented by WKB waves

$$\begin{aligned} u^{(\mathrm{s})}(r) &\overset{r\to 0}{\sim} \frac{A_{\mathrm{s}}}{\sqrt{p_E^{\mathrm{tail}}(r)}} \sin\left(\frac{1}{\hbar}\int_{r_E}^{r} p_E^{\mathrm{tail}}(r')dr' - \phi_{\mathrm{s}}\right) , \\ u^{(\mathrm{c})}(r) &\overset{r\to 0}{\sim} \frac{A_{\mathrm{c}}}{\sqrt{p_E^{\mathrm{tail}}(r)}} \cos\left(\frac{1}{\hbar}\int_{r_E}^{r} p_E^{\mathrm{tail}}(r')dr' - \phi_{\mathrm{c}}\right) , \end{aligned} \tag{3.29}$$

with r_E given by $V_{\mathrm{tail}}(r_E) = -E$, as in Eq. (3.9), and real nonnegative amplitudes A_{s} and A_{c}. Explicit expressions (3.29) for the fundamental solutions in the inner region can obviously be obtained from the exact solutions of the radial Schrödinger equation (2.6) with the reference potential $V_{\mathrm{tail}}(r)$ in the limit $r \to 0$, where the WKB approximation is accurate. The amplitudes A_{s} and A_{c} as well as the phases ϕ_{s} and ϕ_{c}, which all depend on the energy, are thus determined solely by the reference potential $V_{\mathrm{tail}}(r)$.

Relating the phase of the tail based expression (3.8) of the regular solution $u_{\mathrm{reg}}(r)$ in the inner region of the tail potential to the phase of the corresponding linear combination (3.28) of the two fundamental solutions (3.29) in the inner region yields

$$\tan\delta_0 = \frac{A_\mathrm{s}}{A_\mathrm{c}} \frac{\sin\left(\Delta_\mathrm{th}\pi - \xi_\mathrm{t} + \phi_\mathrm{s}\right)}{\cos\left(\Delta_\mathrm{th}\pi - \xi_\mathrm{t} + \phi_\mathrm{c}\right)} \tag{3.30}$$

for the s-wave phase shift δ_0 for scattering by the full potential $V(r)$ that has a singular attractive tail $V_{\mathrm{tail}}(r)$. The right-hand side of Eq. (3.30) contains four functions, which depend only on the tail potential. The phase ξ_t stems from the tail-based representation (3.8) of the regular solution at short distances and is explicitly given by the corresponding terms in Eq. (3.9). The ratio $A_\mathrm{s}/A_\mathrm{c}$ and the phases ϕ_s and ϕ_c, which are defined via (3.29), are solely determined by the tail potential $V_{\mathrm{tail}}(r)$. They can be determined by comparing the WKB expressions (3.29) to analytically known solutions for the tail potential, if available. Otherwise they can easily be calculated by numerically integrating the radial Schrödinger equation (2.6) with $V_{\mathrm{tail}}(r)$ for any desired energy.

Properties related to the short-range part of the potential enter Eq. (3.30) — to first order — via the remainder Δ_th. Higher-order short-range effects can be accounted for by replacing the remainder Δ_th in Eq. (3.30) by the full short-range parametrization $\Delta_\mathrm{th} + \gamma(E)$ [cf. Eq. (3.8)].

3.3.2 Connection to the properties of quantum reflection

The two fundamental solutions $u^{(\mathrm{s})}(r)$ and $u^{(\mathrm{c})}(r)$ [see Eqs. (3.27) and (3.29)] to the radial Schrödinger equation (2.6) with the reference potential $V_{\mathrm{tail}}(r)$ have been chosen for reasons of convenience. They, themselves, do not represent any actual physically meaningful quantum state. However, the amplitudes and phases that enter the parametrization (3.30) of the phase shift can be related to the quantities of quantum reflection, which are physically meaningful and tangible properties of the singular attractive tail potential. The basic essentials of this result have already been published in Ref. [61].

Quantum reflection process

A particle approaching an attractive force field can be reflected far away from the center of the potential. This process is called quantum reflection [62] and is a purely quantum mechanical phenomenon without any classical analog. Its occurrence in atomic physics has been established in various experiments [63, 64]. For typical interatomic interactions, it has been shown that quantum reflection takes place at rather large distances [65] and is therefore an effect due to the potential tail.

For attractive potentials $V_{\mathrm{tail}}(r)$ that are more singular than $-1/r^2$ at the origin and vanish faster than $-1/r^2$ asymptotically, there are two distinct regions of WKB validity. The WKB approximation becomes increasingly accurate in the limit of small radii close to the singularity, as well as in the limit of large radii where the potential becomes negligible. These regions are separated by an anticlassical region that extends around the distance r_E with $V_{\mathrm{tail}}(r_E) = -E$, where the WKB criterion (2.38) is not well fulfilled. As already

discussed in Section 2.2.1, the wave function can be split up into an inward and an outward traveling part, wherever the WKB approximation is valid.

The process of quantum reflection can thus be described by a stationary solution $u_{\rm refl}(r)$ of the radial Schrödinger equation that is a superposition of an inward traveling wave and an outward traveling reflected wave in the outer asymptotic region ($r \to \infty$). This wave function can be given in terms of free-particle waves

$$u_{\rm refl}(r) \overset{r\to\infty}{\sim} \frac{1}{\sqrt{\hbar k}} \exp(-ikr) + \frac{R}{\sqrt{\hbar k}} \exp(ikr)\,, \tag{3.31}$$

with the wave number $k = \sqrt{2\mu E}/\hbar$ as long as the potential vanishes faster than $1/r^2$ at large distances. The complex coefficient $R = |R| \exp(i\phi_R)$ is the reflection amplitude with $|R| \leq 1$. A detailed description of the modulus and phase of the quantum reflection amplitude can be found in Refs. [65–67]. An alternative representation of this solution is

$$u_{\rm refl}(r) \overset{r\to\infty}{\propto} \frac{1}{\sqrt{\hbar k}} \sin(kr) + \frac{\mathcal{K}_{\rm refl}}{\sqrt{\hbar k}} \cos(kr)\,. \tag{3.32}$$

The complex coefficient $\mathcal{K}_{\rm refl}$ can be related to a complex phase shift for the quantum reflection process [67] and is connected to the reflection amplitude R via the relation

$$\mathcal{K}_{\rm refl} = i\left(\frac{1+R}{1-R}\right)\,. \tag{3.33}$$

In the limit of small radii the solution $u_{\rm refl}(r)$ is an inward-traveling wave representing the transmitted part of the incoming wave. Since the potential is not a constant in the inner region of WKB validity, the inward-traveling wave cannot be expressed as a free wave. We need to use the WKB expression

$$u_{\rm refl}(r) \overset{r\to 0}{\sim} \frac{T}{\sqrt{p_E^{\rm tail}(r)}} \exp\left(-\frac{i}{\hbar}\int_{r_E}^{r} p_E^{\rm tail}(r')dr'\right) \tag{3.34}$$

instead. The complex transmission amplitude T can be given in terms of its modulus and phase by $|T| \exp(i\phi_T)$.

Since the radial flux density

$$j_r = \frac{\hbar}{2\mu i}\left(u^* \frac{du}{dr} - u\frac{du^*}{dr}\right) \equiv \text{const}\,. \tag{3.35}$$

is conserved,[2] the amplitudes for transmission and reflection necessarily need to fulfill the relation

$$|R|^2 + |T|^2 = 1\,. \tag{3.36}$$

The quantities $|T|^2$ and $|R|^2$ can thus be thought of as the probabilities for transmission through and quantum reflection by the anticlassical region around r_E in the attractive interaction potential.

[2]The requirement that the flux is conserved is an immediate consequence of the Wronskian $W(u, u^*)$ being independent of r for any solution $u(r)$ of an ordinary second-order differential equation.

Quantum capture process

The process that will, in the following, be referred to as *quantum capture* is described as follows: A particle moving in the inner region of an attractive potential $V_{\mathrm{tail}}(r)$ can be captured on the inside, despite the fact that its energy is actually above the dissociation threshold. This is due to reflection by the anticlassical region in the potential. Therefore, this process is also referred to as *near-side quantum reflection* [68].

The stationary solution $u_{\mathrm{capt}}(r)$ that describes the quantum capture of a particle incidentally traveling outwards is — in the inner spatial region — given by

$$u_{\mathrm{capt}}(r) \overset{r\to 0}{\sim} \frac{1}{\sqrt{p_E(r)}} \left[\exp\left(\frac{i}{\hbar} \int_{r_E}^{r} p(r')dr' \right) + \mathcal{C} \exp\left(-\frac{i}{\hbar} \int_{r_E}^{r} p(r')dr' \right) \right], \tag{3.37}$$

representing an outward traveling WKB wave and a *captured* inward traveling wave with the complex capture amplitude $\mathcal{C}$. The wave function (3.37) can be constructed from superposition of the solution $u_{\mathrm{refl}}(r)$ which describes the quantum reflection of an inward traveling wave, and its complex conjugate. From this connection to the quantum reflection process, the relation

$$\mathcal{C} = -R^* \frac{T}{T^*} \tag{3.38}$$

is derived, which connects the amplitudes for reflection, transmission and capture. A general form of this relation is given in Refs. [54, 69] for quantum reflection from the left- and the right-hand side. On the outside of the anticlassical region in the potential $V_{\mathrm{tail}}(r)$, the wave function can simply be given by an outward traveling, transmitted wave

$$u_{\mathrm{capt}}(r) \overset{r\to\infty}{\sim} \frac{T}{\sqrt{\hbar k}} \exp(ikr), \tag{3.39}$$

where the transmission amplitude is just the same as in Eq. (3.34) for the quantum reflection process [68, 69]. Its squared modulus $|T|^2$ gives the probability for the particle to escape from the inner region of WKB validity.

Relation to fundamental solutions

From the wave function $u_{\mathrm{capt}}(r)$ describing the quantum capture, the phases and amplitudes of the previously defined fundamental solutions $u^{(\mathrm{s})}(r)$ and $u^{(\mathrm{c})}(r)$ [see Eqs. (3.27) and (3.29)] can be related to the amplitudes for reflection and transmission. The fundamental solution $u^{(\mathrm{s})}(r)$ which is a sine in the outer asymptotic region [cf. Eq. (3.27)] can be expressed in terms of the wave function (3.39) of the quantum capture process

$$u^{(\mathrm{s})}(r) = \mathrm{Im}\left[\frac{\sqrt{\hbar k}}{T} u_{\mathrm{capt}}(r) \right] \tag{3.40}$$

in all of the coordinate space. By making use of Eqs. (3.37) and (3.38) and using well-known trigonometric identities, this wave function can — in the inner region — be written as

$$\begin{aligned} u^{(\mathrm{s})}(r) \overset{r\to 0}{\sim} \frac{1}{\sqrt{p_E^{\mathrm{tail}}(r)}} \frac{\sqrt{\hbar k}}{|T|} \Big\{ \Big[1 + |R| \cos(\phi_R) \Big] \sin\left(\frac{1}{\hbar} \int_{r_E}^{r} p(r')dr' - \phi_T \right) \\ + |R| \sin(\phi_R) \cos\left(\frac{1}{\hbar} \int_{r_E}^{r} p(r')dr' - \phi_T \right) \Big\}. \end{aligned} \tag{3.41}$$

This form can, by making use of the identities

$$\begin{aligned} 1 + |R|\cos(\phi_R) &= \mathrm{Re}\,(1+R) = |1+R|\cos\left(\arg(1+R)\right)\,, \\ |R|\sin(\phi_R) &= \mathrm{Im}\,(1+R) = |1+R|\sin\left(\arg(1+R)\right)\,, \end{aligned} \tag{3.42}$$

be reformulated as

$$u^{(\mathrm{s})}(r) \overset{r\to 0}{\sim} \sqrt{\hbar k}\frac{|1+R|}{|T|}\frac{1}{\sqrt{p_E^{\mathrm{tail}}(r)}}\sin\left(\frac{1}{\hbar}\int_{r_E}^{r} p(r')dr' - \phi_T + \arg(1+R)\right)\,. \tag{3.43}$$

By comparing this expression to Eq. (3.29), we can establish the relations

$$A_{\mathrm{s}} = \sqrt{\hbar k}\,\frac{|1+R|}{|T|}\,, \quad \text{and} \quad \phi_{\mathrm{s}} = \phi_T - \arg(1+R)\,. \tag{3.44}$$

Using the corresponding identity

$$u^{(\mathrm{c})}(r) = \mathrm{Re}\left[\frac{\sqrt{\hbar k}}{T}u_{\mathrm{capt}}(r)\right] \tag{3.45}$$

for the solution $u^{(\mathrm{c})}(r)$ that is a cosine in the outer asymptotic region [cf. Eq. (3.27)] and performing similar conversions, we find

$$A_{\mathrm{c}} = \sqrt{\hbar k}\,\frac{|1-R|}{|T|}\,, \quad \text{and} \quad \phi_{\mathrm{c}} = \phi_T - \arg(1-R)\,. \tag{3.46}$$

The ratio of amplitudes can then be given as

$$\frac{A_{\mathrm{s}}}{A_{\mathrm{c}}} = \left|\frac{1+R}{1-R}\right| = |\mathcal{K}_{\mathrm{refl}}|\,. \tag{3.47}$$

It is found to be identical to the absolute value of the coefficient $\mathcal{K}_{\mathrm{refl}}$ for quantum reflection [cf. Eq. (3.32)]. Equation (3.30) can thus be reformulated using only the properties of quantum reflection

$$\tan\delta_0 = \left|\frac{1+R}{1-R}\right|\frac{\sin(\Delta_{\mathrm{th}}\pi - \xi_t + \phi_T - \arg(1+R))}{\cos(\Delta_{\mathrm{th}}\pi - \xi_{\mathrm{t}} + \phi_T - \arg(1-R))}\,. \tag{3.48}$$

In formula (3.48) the influence of the potential tail now enters via its tangible physical properties, i.e., the amplitudes for transmission and quantum reflection.

3.3.3 Limiting expansions

As for the case of quantization (see Section 3.2.2), analytical expansions of the tail functions both at low and at high energies can be derived from the zero-energy solutions in the potential $V_{\mathrm{tail}}(r)$ also for energies above the dissociation threshold ($E > 0$).

Low collision energies

The low-energy behavior of the wave function $u^{(\mathrm{s})}(r)$, defined by its asymptotic behavior (3.27), can be given by

$$u^{(\mathrm{s})}(r) \overset{kr\to 0}{\sim} k w_1(r) \overset{r\to\infty}{\sim} kr\,, \tag{3.49}$$

where $w_1(r)$ is the zero-energy solution of the radial Schrödinger equation (2.6) with the reference potential $V_{\mathrm{tail}}(r)$ alone, which has already been defined in Eq. (3.19). As in Section 3.2.2, this formulation is valid as long as the reference potential vanishes faster than $-1/r^3$ asymptotically. We compare both sides of relation (3.49) in the limit $r \to 0$ using Eqs. (3.20) and (3.29). This explicitly yields

$$\frac{A_{\mathrm{s}}}{\sqrt{p_E^{\mathrm{tail}}(r)}} \sin\left(\frac{1}{\hbar}\int_{r_E}^{r} p_E^{\mathrm{tail}}(r')dr' - \phi_{\mathrm{s}}\right) = \frac{D_1 k}{\sqrt{p_0^{\mathrm{tail}}(r)}} \cos\left(\frac{1}{\hbar}\int_{r}^{\infty} p_0^{\mathrm{tail}}(r')dr' - \frac{\phi_1}{2}\right)\,. \tag{3.50}$$

In the limit of small distances, the local classical momentum $p_E^{\mathrm{tail}}(r)$ approaches its zero-energy correspondent $p_0^{\mathrm{tail}}(r)$ due to the distinct singularity of the reference potential at $r = 0$. The low-energy expression for the amplitude can just be read off Eq. (3.50),

$$A_{\mathrm{s}} \overset{k\to 0}{\sim} D_1 k\,. \tag{3.51}$$

Equating the phases gives the low-energy behavior of the corresponding phase

$$\phi_{\mathrm{s}} \overset{k\to 0}{\sim} -\frac{\phi_1}{2} - \frac{\pi}{2} + \frac{1}{\hbar}\int_{r_E}^{\infty} p_0^{\mathrm{tail}}(r)dr + \frac{1}{\hbar}\int_{0}^{r_E} \left[p_0^{\mathrm{tail}}(r) - p_E^{\mathrm{tail}}(r)\right] dr\,, \tag{3.52}$$

where the action integrals that occur, are — in accordance with the behavior at energies below the dissociation threshold ($E < 0$) — of lower order in the energy than the wave number $k = \sqrt{2\mu E}/\hbar$.

The same procedure is applied for the solution $u^{(\mathrm{c})}(r)$. Its asymptotic low-energy behavior is expressed by

$$u^{(\mathrm{c})}(r) \overset{kr\to 0}{\sim} w_0(r) \overset{r\to\infty}{\sim} 1\,, \tag{3.53}$$

which is valid for all singular attractive potential tails that vanish faster than $-1/r^2$ asymptotically. Equating the corresponding expressions from Eqs. (3.20) and (3.29) in the limit of small distances yields

$$\frac{A_{\mathrm{c}}}{\sqrt{p_E^{\mathrm{tail}}(r)}} \sin\left(\frac{1}{\hbar}\int_{r_E}^{r} p_E^{\mathrm{tail}}(r')dr' - \phi_{\mathrm{c}}\right) = \frac{D_0}{\sqrt{p_0^{\mathrm{tail}}(r)}} \cos\left(\frac{1}{\hbar}\int_{r}^{\infty} p_0^{\mathrm{tail}}(r')dr' - \frac{\phi_0}{2}\right)\,. \tag{3.54}$$

It is thus found that the amplitude A_{c} approaches a finite value in the limit of zero energy

$$A_{\mathrm{c}} \overset{k\to 0}{\sim} D_0\,. \tag{3.55}$$

The corresponding phase is just given by

$$\phi_{\mathrm{c}} \overset{k\to 0}{\sim} -\frac{\phi_0}{2} + \frac{1}{\hbar}\int_{r_E}^{\infty} p_0^{\mathrm{tail}}(r)dr + \frac{1}{\hbar}\int_{0}^{r_E} \left[p_0^{\mathrm{tail}}(r) - p_E^{\mathrm{tail}}(r)\right] dr\,. \tag{3.56}$$

Having derived the low-energy behavior of all the tail-related functions that enter formula (3.30) for the s-wave phase shift due to the full potential $V(r)$, we can specify

the low-energy behavior of the phase shift itself. In this limit, the ratio of the amplitudes, which has the dimension of a length, is given by

$$\frac{A_\mathrm{s}}{A_\mathrm{c}} \overset{k\to 0}{\sim} \frac{D_1}{D_0} k\,. \tag{3.57}$$

The zero-energy value of the fraction of sine and cosine in (3.30) is found by inserting the zero-energy values of the phases ϕ_s and ϕ_c given in (3.52) and (3.56). After some simple conversions the low-energy limit of Eq. (3.30) yields

$$\tan\delta_0 \overset{k\to 0}{\sim} -\frac{D_1}{D_0}\left[\cos\left(\frac{\phi_0-\phi_1}{2}\right) + \sin\left(\frac{\phi_0-\phi_1}{2}\right)\cot(\Delta_\mathrm{th}\pi)\right] k \tag{3.58}$$

The terms containing the action integrals in both ξ_t [cf. Eq. (3.9) and $\phi_\mathrm{s,c}$ [cf. Eqs. (3.52) and (3.56)] might be of lower order than the wave number k, but in the limit of low energies they cancel exactly. The result (3.58) is by no means surprising; it just gives the first term of the well-established effective-range expansion (see, e.g., Ref. [27])

$$\tan\delta_0 \overset{k\to 0}{\sim} -ak\,, \tag{3.59}$$

which is determined by the *scattering length* a, that was first introduced by Fermi in the context of scattering of slow neutrons [30]. Whenever the interaction potential vanishes faster than $-1/r^3$, a scattering length exists. In our case, Eq. (3.58) yields

$$a = \bar{a} + \frac{b}{\tan(\Delta_\mathrm{th}\pi)}\,, \tag{3.60}$$

where we introduced an additional length scale, the *mean scattering length*

$$\bar{a} = \frac{D_1}{D_0}\cos\left(\frac{\phi_0-\phi_1}{2}\right)\,, \tag{3.61}$$

and b is just the threshold length, as defined in Eq. (3.24). Equation (3.60) shows that the scattering length depends on the two length scales $\bar{a}$ and b, that both are properties of the tail potential. Short-range effects enter the scattering length solely via the threshold quantum number's remainder Δ_th. Further short-range corrections enter the expansion (3.59) only in higher-order terms of the wave number k, according to the formula (3.30) for the scattering phase shift.

Effective-range expansion for ϕ_s

In the following, an effective-range expansion is performed in order to obtain an expression for the phase $\phi_\mathrm{s}(k)$. For this purpose, we consider the fundamental solution $u^{(\mathrm{s})}(r)$ that behaves like a sine asymptotically, according to Eq. (3.27), in the reference potential $V_\mathrm{tail}(r)$. We define $u_k(r) \equiv u^{(\mathrm{s})}(r)$ for this solution at a given asymptotic wave number $k = \sqrt{2\mu E}/\hbar$. Its behavior in the inner region of the reference potential $V_\mathrm{tail}(r)$ is given by Eq. (3.29).

We consider two possible solutions u_{k_1}, u_{k_2} in the same reference potential $V_{\text{tail}}(r)$ at different asymptotic wave numbers k_1, k_2. The corresponding radial Schrödinger equations are then given by

$$-u''_{k_i}(r) - \frac{2\mu}{\hbar^2} V_{\text{tail}}(r) u_{k_i}(r) = k_i^2 u_{k_i}(r) \tag{3.62}$$

Multiplying each of the two equations with the solution of the other and subtracting one from the other leads to

$$u_{k_1} u''_{k_2} - u''_{k_1} u_{k_2} = \left(k_1^2 - k_2^2\right) u_{k_1} u_{k_2} \,. \tag{3.63}$$

Intergrating this equation from an arbitrary lower bound r_l to an upper bound r_u gives

$$\int_{r_l}^{r_u} \left(u_{k_1} u''_{k_2} - u''_{k_1} u_{k_2}\right) dr = \left(k_1^2 - k_2^2\right) \int_{r_l}^{r_u} u_{k_1} u_{k_2} dr \,. \tag{3.64}$$

Partial integration of the left-hand side gives

$$\left[u_{k_1} u'_{k_2} - u'_{k_1} u_{k_2}\right]_{r_l}^{r_u} = \left(k_1^2 - k_2^2\right) \int_{r_l}^{r_u} u_{k_1} u_{k_2} dr \,. \tag{3.65}$$

Since the limits of integration are completely arbitrary, we are free to choose $r_l \to 0$ and $r_u \to \infty$. In order to obtain the contribution from the lower bound to the left-hand side, we need to know not only the wave function [see upper relation of Eq. (3.29)] in the inner region of WKB validity in the potential tail, but also its derivative, which is given by

$$u'_{k_i}(r) = \frac{A_{\text{s}}(k_i)}{\sqrt{p_{k_i}(r)}} \left\{ \frac{p_{k_i}(r)}{\hbar} \cos\Omega_{k_i}(r) - \frac{1}{2} \frac{p'_{k_i}(r)}{p_{k_i}(r)} \sin\Omega_{k_i}(r) \right\} , \tag{3.66}$$

where we used the abbreviation

$$\Omega_{k_i}(r) \equiv \frac{1}{\hbar} \int_{r_{k_i}}^{r} p_{k_i}^{\text{tail}}(r') dr' - \phi_{\text{s}}(k_i) \,. \tag{3.67}$$

In the limit of interest, i.e., $r \to 0$, expression (3.66) for the wave function's derivative is further simplified

$$u'_{k_i}(r) \overset{r\to 0}{\sim} \frac{A_{\text{s}}(k_i)}{\sqrt{p_0(r)}} \frac{p_0(r)}{\hbar} \cos\Omega_{k_i}(r) \,. \tag{3.68}$$

The contribution from the lower limit in Eq. (3.65) can thus be given as

$$\left[u_{k_1} u'_{k_2} - u'_{k_1} u_{k_2}\right]_{r_l \to 0} = \frac{A_s(k_1)\, A_s(k_2)}{\hbar} \sin\left[\Omega_{k_2}(0) - \Omega_{k_1}(0)\right] \,. \tag{3.69}$$

In order to evaluate the upper limit in Eq. (3.65), we make use of the solutions of the free Schrödinger equation $v_{k_i}(r)$ obeying the same boundary conditions as the solutions $u_{k_i}(r)$ with a given potential

$$u_{k_i}(r) \overset{r\to\infty}{\sim} v_{k_i}(r) \equiv \sin(k_i r) \,. \tag{3.70}$$

Taking the same steps that led to Eq. (3.65) but for the free solutions $v_{k_i}(r)$, we obtain

$$\left[v_{k_1} v'_{k_2} - v'_{k_1} v_{k_2}\right]_{r_l}^{r_u} = \left(k_1^2 - k_2^2\right) \int_{r_l}^{r_u} v_{k_1} v_{k_2} dr \,. \tag{3.71}$$

The evaluation of the lower bound yields

$$\left[v_{k_1} v'_{k_2} - v'_{k_1} v_{k_2}\right]_{r_l} = \sin\left[(k_2 - k_1)\, r_l\right] \overset{r_l \to 0}{\to} 0\,. \tag{3.72}$$

In the limit $r_u \to \infty$, the identity

$$\left[v_{k_1} v'_{k_2} - v'_{k_1} v_{k_2}\right]^{r_u \to \infty} = \left[u_{k_1} u'_{k_2} - u'_{k_1} u_{k_2}\right]^{r_u \to \infty} \tag{3.73}$$

holds and the relation

$$\left[u_{k_1} u'_{k_2} - u'_{k_1} u_{k_2}\right]^{r_u \to \infty} = \left(k_1^2 - k_2^2\right) \int_0^\infty v_{k_1} v_{k_2} dr \tag{3.74}$$

is obtained, which is then inserted in Eq. (3.65), together with Eq. (3.69). This yields

$$\frac{A_s(k_1)\, A_s(k_2)}{\hbar} \sin\left[\Omega_{k_2}(0) - \Omega_{k_1}(0)\right] = \left(k_1^2 - k_2^2\right) \int_0^\infty \left(u_{k_1} u_{k_2} - v_{k_1} v_{k_2}\right) dr \tag{3.75}$$

and therefore

$$\sin\left[\Omega_{k_2}(0) - \Omega_{k_1}(0)\right] = \hbar \left(k_1^2 - k_2^2\right) \int_0^\infty \frac{u_{k_1} u_{k_2} - v_{k_1} v_{k_2}}{A_{\mathrm{s}}(k_1)\, A_{\mathrm{s}}(k_2)} dr\,. \tag{3.76}$$

Without any loss of generality, the wave number k_2 is renamed to k and the limit $k_1 \to 0$ is performed. Using the known low-energy identities (3.49) and (3.51) and expanding the sine in Eq. (3.70) gives

$$\sin\left[\Omega_k(0) - \Omega_0(0)\right] = -\hbar k^2 \frac{1}{D_1} \int_0^\infty \frac{w_1 u_k - r v_k}{A_{\mathrm{s}}(k)} dr\,. \tag{3.77}$$

Since the present effective-range expansion is only correct up to $\mathcal{O}(k^2)$, the term on the left-hand side is expanded in terms of the wave number k. Solving for $\phi_{\mathrm{s}}(k)$ yields

$$\begin{aligned} \phi_{\mathrm{s}}(k) \overset{k \to 0}{\sim} \phi_{\mathrm{s}}(0) &+ \frac{1}{\hbar} \int_{r_E}^\infty p_0^{\mathrm{tail}}(r) dr \\ &+ \frac{1}{\hbar} \int_0^{r_E} \left[p_0^{\mathrm{tail}}(r) - p_E^{\mathrm{tail}}(r)\right] dr - h_{\mathrm{s}} k^2 + \mathcal{O}(k^3)\,, \end{aligned} \tag{3.78}$$

with the coefficient h_{s}, which has the units of an area and is defined via

$$h_{\mathrm{s}} = \frac{\hbar}{D_1^2} \int_0^\infty \left[r^2 - w_1(r)^2\right] dr\,. \tag{3.79}$$

In accordance with the ordinary effective-range expansion [31–33] for the scattering phase shift and corresponding expansions [67], the integral in Eq. (3.79) converges for all reference potentials that fall off faster than $-1/r^5$ asymptotically. The threshold value $\phi_{\mathrm{s}}(0) = -\phi_1/2 - \pi/2$ is found by comparing to Eq. (3.52).

Effective-range expansion for ϕ_c

The effective-range expansion for the phase $\phi_\mathrm{c}(k)$ can be performed in a similar fashion. In fact, the actual evaluation of the occurring terms is even less demanding than for the phase $\phi_\mathrm{s}(k)$, since the amplitude $A_\mathrm{c}(k)$ reaches a finite value as $k \to 0$ [cf. Eq. (3.55)]. This procedure yields

$$\begin{aligned}\phi_\mathrm{c}(k) \overset{k\to 0}{\sim} \phi_\mathrm{c}(0) &+ \frac{1}{\hbar}\int_{r_E}^{\infty} p_0^{\mathrm{tail}}(r)dr \\ &+ \frac{1}{\hbar}\int_0^{r_E}\left[p_0^{\mathrm{tail}}(r) - p_E^{\mathrm{tail}}(r)\right]dr - h_\mathrm{c}k^2 + \mathcal{O}(k^3)\,. \end{aligned} \tag{3.80}$$

The effective area h_c is given by

$$h_\mathrm{c} = \frac{\hbar}{D_0^2}\int_0^{\infty}\left[1 - w_0(r)^2\right] = \frac{\hbar}{D_0^2}\,\rho_\mathrm{eff} = b\,\rho_\mathrm{eff}\,, \tag{3.81}$$

where the relation (B.13) has been used to obtain the third identity. The zero-energy solution $w_0(r)$ is defined in Eq. (3.19) and ρ_eff is the *subthreshold effective range* defined in Ref. [13], which also determines the next-to-leading term in the quanitzation function (3.16). It can explicitly be evaluated for any potential with a tail that vanishes faster than $-1/r^3$ asymptotically. The threshold value $\phi_\mathrm{c}(0) = -\phi_0/2$ is found by comparing to Eq. (3.56).

High collision energies

In the limit of high energies, we find that the quantality function (2.37) tends to zero at all distances,

$$\lim_{E\to\infty} \mathcal{Q}_E(r) = 0 \quad \forall r > 0\,, \tag{3.82}$$

for reference potentials that fall off faster than $1/r^2$ asymptotically and are more singular than $-1/r^2$ at the origin. This means that the criterion (2.38) for the validity of the WKB approximation is fulfilled in all of coordinate space. Therefore, we can identify the fundamental solutions defined in Eq. (3.27) with their WKB behavior (3.29), which was originally restricted to the inner region of the potential tail, but is — in the limit of high energies — valid for all distances r. We thus obtain the identities

$$\frac{A_\mathrm{s/c}}{\sqrt{p_E^{\mathrm{tail}}(r)}}\sin/\cos\left(\frac{1}{\hbar}\int_{r_E}^{r} p_E^{\mathrm{tail}}(r')dr' - \phi_\mathrm{s/c}\right) \overset{r\to\infty}{\sim} \sin/\cos(kr) \tag{3.83}$$

for both the fundamental solution $u^{(\mathrm{s})}(r)$ and the fundamental solution $u^{(\mathrm{c})}(r)$. In the limit of large distances, $r \to \infty$, the local classical momentum reaches the free-particle limit $p_E^{\mathrm{tail}}(r) \to \hbar k$ and we can immediately read off the high-energy behavior of the amplitudes

$$A_\mathrm{s/c} \overset{E\to\infty}{\sim} \sqrt{\hbar k}\,, \tag{3.84}$$

which obviously yields

$$\frac{A_\mathrm{s}}{A_\mathrm{c}} \overset{E\to\infty}{\sim} 1 \tag{3.85}$$

for their ratio. This limit can also be obtained from the identity (3.47) in a very intuitive way.

The high-energy limits of the phases ϕ_s and ϕ_c are obtained by comparing the arguments of the trigonometric functions in Eq. (3.83), which yields

$$\begin{aligned}\phi_{\mathrm{s/c}} &\overset{E\to\infty}{\sim} \lim_{r\to\infty}\left[\frac{1}{\hbar}\int_{r_E}^{r} p_E^{\mathrm{tail}}(r')dr' - kr\right] \\ &= -kr_E + \frac{1}{\hbar}\int_{r_E}^{\infty}\left[p_E^{\mathrm{tail}}(r) - \hbar k\right]dr\,. \end{aligned} \tag{3.86}$$

According to the relations (3.44) and (3.46), this is also the high-energy expansion of the phase ϕ_T of the transmission amplitude, which enters the wave function (3.34) for the quantum reflection process.

Inserting the high-energy expansions (3.85) and (3.86) into the expression (3.30) for the phase shift and using the explicit form (3.9) of the phase ξ_t yields

$$\begin{aligned}\delta_0 &\overset{E\to\infty}{\sim} n_\mathrm{th}\pi - \xi_\mathrm{t} + \phi_{\mathrm{s/c}} \\ &= n_\mathrm{th}\pi + \frac{\phi_\mathrm{out}(0)}{2} + \frac{\pi}{2} + \frac{1}{\hbar}\int_0^{\infty}\left[p_E^{\mathrm{tail}}(r) - p_0^{\mathrm{tail}}(r) - \hbar k\right]dr\,. \end{aligned} \tag{3.87}$$

In the limit of high energies, the threshold quantum number n_th thus enters the phase shift only as a simple offset, while the energy dependence is determined by the tail of the interaction potential. The validity of Eq. (3.87) is limited to near-threshold energies, which can, however, be larger than the characteristic energy scales of the tail potential by orders of magnitude. Further short-range corrections are omitted, but could in principle be included by simply adding $\pi\gamma(E)$ to the right-hand side of Eq. (3.87).

The phase shift δ_0 is defined only up to an integer multiple of π. Choosing the full threshold quantum number n_th in (3.87) instead of its remainder Δ_th and assuming that the phase shift is a continuous function, ensures that $\delta_0(0)$ is $N_\mathrm{b}\pi$, where $N_\mathrm{b} = \lfloor n_\mathrm{th}\rfloor + 1$ is the number of bound states supported by the full potential well. This is reminiscent of Levinson's Theorem[3] [28, 29]. However, expression (3.87) does not tend to zero in the limit of high energies. This is due to the fact that, at energies beyond the validity of Eq. (3.87), the behavior of the phase shift is actually not governed by the potential tail, but by the behavior of the potential in the inner region.

3.4 Summary of results

For interaction potentials with tails that fall off faster than $1/r^2$ asymptotically and are more singular than $-1/r^2$ at the origin, a separation of the influence of this tail potential on the bound-state spectrum and the scattering properties has been achieved. Utilizing the

[3]Note that the applicability of Levinson's Theorem is restricted to a very special class of potentials. It is in particular not applicable for potentials that have a repulsive core more singular than $1/r^2$ at the origin.

modified WKB approximation of Section 2.2, where appropriate, a parametrization of the short-range solution (3.8) in interaction potentials with singular attractive tails has been given, which offers an appropriate boundary condition for the singular tail potential. It is essentially determined by the noninteger remainder Δ_{th} of the threshold quantum number n_{th} and a further short-range correction $\gamma(E)$ that is a smooth and small function of energy which vanishes at $E = 0$. At near-threshold energies, it can thus be approximated by its leading-order term $\gamma_{\mathrm{sr}}E$ or even be completely neglected. From the short-range parametrization, the scattering properties as well as the bound-state spectrum can be obtained from the solutions of the Schrödinger equation with only the singular tail potential as reference.

The present formulation is particularly convenient in the case that the deviation of the full interaction potential from the singular form of its tail is restricted to distances that are small compared to the typical length scales of the tail potential, i.e., the full potential is deep in the sense that it supports a large number of bound states. This requirement is typically well fulfilled by interatomic potentials, that have tails that are essentially due to induced electrostatic interactions (see Appendix A).

The quantization function $F(E)$, which enters the quantization condition (3.14), is — for near-threshold energies — essentially determined by its tail part (3.16), which can be obtained from the solutions in the tail potential. Its fundamental difference to the purely semiclassical LeRoy-Bernstein function (3.18), which might offer a good description of the progression of bound-state levels for high binding energies, has been pointed out. The quantization function's low-energy behavior (3.25) is found to be universally determined by the threshold length b [cf. Eq. (3.24)].

For continuum states ($E > 0$), the scattering phase shift has been expressed in terms of functions that depend on the potential tail only; the short-range effects on the scattering properties are completely described via the threshold quantum number n_{th} and the small short-range correction $\gamma(E)$. The tail functions have been expressed in terms of the properties of quantum reflection, i.e., via the tangible properties of the tail potential. At high collision energies, the threshold quantum number n_{th} is manifest in the scattering phase shift as a constant offset [cf. Eq. (3.87)]. In the limit of low collision energies the scattering process is, for potentials falling off faster than $-1/r^3$, determined by the scattering length a (3.59) that can be expressed (3.60) via the mean scattering length $\bar{a}$ [cf. Eq. (3.61)], the threshold length b and the remainder Δ_{th} that parametrizes the effects due to the short-range part of the full interaction potential.

Chapter 4

Application to inverse-power tails

The formalism for the description of quantization and scattering that has been derived in the preceding Chapter 3 is particularly powerful in the presence of pure inverse-power potential tails, as can occur in the interaction of two compound particles such as atoms, ions and molecules. At large distances, the interaction energy can be given in terms of a multipole expansion (cf. Appendix A), that is essentially an expansion in powers of $1/r$.

If one of the interacting compound particles has zero net charge, the lowest-order terms in this multipole expansion vanish and the resulting potential tail fulfills the preconditions for the present treatment. Whenever the leading-order term of the multipole expansion dominates the interaction way down to small distances, where the WKB criterion (2.38) is fulfilled for this potential, it will be sufficient to include only that term in the definition of the reference potential $V_{\text{tail}}(r)$ for a correct description of quantization and scattering at near-threshold energies. For inverse-power reference potentials, the quantities defined in the previous section are given explicitly in this chapter.

The first part of this chapter is devoted to general properties that hold for all inverse-power potentials. The subsequent section deals with the quantization function in the presence of inverse-power tails. An explicit form of the tail part $F_{\text{tail}}(E)$ of the quantization function is presented for the case of inverse-cube interactions. The effects of long-range inverse-power potential tails on the collisional properties is studied in the last section of this chapter. For the most prominent cases of inverse-power potentials the scattering phase shift according to Eq. (3.30) is given explicitly.

4.1 Generalities for inverse-power tails

The inverse-power tails, that fulfill the requirements for the applicability of the present formalism, i.e., are more singular than $-1/r^2$ at the origin and vanish faster than $-1/r^2$ asymptotically, can be given by

$$V_\alpha(r) = -\frac{C_\alpha}{r^\alpha} = -\frac{\hbar^2}{2\mu}\frac{\beta_\alpha^{\alpha-2}}{r^\alpha}\,, \quad \alpha > 2\,. \tag{4.1}$$

The strength of the interaction is given by the strength coefficient C_α, or alternatively by

the length β_α. Relating the interaction strength to the length scale β_α is quite convenient, since it also introduces a corresponding energy scale

$$\mathcal{E}_\alpha = \frac{\hbar^2}{2\mu}\frac{1}{\beta_\alpha^2}\,. \tag{4.2}$$

Expressing all energies in units of this energy and all length in units of β_α allows a significant simplification of the radial Schrödinger equation (2.6) with the tail potential (4.1)

$$\left[\frac{d^2}{d\rho^2} + \frac{1}{\rho^\alpha} + \chi\right] u(\rho) = 0\,, \tag{4.3}$$

where ρ is the dimensionless radius r/β_α and $\chi \equiv E/\mathcal{E}_\alpha$. Depending on whether the energy is below or above the dissociation threshold ($E = 0$), we can also write

$$\chi = \frac{E}{\mathcal{E}_\alpha} = \begin{cases} (k\beta_\alpha)^2\,, & E > 0 \\ -(\kappa\beta_\alpha)^2\,, & E < 0 \end{cases} \tag{4.4}$$

with the asymptotic wave number $k = \sqrt{2\mu E}/\hbar$ or the inverse penetration depth $\kappa = \sqrt{-2\mu E}/\hbar$, respectively.

Equation (4.3) emphasizes a particular feature of homogeneous potentials such as $V_\alpha(r)$ (4.1); all properties of the corresponding solutions do not depend on the energy and the potential strength separately, but only on the product $(\kappa\beta_\alpha)$ or $(k\beta_\alpha)$ respectively. So does, e.g., the local classical momentum (2.29), that is now given by

$$p_E^{\text{tail}}(\rho) = \frac{\hbar}{\beta_\alpha}\sqrt{\chi + \rho^{-\alpha}}\,. \tag{4.5}$$

Regions of WKB validity

For inverse-power potentials (4.1), we can explicitly identify the regions of WKB validity by evaluating the quantality function $\mathcal{Q}_E(r)$ as defined in (2.37). With the local classical momentum given by Eq. (4.5) this yields

$$\mathcal{Q}_E(\rho) = \frac{\alpha}{16}\rho^{\alpha-2}\,\frac{\alpha - 4 - 4(\alpha+1)\chi\rho^\alpha}{(1+\chi\rho^\alpha)^3}\,. \tag{4.6}$$

We find that, at small ρ, the quantality function behaves as

$$\mathcal{Q}_E(\rho) \overset{\rho\to 0}{\sim} \frac{\alpha\,(\alpha-4)}{16}\rho^{\alpha-2}\,, \tag{4.7}$$

except for the case of $\alpha = 4$, where the quantality function starts proportional to ρ^6. Therefore, for all inverse-power potentials $V_\alpha(r)$ [cf. Eq. (4.1)], the accuracy of the WKB approximation increases with decreasing r and becomes exact in the limit $r \to 0$, independent of the system's energy. For large ρ the quantality function behaves as

$$\mathcal{Q}_E(\rho) \overset{\rho\to\infty}{\sim} -\frac{\alpha(\alpha+1)}{4}\frac{1}{\chi^2}\rho^{-(\alpha+2)}\,, \tag{4.8}$$

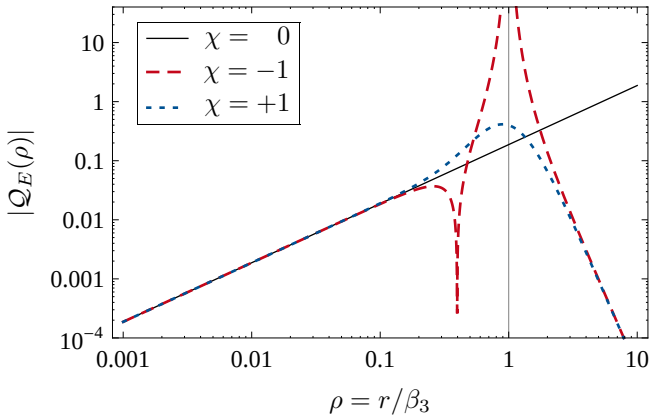

Figure 4.1: The absolute value of the quantality function $\mathcal{Q}_E(\rho)$ for the potential $V_3(r) = -C_3/r^3$ is plotted against the dimensionless radius $\rho = r/\beta_\alpha$ for zero energy (solid line) and for both a negative energy $\chi = -1$ (dashed line) and a positive energy $\chi = +1$ (dotted line). The value quantality function $\mathcal{Q}_E(\rho)$ tends to zero both in the limit $\rho \to \infty$ (for nonzero energies) and in the limit $\rho \to 0$ (for every energy). At negative energy ($\chi = -1$) a classical turning point exists at $\rho = 1$ and the corresponding quantality function (dashed line) diverges at this point.

so that the WKB approximation becomes increasingly accurate in the limit $r \to \infty$ too for any given nonzero energy. This is actually not very surprising, since the potential $V_\alpha(r)$ vanishes in the limit $r \to \infty$ and each solutions can be written as a linear combination of $\exp(\pm ikr)$ for positive energies or $\exp(\pm\kappa r)$ for negative energies. These are just particular cases of WKB waves (2.35) in a constant potential.

At a classical turning point, i.e., at r_E for negative energies in attractive inverse-power potentials (4.1), the quantality function diverges (cf. Section 2.2). For positive energies, the absolute value of the quantality function does not diverge but has a maximum at around r_E,[1] which is given by

$$r_E = |\chi|^{-1/\alpha}\beta_\alpha = \begin{cases} (\kappa\beta_\alpha)^{-2/\alpha}\,\beta_\alpha & E < 0 \\ (k\beta_\alpha)^{-2/\alpha}\,\beta_\alpha & E > 0 \end{cases} . \tag{4.9}$$

As an example, Figure 4.1 shows the behavior of the quantality function (4.6) for the inverse-cube potential $V_3(r) = -C_3/r^3$ for different energies. The absolute value of the quantality function is plotted against the dimensionless radius $\rho = r/\beta_3$ for the energies $E = 0, -\mathcal{E}_3, +\mathcal{E}_3$. We find that, in the limit of small radii (4.7), it is essentially independent of the energy. For the negative energy value $E = -\mathcal{E}_3$ (dashed line), $r_E = \beta_3$ is the classical turning point and the quantality function diverges. For the positive energy value $E = +\mathcal{E}_3$ (dotted line) the behavior at small and large ρ is the same as for $E = -\mathcal{E}_3$, since neither the low-ρ asymptote (4.7) nor the high-ρ asymptote (4.8) depends on the sign of the energy.

[1] The absolute value of the quantality function can obviously be determined by explicitly differentiating Eq. (4.6) with respect to ρ. This actually yields a distance that is r_E times a factor close to unity in the cases considered here (cf. Ref. [70]).

Zero-energy solutions

Two linearly independent zero-energy solutions (3.19) of the radial Schrödinger equation (4.3) with the tail potential $V_\alpha(r)$ are needed for the calculation of the low-energy expansions of the quantization function (see Section 3.2.2) and the tail functions for the description of unbound scattering states (see Section 3.3.3). These functions can be given analytically

$$w_0(r) = \frac{\Gamma(1+\nu)}{\nu^\nu}\sqrt{\frac{r}{\beta_\alpha}}J_\nu(z)\,, \quad w_1(r) = \Gamma(1-\nu)\nu^\nu\sqrt{\beta_\alpha r}J_{-\nu}(z)\,, \tag{4.10}$$

where $J_{\pm\nu}(z)$ denotes the Bessel function of the first kind[2] of order $\pm\nu$, with

$$\nu = \frac{1}{\alpha-2}\,, \quad \text{and} \quad z = 2\nu\left(\frac{\beta_\alpha}{r}\right)^{1/(2\nu)} \tag{4.11}$$

being the argument. The gamma function $\Gamma(x)$ is real-valued for real arguments x. In the limit $r \to 0$, the argument z of the Bessel functions diverges to infinity. The asymptotic expansion for large arguments [48] of the Bessel functions can then be compared to the inner WKB form (3.20) to determine the amplitudes $D_{0,1}$ and the phases $\phi_{0,1}$ (see, e.g., [54]). This yields

$$\begin{aligned} D_0 &= \sqrt{\frac{\hbar}{\pi\nu\beta_\alpha}}\,\frac{\Gamma(1+\nu)}{\nu^\nu}\,, \quad \phi_0 = \frac{\pi}{2}+\nu\pi\,, \\ D_1 &= \sqrt{\frac{\hbar\beta_\alpha}{\pi\nu}}\,\Gamma(1-\nu)\nu^\nu\,, \quad \phi_1 = \frac{\pi}{2}-\nu\pi\,. \end{aligned} \tag{4.12}$$

These amplitudes and phases determine the parameters that enter the low-energy identities that have been formulated in Section 3.2.2 for the quantization function $F(E)$ and in Section 3.3.3 for the tail functions ϕ_s, ϕ_c and $A_\mathrm{s}/A_\mathrm{c}$ that characterize the continuum states above threshold.

The threshold length, which is defined in Eq. (3.24) and determines the leading-order energy dependence of the quantization function [cf. Eq. (3.25)], is given by

$$b_\alpha = \nu^{2\nu}\frac{\Gamma(1-\nu)}{\Gamma(1+\nu)}\sin(\nu\pi)\beta_\alpha\,. \tag{4.13}$$

This expression can easily be evaluated for any $\alpha > 3$ and, in addition, takes a finite value in the limit $\alpha \to 3$. A threshold length b_3 thus exists for the reference potential $V_3(r)$. The mean scattering length (3.61) determines, together with the threshold length b_α, the threshold law (3.60) for elastic scattering. For inverse-power tails $V_\alpha(r)$ with $\alpha > 3$ it is given by

[2] For integer orders ν the Bessel functions fulfill $J_{-\nu}(z) = (-1)^\nu J_\nu(z)$ and are therefore not linearly independent. As far as our considerations are concerned, this is only important in the case of $\alpha = 3$; a solution linearly independent of $w_0(r)$ (4.10) is asymptotically given by $r + \ln r$ instead of r.

α	3	4	5	6	7	$\alpha \to \infty$
b_α/β_α	π	1	0.631342	0.477989	0.391514	$\pi/(\alpha-2)$
$\bar{a}_\alpha/\beta_\alpha$	—	0	0.364506	0.477989	0.538872	1

Table 4.1: Values of the threshold length b_α and of the mean scattering length $\bar{a}_\alpha$ for inverse-power tail potentials $V_\alpha(r)$ (4.1) with different values of the power α.

$$\bar{a}_\alpha = \nu^{2\nu}\frac{\Gamma(1-\nu)}{\Gamma(1+\nu)}\cos(\nu\pi)\beta_\alpha\,. \tag{4.14}$$

In the particular limit of $\alpha \to 3$ the mean scattering length $\bar{a}_\alpha$ diverges to $-\infty$; a finite scattering length does not exist for potentials with inverse-cube tails $V_3(r)$. Explicit values for b_α and $\bar{a}_\alpha$ are given in Table 4.1.

4.2 Quantization for inverse-power tails

The general form of the tail part $F_{\text{tail}}(E)$ of the quantization function that enters the quantization rule (3.14) via Eq. (3.15) has been given in Refs. [13, 43] for inverse-power tails and will briefly be summarized in the following. Explicit expressions for the tail part of the quantization function in the presence of tail potentials proportional to $-1/r^6$ [13, 43] and $-1/r^4$ [42, 43] have also been given before. We thus do not recapitulate these quantization functions, but derive an explicit, analytical expression for the tail part of the quantization function only for the case of inverse-cube tails $V_3(r)$ in Section 4.2.2.

4.2.1 The general case $-C_\alpha/r^\alpha$ with $\alpha > 2$

In this section, the constituents of the tail part $F_\alpha(E)$ of the quantization function for the class of inverse-power potentials $V_\alpha(r)$ with $\alpha > 2$ [see Eq. (4.1)] are explicitly given. Limiting expansions for the outer reflection phase $\phi_{\text{out}}(E)$ are given in an analytical form and the corresponding implications on the quantization function are studied.

For inverse-power tail potentials (4.1), the difference of the two action integrals that occurs in Eqs. (3.16), (3.18) and (3.23) can be evaluated analytically, which yields

$$\begin{aligned}
F_\alpha^{\text{NDE}}(E) &= \frac{1}{\pi\hbar}\left[S_{\text{tail}}(0) - S_{\text{tail}}(E)\right] \\
&= \frac{1}{\pi\hbar}\int_{r_E}^{\infty} p_0^{\text{tail}}(r)dr + \frac{1}{\pi\hbar}\int_0^{r_E}\left[p_0^{\text{tail}}(r) - p_E^{\text{tail}}(r)\right]dr \\
&= \frac{1}{\pi}\int_{(\kappa\beta_\alpha)^{-2/\alpha}}^{\infty}\rho^{-\alpha/2}d\rho + \frac{1}{\pi}\int_0^{(\kappa\beta_\alpha)^{-2/\alpha}}\left[\rho^{-\alpha/2} - \sqrt{(\kappa\beta_\alpha)^2 - \rho - \alpha}\right]d\rho \\
&= \frac{1}{\pi}\left\{\frac{2}{\alpha-2} + \int_0^1 x^{-\alpha/2}\left[1-\sqrt{1-x^\alpha}\right]\right\}(\kappa\beta_\alpha)^{1-2/\alpha} \\
&= \frac{G_\alpha}{\pi}(\kappa\beta_\alpha)^{1-2/\alpha}\,,
\end{aligned} \tag{4.15}$$

α	3	4	5	6	7	$\alpha \to \infty$
ϕ_0/π	3/2	1	5/6	3/4	7/10	1/2
G_α	2.24050	1.19814	0.835265	0.646777	0.529983	π/α

Table 4.2: Values of the outer reflection phase at zero energy ϕ_0 and of the coefficient G_α for inverse-power tail potentials $V_\alpha(r)$ (4.1) with different values of the power α.

where we substituted $\rho \to (\kappa\beta_\alpha)^{-2/\alpha}x$ to obtain the third identity. The distance r_E is, for $E < 0$, just given by the outer classical turning point $r_E = (\kappa\beta_\alpha)^{-2/\alpha}\beta_\alpha$, according to its definition (4.9). By expanding the square root in the integrand, an analytical solution can be found which yields

$$G_\alpha = \frac{\sqrt{\pi}}{\alpha - 2}\frac{\Gamma\left(\frac{1}{2} + \frac{1}{\alpha}\right)}{\Gamma\left(1 + \frac{1}{\alpha}\right)} \tag{4.16}$$

for the coefficient G_α. Equation (4.15) constitutes the LeRoy-Bernstein quantization function $F_{\text{tail}}^{\text{NDE}}(E)$ [cf. Eq. (3.18)] that was obtained for inverse-power potentials $V_\alpha(r)$ with $\alpha > 2$ in 1970 [14, 15]. It exhibits the typical semiclassical energy dependence on the *reduced outer classical turning point*

$$s = \kappa r_E = (\kappa\beta_\alpha)^{1-2/\alpha}\,. \tag{4.17}$$

The LeRoy-Bernstein quantization function $F_\alpha^{\text{NDE}}(E)$ is, however, not exact for binding energies very close to the dissociation threshold $E = 0$, which is the anticlassical limit for these kinds of potentials [4]. To account for purely quantum mechanical effects at low binding energies it needs to be modified via the correct values of the outer reflection phase

$$F_\alpha(E) = F_\alpha^{\text{NDE}}(E) - \frac{\phi_0 - \phi_{\text{out}}(E)}{2\pi}\,. \tag{4.18}$$

At low energies the outer reflection phase $\phi_{\text{out}}(E)$ is in general given by Eq. (3.23). With ϕ_0 from Eq. (4.12), the difference of the action integrals evaluated above [Eq. (4.15)], and the threshold length b_α defined in Eq. (4.13), this yields

$$\phi_{\text{out}}(E) \overset{\kappa\to 0}{\sim} \phi_0 - 2G_\alpha(\kappa\beta_\alpha)^{1-2/\alpha} + 2b_\alpha\kappa + \mathcal{O}(\kappa^2)\,. \tag{4.19}$$

The phase ϕ_0 and the coefficient G_α are explicitly given in Table 4.2 for different values of the power α. For inverse-power tail potentials $V_\alpha(r)$ with $\alpha \geq 4$ the subsequent term $\mathcal{O}(\kappa^2)$ can in general be obtained analytically. The corresponding scheme is not revisited here. For further reading see Ref. [13]. With the difference of the action integrals given by Eq. (4.15) and the low-energy limit (4.19) of the outer reflection phase, the low energy limit of the quantization function is

$$F_\alpha(E) \overset{\kappa\to 0}{\sim} \frac{b_\alpha}{\pi}\kappa + \mathcal{O}(\kappa^2)\,, \tag{4.20}$$

which is in accordance with the more general formulation of Eq. (3.25).

D_1	D_3	D_5	D_7
$\frac{1}{9}\sqrt{\pi}\frac{\Gamma(1/6)}{\Gamma(2/3)}$	0	$\frac{17}{486}\sqrt{\pi}\frac{\Gamma(5/6)}{\Gamma(-2/3)}$	$-\frac{1093}{29160}\sqrt{\pi}\frac{\Gamma(7/6)}{\Gamma(-4/3)}$
0.809550	0	−0.0174159	−0.0202295

Table 4.3: Analytical and numerical values for the coefficients of the high-energy expansion (4.21) of the outer reflection phase in the case of an inverse-power tail potential (4.1) with $\alpha = 3$.

In the limit $\kappa \to \infty$, the outer reflection phase approaches the conventional WKB value of $\pi/2$. Taking higher-order corrections to the WKB approximation in Eq. (2.31) into account, the high-κ expansion of the outer reflection phase is

$$\phi_{\text{out}}(E) \overset{\kappa\to\infty}{\sim} \frac{\pi}{2} + \sum_{j=1}^{j_{\max}} \frac{D_j}{s^j}\,, \tag{4.21}$$

where s again stands for the reduced outer classical turning point (4.17). Explicit expressions for the coefficients D_j are given, for any power $\alpha > 2$, up to $j = 7$ in Ref. [42]. For arbitrary α, only terms with odd j which are not integer multiples of α give a nonvanishing contribution to the high-κ expansion (4.21). In the limit of high energies, the tail part of the quantization function for inverse-power tails is given by

$$F_\alpha(E) \overset{\kappa\to\infty}{\sim} F_\alpha^{\text{NDE}}(E) - \frac{\nu}{2}\,, \tag{4.22}$$

with $F_\alpha^{\text{NDE}}(E)$ given in Eq. (4.15), according to Eq. (3.26). We thus find that, except for a constant offset, the near-dissociation expansion given by LeRoy and Bernstein [14] gives the correct progression of bound-state energies in the limit of high binding energies, but fails near the dissociation threshold $E = 0$. However, one should keep in mind that, at higher binding energies, the short-range part $F_{\text{sr}}(E)$ of the quantization function is most certainly not negligible.

4.2.2 Dipole-dipole interaction ($\alpha = 3$)

We now study the near-threshold quantization for potentials that have inverse-cube tails $V_3(r) = -C_3/r^3$. Isotropic interaction potentials with these tails can occur in the interaction between two atoms of the same species, but in different internal states (see Appendix A). Exact values for the outer reflection phase are presented. With these values the correct form of the tail part $F_{\alpha=3}(E)$ of the quantization function is obtained. In order to present a simple form for this quantization function, a simple rational expression is presented, which accurately approximates the outer reflection phase. The results for the quantization function in the presence of inverse-cube tails have already been published in Ref. [71].

Outer reflection phase

For the inverse-cube reference potential $V_3(r)$ the threshold value of the reflection phase is given by $3\pi/2$ (see Eq. 4.10 and Table 4.2). and $\phi_{\text{out}}(E)$ decreases to its semiclassical

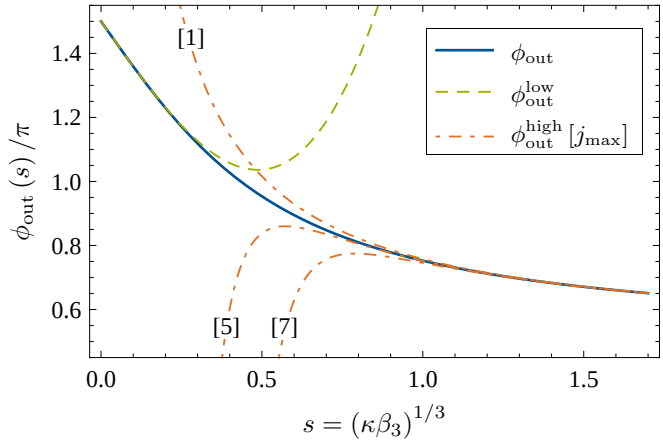

Figure 4.2: Exact values of the outer reflection phase $\phi_{\rm out}$ as obtained with an inverse-cube reference potential. They are plotted against the reduced outer classical turning point (4.17) (solid line) together with the analytical low-energy expansion (4.23) (dashed line) and the high-energy expansion (4.21) for different values of $j_{\rm max}$ (dot-dashed lines).

value $\pi/2$ as the asymptotic inverse penetration depth κ increases ($\kappa \to \infty$), according to Eq. (4.21). Exact values for the outer reflection phase are shown as the solid line in Figure 4.2. They have been calculated by solving the Schrödinger equation (4.3) numerically with bound-state boundary conditions (3.11) and are plotted against the reduced outer classical turning point $s = (\kappa\beta_3)^{1/3}$ of the reference potential $V_3(r) = -C_3/r^3$, with the characteristic length $\beta_3 = 2\mu C_3/\hbar^2$.

The low-energy expansion $\phi_{\rm out}^{\rm low}(E)$ of the outer reflection phase $\phi_{\rm out}(E)$ is depicted as the dashed line in Figure 4.2. It is defined via the expansion

$$\phi_{\rm out}^{\alpha=3}(E) \overset{\kappa\to 0}{\sim} \frac{3\pi}{2} - 2G_3(\kappa\beta_3)^{1/3} + 2\pi(\kappa\beta_3) \overset{\rm def}{=} \phi_{\rm out}^{\rm low}(E)\,, \tag{4.23}$$

where the next term is of the order κ^2, but can not be obtained analytically for the case of inverse-cube tail potentials $V_3(r)$. According to Eq. (4.16) the coefficient G_3 is given by

$$G_3 = \sqrt{\pi}\frac{\Gamma\,(5/6)}{\Gamma\,(4/3)} \approx 2.24050\,, \tag{4.24}$$

as already listed in Table 4.2. Note that this contribution from the outer reflection phase cancels exactly with the contribution of the action integrals to the quantization function (3.16). The threshold length b_3 that enters the expansion (4.23) is just $b_3 = \pi\beta_3$ as already stated in Table 4.1.

The high-energy expansion $\phi_{\rm out}^{\rm high}(E)$ is given by Eq. 4.21 with $s = (\kappa\beta_3)^{1/3}$. The coefficients D_j for the inverse-power tail potential (4.1) with $\alpha = 3$ are gathered in Table 4.3. The high-energy expansions (4.21) obtained with $j_{\rm max} = 1, 5, 7$ are shown as dot-dashed lines in Figure 4.2. We can clearly see from Figure 4.2 that the high-energy expansion $\phi_{\rm out}^{\rm high}(E)$ is an asymptotic expansion; the inclusion of higher order terms does not necessarily increase the range of applicability. However, there is only a small energy regime $0.2 \lesssim s \lesssim 1$ that is not well covered by the expansions (4.23) and (4.21) at low and high energies respectively.

Interpolation scheme

Our goal is to find an analytical expression approximating the energy-dependent behavior of the outer reflection phase for all energies, and consequently of the quantization function (3.16), in order to provide an accurate form of the quantization rule (3.14), that can be applied to realistic situations.

Starting from the low-energy expansion (4.23) and the high-energy expansion (4.21) some effort has been put into the interpolation between these two regimes. In previous works, several different types of fitting functions have been used to approximate the exact behavior of the outer reflection phase. A first attempt was undertaken by Trost et al. [59]. An even simpler expression was given by Côté et al. in 2004 [72]. The most accurate fit for the reflection phase over the whole energy range so far has been found by introducing an interpolation function of the form

$$\phi_{\text{out}}^{\text{fit}}(E) = A(E) \cdot \phi_{\text{out}}^{\text{low}}(E) + [1 - A(E)] \cdot \phi_{\text{out}}^{\text{high}}(E)\,, \tag{4.25}$$

with an appropriate choice of the function $A(E)$. The expression (4.25) has been able to approximate the exact reflection phase up to an accuracy of at least 10^{-3} over the whole energy range for inverse-power tail potentials $V_\alpha(r)$ with $\alpha = 6$ [13] and $\alpha = 4$ [42].

For the special case of the tail potential $V_3(r)$, finding such an interpolation function is a challenging task; the deviation from the exact values needs to be a lot smaller in this case, in order to account for the increased density of states near the dissociation threshold $E = 0$. The density of states diverges as the energy approaches the dissociation threshold for all inverse-power tails (4.1) with $\alpha > 2$, while the total number of bound states remains finite. However, the density of near-threshold bound states increases the closer the power α in (4.1) comes to the value 2, below which the number of bound states is infinite [73]. We thus try an alternative to the interpolation scheme of Eq. (4.25) in order to obtain an accurate analytical approximation to the exact values of the reflection phase.

One alternative is to consider a rational function of s to approximate the reflection phase

$$\frac{\phi_{\text{out}}^{\text{rat}}(s)}{\pi} = \frac{3 + \sum_{i=1}^{i_{\max}} c_i s^i}{2 + \sum_{i=1}^{i_{\max}} d_i s^i}\,. \tag{4.26}$$

This is particularly useful for inverse-power tail potentials (4.1) with $\alpha = 3$ because $\kappa\beta_3$ is an integer power of the reduced classical turning point s, in contrast to $\alpha = 6$, where $\kappa\beta_6 = s^{3/2}$.

The limiting cases (4.23), (4.21) impose several constraints on the rational function (4.26). First of all, to make sure that the expression reaches $3/2$ as $s \to 0$ [cf. Eq. (4.23)], the zeroth-order terms in the numerator and denominator are given by 3 and 2 respectively. Furthermore, the highest order $i_{\max}$ must be the same in numerator and denominator, since ϕ_{out} approaches a constant value as $s \to \infty$. This constant is $\pi/2$ so we can conclude that $c_{i_{\max}} = d_{i_{\max}}/2$. According to this principle we equip the expression (4.26) with the correct limiting expansions (4.23), (4.21). If we consider the low-energy expansion up to $\mathcal{O}(\kappa) = \mathcal{O}(s^3)$ and the high-energy expansion up to and including $\mathcal{O}(s^{-5})$, we get another eight constraints to the c_i and d_i.

We have experienced that this procedure is very efficient for the case $i_{\max} = 8$, in which

i	c_i	d_i
1	8.198894514574	7.367727350550
2	38.229531850326	32.492317936470
3	85.724646494548	85.380005002970
4	147.081920247084	169.428485967491
5	185.465618264420	242.028021052411
6	141.484936909078	250.115055730896
7	60.927524697423	63.749260455229
8	56.372265754601	112.744531509202

Table 4.4: Coefficients for the rational expression $\phi_{\text{out}}^{\text{rat}}(E)$ [Eq. (4.26)] with $i_{\max} = 8$ for the outer reflection phase ϕ_{out}. The coefficients are obtained via a χ^2-fit to the numerically exact values of the reflection phase as depicted in Figure 4.2.

(4.26) contains 16 parameters.[3] This leaves us with seven free fit parameters, considering the limiting expansions mentioned above. Fitting to a set of numerically exact values for the reflection phase yields the values for the coefficients $(c_1, \ldots, c_8, d_1, \ldots, d_8)$ gathered in Table 4.4.

The analytical expression (4.26) obtained by this fitting procedure fulfills the relations (4.23) and (4.21) with $j_{\max} = 5$ by construction. The absolute value of the deviation from the numerically exact values is shown in Figure 4.3. It can be seen that the rational expression (4.26) approximates the outer reflection phase with an accuracy of $10^{-7}\pi$ in the whole range from threshold ($\kappa = 0$) to the high-κ limit. This is an appreciable improvement over the interpolation scheme of Eq. (4.25).

The expression (4.26) contains more fitted parameters than the expressions (4.25) used for the $-1/r^6$ [13] and for the $-1/r^4$ [42] potentials, but it has a transparent structure and it fulfills the high-accuracy requirements of the $-1/r^3$ case. All these interpolated expressions are superior to the earlier attempts [59, 72], where either the low-κ or the high-κ expression for $\phi_{\text{out}}(E)$ is only correct to leading order.

Explicit expression for the quantization function

The tail contribution to the quantization function is constructed according to (3.16) with the analytical expression (4.26) for the outer reflection phase

$$\begin{aligned} F_{\alpha=3}(s) &= \frac{G_3}{\pi} \cdot s - \frac{\phi_0 - \phi_{\text{out}}^{\text{rat}}(s)}{2\pi} \\ &= \frac{\Gamma(5/6)}{\sqrt{\pi}\Gamma(4/3)} s + \frac{3 + \sum_{i=1}^{i_{\max}} c_i s^i}{4 + 2\sum_{i=1}^{i_{\max}} d_i s^i} - \frac{3}{4} \end{aligned} \tag{4.27}$$

with the corresponding coefficients listed in Table 4.4. This quantization function (4.27) accounts for all effects originating from the potential tail up to an accuracy of 5×10^{-8}

[3] There is no analytical expression reproducing the characteristics of the reflection phase exactly in every energy region and so there is no approximate expression to be preferred for other reasons than accuracy and handling.

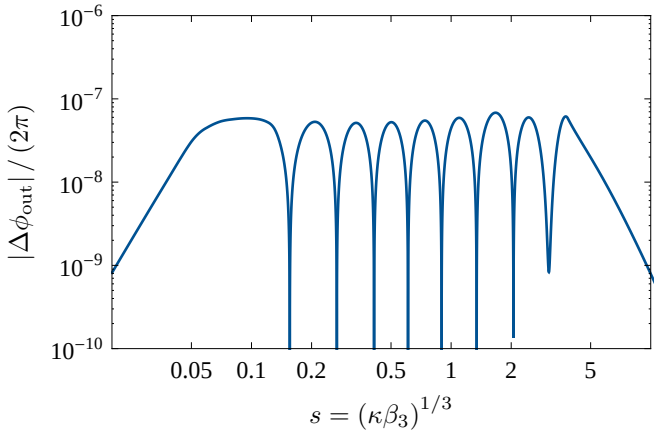

Figure 4.3: The absolute value of the deviation of the rational expression (4.26) for the outer reflection phase from its numerical values is plotted against the reduced classical turning point s on a doubly-logarithmic scale. From $s \gtrsim 4$ on, the high-energy expansion (4.21) of the reflection phase with $j_{\max} = 7$ is closer to the exact value of the reflection phase than the numerical values. Therefore the expansion (4.21) is the reference for the rational function (4.26) in this energy regime.

(see Figure 4.3).

The left panel of Figure 4.4 shows both $F_{\alpha=3}$ and $F_{\alpha=3}^{\mathrm{NDE}}$ as functions of $\kappa\beta_3 = s^3$. Taking either the low-energy expansion (4.23) or the interpolated expression (4.26) for the outer reflection phase, we find that the quantization function for potential tails (4.1) with $\alpha = 3$ behaves as

$$F_{\alpha=3}(E) \overset{\kappa\to 0}{\sim} \kappa\beta_3 = s^3 \overset{\mathrm{def}}{=} F_{\alpha=3}^{\mathrm{low}}(E) \tag{4.28}$$

at low energies (dashed line in Figure 4.4). The contributions of the actions integrals ($\propto s$) in (3.16) cancel exactly. As shown in previous works [13, 41, 42], this gives the universal behavior of quantization functions for potentials with tails vanishing faster than $-1/r^2$ asymptotically [cf. Eq. (3.25)]. This is in strict contrast to the LeRoy-Bernstein function (4.15) which neglects the energy dependence of the outer reflection phase and starts linearly in the reduced outer classical turning point s.

Using the high-energy expansion of the reflection phase for the quantization function (3.16) we obtain

$$F_{\alpha=3}(E) \overset{\kappa\to\infty}{\sim} \frac{G_3}{\pi} \cdot s + \frac{1}{2\pi} \sum_{j=1}^{j_{\max}} \frac{D_j}{s^j} - \frac{1}{2} \overset{\mathrm{def}}{=} F_{\alpha=3}^{\mathrm{high}}(E)\,. \tag{4.29}$$

This expression resembles the near-dissociation expansion for high energies, but it is offset by $-1/2$. This offset is, for given α, equal to $\nu/2 = 1/[2(\alpha-2)]$, according to Eq. (4.22). Thus the discrepancy between the LeRoy-Bernstein function (4.15) and the correct quantization function (4.27) increases as $\alpha \to 2$. The constant offset of $-1/2$ is depicted in the right panel of Figure 4.4, where the quantization functions $F_{\alpha=3}$ and $F_{\alpha=3}^{\mathrm{NDE}}$ are plotted against the reduced outer classical turning point s up to higher energies ($\kappa\beta_3 \approx 64$).

It is still widely believed, that the near-dissociation expansion offers a good description of the highest-lying states in a potential well with a long-range tail [74–77]. The accuracy of both the LeRoy-Bernstein function (4.15) and the correct quantization function (4.27)

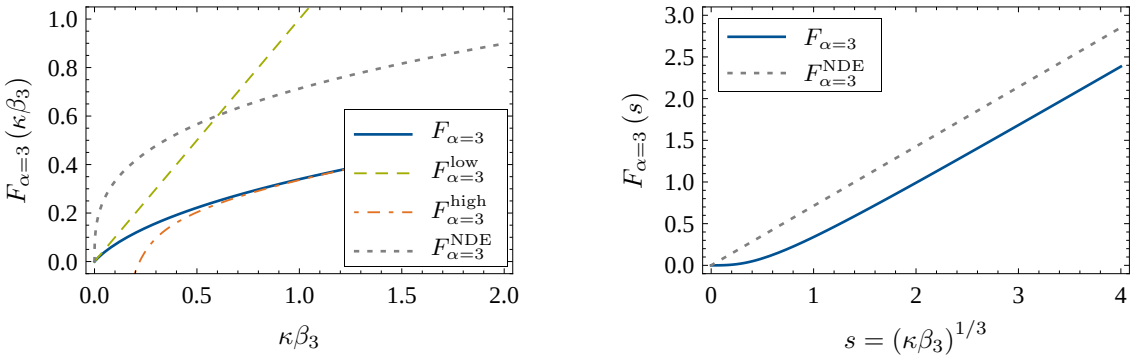

Figure 4.4: The left panel shows the quantization function (4.27) for inverse-cube potential tails, i.e. (4.1) with $\alpha = 3$ plotted against the product of the inverse penetration depth κ and the length parameter β_3. The correct quantization function (4.27) (solid line) starts linearly in $\kappa\beta_3$, whereas the quantization function (4.15) derived from the near-dissociation expansion (LeRoy-Bernstein function) shows a wrong near-threshold behavior (dotted line). The low-κ and high-κ expansions of the correct quantization function (4.28) and (4.29) are also shown (dashed line, dot-dashed line). The right panel shows the quantization function (4.27) for an inverse-cube potential tail, i.e. (4.1) with $\alpha = 3$, as function of the reduced outer classical turning point s (solid line). The corresponding quantization function resulting from the near-dissociation expansion, the LeRoy-Bernstein function (4.15), is also shown (dotted line).

deteriorates with increasing separation from the threshold, due to short-range effects, that vanish in the limit $E \to 0$. But only the quantization function (4.27), accounting for the energy dependence of the outer reflection phase provides the correct description of quantization in the near-threshold regime. The near-dissociation expansion fails there too, because it is based on the conventional semiclassical approximation which breaks down near threshold for potentials with inverse-power tails $V_\alpha(r)$ with $\alpha > 2$.

4.3 Scattering for inverse-power tails

In Chapter 3, a formalism has been developed that allows the treatment of scattering processes given that the considered interaction potential has an attractive tail $V_{\mathrm{tail}}(r)$ that vanishes faster than $1/r^2$ asymptotically and is more singular than $-1/r^2$ at the origin. The singular form of the tail potential provides the possibility of separating the influence of the attractive tail on the scattering properties from effects due to the deviation of the full potential from the singular form of its tail.

Analytical expansions of the scattering tail functions are given for inverse-power tail potentials $V_\alpha(r) = -C_\alpha/r^\alpha$ for general $\alpha > 2$ and explicitly for the integer cases $-1/r^6$ to $-1/r^3$, including the rather rare case of isotropic $-1/r^5$ interactions for reasons of completeness. For each of these cases, the effective-range expansion for the s-wave scattering phase shift is reformulated and the low-energy scattering parameters are expressed in terms of the threshold quantum number n_{th} and further short-range parameters, if needed.

4.3.1 The general case $-C_\alpha/r^\alpha$ with $\alpha > 2$

The preconditions that have been formulated in Chapter 3 for the shape of the tail potential $V_{\mathrm{tail}}(r)$ are perfectly fulfilled by the inverse-power potential $V_\alpha(r)$ with $\alpha > 2$. In the following, we study the peculiarities of the scattering parameters that arise for certain shapes of the inverse-power tail, i.e., for different powers α. The tail functions for scattering are given and their implications for the scattering phase shift are studied.

Tail functions

In order to evaluate the formula (3.30) or (3.48) for the scattering phase shift and to obtain explicit expressions for the low-energy scattering parameters, we need to provide the tail functions ξ_{t}, $A_{\mathrm{s}}/A_{\mathrm{c}}$, ϕ_{s}, and ϕ_{c} in an explicit form. We thus present — for the general case of an inverse-powers tail (4.1) — limiting analytical expressions of these, both at high collision energies and at low collision energies.

Evaluation of the phase ξ_{t}

To find an explicit expression for the phase ξ_{t} (3.9) that enters the expression (3.8) for the regular solution in the short-range region of the potential tail, as well as the formulae (3.30) and (3.48) for the scattering phase shift, we need to evaluate the integrals occurring in Eq. (3.9) for each tail potential $V_\alpha(r)$. With the local classical momentum given by Eq. (4.5) and the distance r_E given by Eq. (4.9), we find

$$\begin{aligned}
&\frac{1}{\hbar}\int_{r_E}^{\infty} p_0^{\mathrm{tail}}(r)dr + \frac{1}{\hbar}\int_0^{r_E}\left[p_0^{\mathrm{tail}}(r) - p_E^{\mathrm{tail}}(r)\right]dr \\
&\qquad = \int_{(k\beta_\alpha)^{-2/\alpha}}^{\infty} \rho^{-\alpha/2}d\rho + \int_0^{(k\beta_\alpha)^{-2/\alpha}}\left[\rho^{-\alpha/2} - \sqrt{(k\beta_\alpha)^2+\rho^{-\alpha}}\right]d\rho \\
&\qquad = \left[\int_1^{\infty} x^{-\alpha/2}dx - \int_0^1 x^{-\alpha/2}\left(\sqrt{1+x^\alpha}-1\right)dx\right](k\beta_\alpha)^{1-2/\alpha}\,, \qquad (4.30)
\end{aligned}$$

α	3	4	5	6	7	$\alpha \to \infty$
η_α	0.908797	0.847213	0.802904	0.769516	0.743463	$\sqrt{2} - \operatorname{arsinh}(1)$
τ_α	0.769516	0.847213	0.885769	0.908797	0.924102	1

Table 4.5: Values of the coefficients η_α and τ_α for inverse-potential tail $V_\alpha(r)$ (4.1) for different values of the power α.

where we substituted $\rho \to (k\beta_\alpha)^{-2/\alpha}x$ to obtain the second identity. The first integral in the third line of Eq. (4.30) can be evaluated in a straighforward fashion. The second integral can also be evaluated analytically by expanding the square root in the integrand in orders of x^α and integrating each addend separately. Together with $\phi_{\text{out}}(0) = (1/2+\nu)\pi$ [cf. Eqs. (3.23) and (4.12)], Eq. (3.9) yields

$$\xi_{\text{t}} = -\left(\frac{3}{4} + \frac{\nu}{2}\right)\pi + \frac{2}{\alpha-2}\eta_\alpha (k\beta_\alpha)^{1-2/\alpha}\,, \tag{4.31}$$

which is valid for all inverse-power tails $V_\alpha(r)$ with $\alpha > 2$. The coefficient η_α can be expressed in terms of a hypergeometric function

$$\eta_\alpha = \sqrt{2} - \frac{\alpha}{\alpha+2}\,{}_2F_1\left(\frac{1}{2}, \frac{1}{2}+\frac{1}{\alpha}; \frac{3}{2}+\frac{1}{\alpha}; -1\right)\,. \tag{4.32}$$

Explicit values of the coefficient η_α are listed in Table 4.5.

High-energy behavior

At energies much larger than the characteristic energy scale $\mathcal{E}_\alpha$ of the inverse-power potential tail (4.1), it has been shown that the ratio $A_{\text{s}}/A_{\text{c}}$ of the amplitudes approaches unity (3.85) [cf. also Eq. (3.47)]. The high-energy expansion of the corresponding phases ϕ_{s} and ϕ_{c} has been derived in Section 3.3.3. For inverse-power tails (4.1), the integrals occurring in Eq. (3.86) can be evaluated analytically

$$\begin{aligned}
\phi_{\text{s/c}} \overset{E\gg\mathcal{E}_\alpha}{\sim} & - kr_E + \frac{1}{\hbar}\int_{r_E}^{\infty}\left[p_E^{\text{tail}}(r) - \hbar k\right] \\
&= -(k\beta_\alpha)^{1-2/\alpha} + \int_{(k\beta_\alpha)^{-2/\alpha}}^{\infty}\left[\sqrt{(k\beta_\alpha)^2 + \rho^{-\alpha}} - (k\beta_\alpha)\right]d\rho \\
&= -\left[1 - \int_0^1 \frac{1}{y^2}\left(\sqrt{1+y^\alpha} - 1\right)dy\right](k\beta_\alpha)^{1-2/\alpha} \\
&= -\tau_\alpha (k\beta_\alpha)^{1-2/\alpha}
\end{aligned} \tag{4.33}$$

for any $\alpha > 2$. In the third line of Eq. (4.33), we substituted $\rho \to (k\beta_\alpha)^{-2/\alpha}/y$. The high-energy behavior of the phases ϕ_{s} and ϕ_{c} shows the typical semiclassical dependence on the energy, i.e., it is proportional to $(k\beta_\alpha)^{1-2/\alpha}$ (cf. Ref. [54]). The coefficient τ_α can be evaluated again by expanding the integrand in orders of y^α. This procedure yields

$$\tau_\alpha = \sqrt{2} - \frac{\alpha}{2(\alpha-1)}\;{}_2F_1\left(\frac{1}{2}, 1-\frac{1}{\alpha}; 2-\frac{1}{\alpha}; -1\right)\,. \tag{4.34}$$

From this behavior and the complete knowledge of the phase ξ_t (4.31), we can deduce an expression for the high-energy behavior of the scattering phase shift as given in Eq. (3.87)

$$\delta_0 \overset{E\gg\mathcal{E}_\alpha}{\sim} \left(n_\mathrm{th} + \frac{3}{4} + \frac{\nu}{2}\right)\pi - \left(\tau_\alpha + \frac{2}{\alpha-2}\eta_\alpha\right)(k\beta_\alpha)^{1-2/\alpha}\,. \tag{4.35}$$

The coefficient for the typical semiclassical energy dependence of the phase shift can further be simplified, which gives

$$\tau_\alpha + \frac{2}{\alpha-2}\eta_\alpha = \frac{\alpha}{\alpha-2}\frac{\Gamma\left(\frac{1}{2}+\frac{1}{\alpha}\right)\Gamma\left(1-\frac{1}{\alpha}\right)}{\sqrt{\pi}}\,. \tag{4.36}$$

A corresponding expression was already found by Flambaum *et al.* [44] from semiclassical considerations.

Low-energy behavior of the tail functions

For the ratio of the amplitudes $A_\mathrm{s}/A_\mathrm{c}$, we can use its lowest-order expansion as given in Eq. (3.57) with the amplitudes from Eq. (4.12) to obtain

$$\frac{A_\mathrm{s}}{A_\mathrm{c}} \overset{k\to0}{\sim} \nu^{2\nu}\frac{\Gamma(1-\nu)}{\Gamma(1+\nu)}(k\beta_\alpha) = \sqrt{\bar{a}_\alpha^2 + b_\alpha^2}\,k \tag{4.37}$$

for any $\alpha > 3$, where the threshold length b_α and the mean scattering length $\bar{a}_\alpha$ are defined for inverse-power tails in Eqs. (4.13) and (4.14) respectively. In order to obtain an expression for the ratio of the amplitudes, we can alternatively use the identity (3.47) with the result for $\mathcal{K}^\alpha_\mathrm{refl}$ taken from the context of quantum reflection

$$\begin{aligned}\frac{A_\mathrm{s}}{A_\mathrm{c}} = |\mathcal{K}^\alpha_\mathrm{refl}| \overset{k\to0}{\sim} \nu^{2\nu}&\frac{\Gamma(1-\nu)}{\Gamma(1+\nu)}(k\beta_\alpha)\\ &- \nu^{1+6\nu}\frac{\Gamma(-\nu)\Gamma(-2\nu)^2\Gamma(-3\nu)}{\Gamma(\nu)^2\Gamma(-4\nu)}\cos(2\pi\nu)(k\beta_\alpha)^3\\ &+ \frac{\sqrt{\pi}}{4}\frac{\Gamma\left(-\frac{1}{2}-\frac{1}{2\nu}\right)}{\Gamma\left(1+\frac{1}{2\nu}\right)}\cos(\pi\nu)(k\beta_\alpha)^{\alpha-2} + \mathcal{O}(k^5)\,,\end{aligned} \tag{4.38}$$

which gives an expansion up to higher orders of the wave number k. This expression is derived from the expansion of $\mathcal{K}^\alpha_\mathrm{refl}$ that was found by Arnecke *et al.* and is presented in Ref. [78]. It was obtained by expanding the corresponding Jost solutions [29] within the framework established in Ref. [79]. The expansion (4.38) is valid for any $\alpha > 5$, while its first-order term remains valid down to $\alpha > 3$.

The low-energy expansions of the phases ϕ_s and ϕ_c are given in Eqs. (3.78) and (3.80) in general terms. For an explicit expression of these low-energy expansions for inverse-power tails (4.1), the effective areas h_s and h_c that contain integrals involving the zero-energy

solutions (4.10) need to be evaluated. For the effective area h_s (3.79), this yields

$$\begin{aligned} h_\mathrm{s} &= \frac{\hbar}{D_1^2}\int_0^\infty \left[r^2 - w_1(r)^2\right] dr \\ &= \frac{\pi\nu^{1-2\nu}}{\Gamma(1-\nu)^2}\frac{1}{\beta_\alpha}\int_0^\infty \left\{r^2 - \Gamma(1-\nu)^2\nu^{2\nu}\beta_\alpha r\left[J_{-\nu}(z)\right]^2\right\} dr \\ &= \pi\nu^{4\nu+2}\beta_\alpha^2\int_0^\infty \left(\frac{z}{2}\right)^{-4\nu-1}\left\{\left[\frac{(z/2)^{-\nu}}{\Gamma(1-\nu)}\right]^2 - \left[J_{-\nu}(z)\right]^2\right\} dz\,, \end{aligned} \tag{4.39}$$

where the integration variable has been changed to z as defined in Eq. (4.11). It is found that h_s scales with β_α^2. The integrand is, in the limit of small z, of the order of $z^{1-6\nu}$, so that the integral diverges unless $\nu < 1/3$, i.e., $\alpha > 5$. This condition for the existence of an effective-range term was already formulated in Section 3.3.3. Whenever the integral converges to a finite value, we find that

$$\frac{h_\mathrm{s}}{\beta_\alpha^2} = \frac{1}{3\nu}\nu^{4\nu}\frac{\Gamma(4\nu)}{\Gamma(2\nu)^2}\Gamma(1-3\nu)\Gamma(1-\nu)\sin(\pi\nu)\,. \tag{4.40}$$

A similar integration technique can be applied to evaluate the integral in Eq. (3.81). We can, however, also make use of the expression for ρ_eff, that has been derived in previous works [13, 43]

$$\frac{\rho_\mathrm{eff}}{\beta_\alpha} = \frac{\pi(2\nu)^{2\nu}\nu\Gamma\left(\frac{1}{2}+2\nu\right)}{\sin(\pi\nu)\Gamma\left(\frac{1}{2}+\nu\right)\Gamma\left(1+3\nu\right)}\,. \tag{4.41}$$

A finite value for the sub-threshold effective range ρ_eff exists for all inverse-power potentials $V_\alpha(r)$ with $\alpha > 3$. With the threshold length b_α given in Eq. (4.13) and simplifying the expression that is obtained, we find

$$\frac{h_\mathrm{c}}{\beta_\alpha^2} = \frac{1}{3\nu}\nu^{4\nu}\frac{\Gamma(4\nu)}{\Gamma(2\nu)^2}\Gamma(1-3\nu)\Gamma(1-\nu)\sin(3\pi\nu)\,. \tag{4.42}$$

The values for the effective ares h_s and h_c are gathered in Table 4.6 for various values of the power α. Together with the zero-energy phases (4.12) and the explicit form of the integrals obtained in Eq. (4.30), the phases for both the sine (3.78) and the cosine solution (3.80) can be given in terms of α

$$\phi_{\mathrm{s/c}} \overset{k\to 0}{\sim} \left(-\frac{1}{2} \pm \frac{\nu-1/2}{2}\right)\pi + 2\nu\eta_\alpha(k\beta_\alpha)^{1-2/\alpha} - h_{\mathrm{s/c}}^{(\alpha)}k^2 + \mathcal{O}(k^3)\,. \tag{4.43}$$

The validity of this expansion is limited by the existence of the effective areas $h_{\mathrm{s/c}}$. The expansion (4.43) for ϕ_c is therefore valid for all $\alpha > 3$, while the corresponding expansion for ϕ_s is only valid for $\alpha > 5$.

From these results a further term proportional to the energy can also be obtained for the transmission phase ϕ_T, which was defined for the quantum reflection process (3.34) and enters the formula (3.48) for the scattering phase shift. By making use of the relations

$$\phi_T = \phi_\mathrm{s} + \arg(1+R) = \phi_\mathrm{c} + \arg(1-R) \tag{4.44}$$

α	3	4	5	6	7	$\alpha \to \infty$
$h_\mathrm{c}/\beta_\alpha^2$	—	$\pi/3$	0.478821	1/3	0.267278	$\pi/(\alpha-2)$
$h_\mathrm{s}/\beta_\alpha^2$	—	—	—	1/3	0.165187	$\pi/(3(\alpha-2))$

Table 4.6: Values of the effective areas h_c and h_s for inverse-potential tails $V_\alpha(r)$ (4.1) for different values of the power α.

obtained from Eqs. (3.44) and (3.46) together with the relations

$$\arg(1+R) = \arg\left(\frac{2i\mathcal{K}_\mathrm{refl}}{i\mathcal{K}_\mathrm{refl}-1}\right), \quad \arg(1-R) = \arg\left(\frac{2}{1-i\mathcal{K}_\mathrm{refl}}\right) \tag{4.45}$$

as obtained via Eq. (3.33), we can derive the expansions

$$\begin{aligned}\arg(1-R) \overset{k\to 0}{\sim} &- \bar{a}_\alpha k + \frac{\nu^{4\nu}}{2}\frac{\Gamma(1-\nu)^2}{\Gamma(1+\nu)^2}\sin(2\pi\nu)(k\beta_\alpha)^2 \\ &+ \nu^{6\nu}\left[\frac{1}{3}\frac{\Gamma(1-\nu)^3}{\Gamma(1+\nu)^3} - \frac{\Gamma(-2\nu)^2\Gamma(-3\nu)}{\Gamma(\nu)^3\Gamma(-4\nu)\sin(\pi\nu)}\right]\cos(3\pi\nu)(k\beta_\alpha)^3 \\ &+ \mathcal{O}(k^4)\end{aligned} \tag{4.46}$$

and

$$\begin{aligned}\arg(1+R) \overset{k\to 0}{\sim} &\frac{\pi}{2} - \nu\pi - \bar{a}_\alpha k + \frac{\nu^{4\nu}}{2}\frac{\Gamma(1-\nu)^2}{\Gamma(1+\nu)^2}\sin(2\pi\nu)(k\beta_\alpha)^2 \\ &+ \frac{\pi}{2}\nu^{4\nu}\frac{\Gamma(-3\nu)\Gamma(-2\nu)}{\Gamma(-4\nu)\Gamma(\nu)\Gamma(2\nu)}(k\beta_\alpha)^2 \\ &+ \nu^{6\nu}\left[\frac{1}{3}\frac{\Gamma(1-\nu)^3}{\Gamma(1+\nu)^3} - \frac{\Gamma(-2\nu)^2\Gamma(-3\nu)}{\Gamma(\nu)^3\Gamma(-4\nu)\sin(\pi\nu)}\right]\cos(3\pi\nu)(k\beta_\alpha)^3 \\ &- 2^{\alpha-2}\Gamma(1-\alpha)\sin(\alpha\pi/2)\nu^{-2\nu}\frac{\Gamma(\nu)}{\Gamma(-\nu)}(k\beta_\alpha)^{\alpha-3} + \mathcal{O}(k^4)\end{aligned} \tag{4.47}$$

from the expressions for the complex amplitude $\mathcal{K}_\mathrm{refl}^\alpha$ of quantum reflection taken from Ref. [78]. These are valid for all $\alpha > 5$. This procedure immediately yields

$$\begin{aligned}\phi_T \overset{k\to 0}{\sim} &- \frac{\phi_0}{2} + \frac{2}{\alpha-2}\eta_\alpha(k\beta_\alpha)^{2/\alpha} - \bar{a}_\alpha k + \frac{\nu^{4\nu}}{2}\frac{\Gamma(1-\nu)^2}{\Gamma(1+\nu)^2}\sin(2\pi\nu)(k\beta_\alpha)^2 \\ &- \frac{\pi}{3}\nu^{4\nu}\frac{\Gamma(-\nu)\Gamma(4\nu)}{\Gamma(2\nu)^2\Gamma(3\nu)}(k\beta_\alpha)^2 + \mathcal{O}(k^3)\,,\end{aligned} \tag{4.48}$$

which goes beyond the result presented in Appendix B. Our present formulation, which focuses on elastic scattering, does not benefit from this result very much, since the expansions for ϕ_s and ϕ_c were already known up to the order of the energy from the effective-range formalism shown above (Section 3.3.3). It is, however, worth mentioning, since the transmission phase ϕ_T itself is not accessible via a comparable effective-range expansion.

Effective-range expansion

Inserting the expansions (4.43) obtained for ϕ_s and ϕ_c and the expansion (4.38) for the ratio of amplitudes $A_\mathrm{s}/A_\mathrm{c}$ into the formula (3.30) yields the low-energy expansion of the scattering phase shift which is equivalent to the well-known effective-range expansion as easily obtained from scattering theory for short-range potentials (see, e.g., [27–29])

$$\tan\delta_0 \overset{k\to 0}{\sim} -ak - \frac{1}{2}\left(a^2 r_\mathrm{eff}\right)k^3 + \mathcal{O}(k^5)\,. \tag{4.49}$$

It is conventionally given as an expansion of the cotangent of the scattering phase shift

$$k\cot\delta_0 \overset{k\to 0}{\sim} -\frac{1}{a} + \frac{1}{2}r_\mathrm{eff}k^2 + \mathcal{O}(k^4)\,, \tag{4.50}$$

which is more common in the existing literature although the former expansion (4.49) is, in general, considered to be of simpler form and more elegant from the mathematical point of view (see e.g. [34]).

The first-order coefficient is, of course, the scattering length a [30], that exists for any potential with an inverse-power tail $V_\alpha(r)$ [Eq. (4.1)] with $\alpha > 3$. It can, as also shown before [cf. Eq. (3.60)], explicitly be given in terms of the length scales $\bar{a}_\alpha$ and b_α that are given in Eqs. (4.14) and (4.13)

$$a = \bar{a}_\alpha + \frac{b_\alpha}{\tan(n_\mathrm{th}\pi)} = \nu^{2\nu}\frac{\Gamma(1-\nu)}{\Gamma(1+\nu)}\left[\cos(\nu\pi) + \frac{\sin(\nu\pi)}{\tan(\Delta_\mathrm{th}\pi)}\right]. \tag{4.51}$$

From this relation, we can easily see that the scattering length a diverges, when the value of the remainder is

$$\Delta_\mathrm{th}^\infty = 0\,, \tag{4.52}$$

i.e., whenever there is a bound state exactly at the dissociation threshold ($E = 0$)[4] [cf. Eq. (3.25) with (3.14)], and vanishes to zero whenever

$$\Delta_\mathrm{th}^{(0)} = 1 - \nu = \frac{\alpha - 3}{\alpha - 2}. \tag{4.53}$$

We can therefore see, that the distribution of the scattering length in units of the characteristic length scale β_α of the inverse-power tail $V_\alpha(r)$ clearly depends on the power α.

Expanding the expression (3.30) for the scattering phase shift with the ratio of the amplitudes (4.38) and the phases (4.43) up to $\mathcal{O}(k^3)$, the effective range r_eff in expression (4.49) can be given as a function of the scattering length a

$$\frac{r_\mathrm{eff}}{\beta_\alpha} = F_\alpha - G_\alpha\frac{\beta_\alpha}{a} + H_\alpha\left(\frac{\beta_\alpha}{a}\right)^2, \tag{4.54}$$

[4] In the context of ultracold quantum gases, this case is referred to as *unitarity*. The effective interaction strength is independent of the peculiarities of the interaction potential in the limit of low energies.

with the coefficients (according to the nomenclature in Ref. [44])

$$\begin{aligned} F_\alpha &= \frac{2}{3}\frac{\pi}{\sin(\pi\nu)}\nu^{2\nu}\frac{\Gamma(\nu)\Gamma(4\nu)}{\Gamma(2\nu)^2\Gamma(3\nu)} - 2\nu^{1-2\nu}\Gamma(\nu)^2\,\lambda_{\mathrm{sr}}^2 \\ G_\alpha &= \frac{4}{3}\frac{\pi}{\sin(\pi\nu)}\nu^{4\nu}\frac{\Gamma(1-2\nu)\Gamma(4\nu)}{\nu\Gamma(\nu)\Gamma(2\nu)\Gamma(3\nu)} + 4\pi\cot(\pi\nu)\,\lambda_{\mathrm{sr}}^2 \\ H_\alpha &= \frac{2}{3}\frac{\pi}{\sin(\pi\nu)}\nu^{6\nu}\frac{\Gamma(1-3\nu)\Gamma(1-\nu)\Gamma(4\nu)}{\nu^2\Gamma(\nu)^2\Gamma(2\nu)^2} - 2\nu^{2\nu-1}\Gamma(1-\nu)^2\,\lambda_{\mathrm{sr}}^2\,. \end{aligned} \tag{4.55}$$

When expanding the expression (3.30) up to the order of k^3, the lowest order term γ_{sr} of the short-range correction $\gamma(E)$ [cf. Eqs. (3.8) and (3.10)] enters the effective-range term via $\lambda_{\mathrm{sr}}^2 = \gamma_{\mathrm{sr}}\mathcal{E}_\alpha$. Writing $\gamma_{\mathrm{sr}} = 2\mu\beta_{\mathrm{sr}}^2/\hbar^2$ introduces the (generally complex) short-range length scale β_{sr}. Its absolute value is considered to be comparable to the length scale on which the full potential $V(r)$ deviates from the singular form of its inverse-power tail (4.1). The last term of each coefficient F_α, G_α, H_α contains the square of the ratio $\lambda_{\mathrm{sr}} = \beta_{\mathrm{sr}}/\beta_\alpha$.

In the limit that the modulus of the short-range length scale β_{sr} is very small compared to the length scale β_α of the tail potential $V_\alpha(r)$, the ratio λ_{sr} tends to zero and these terms will be negligible. The result obtained for the effective-range r_{eff} is — in this limit ($\lambda_{\mathrm{sr}} \to 0$) — equivalent to the expression that was previously derived by Flambaum *et al.* [44].

Whenever a bound state exists exactly at the dissociation threshold ($E = 0$) the threshold quantum number's remainder Δ_{th} is exactly zero [cf. Eq. 4.52] and the scattering length diverges according to Eq. (4.51). Therefore the effective-range expansion (4.49) is rather useless, since it can not provide for a proper description of the scattering phase shift. However, the formulation (3.30) remains valid and yields

$$\tan\delta_0^\infty \overset{k\to0}{\sim} \frac{2}{r_{\mathrm{eff}}^\infty k} + \mathcal{O}(k)\,, \tag{4.56}$$

with the effective range for this constellation given by $r_{\mathrm{eff}}^\infty = r_{\mathrm{eff}}(a\to\infty) = F_\alpha\beta_\alpha$, according to Eq. (4.54). This leads to a divergence of the scattering cross section in the limit of zero collision energy

$$\sigma_0^\infty \overset{k\to0}{\sim} \frac{4\pi}{k^2} - \pi\,(r_{\mathrm{eff}}^\infty)^2 + \mathcal{O}(k^2). \tag{4.57}$$

This relation can also be obtained by making use of the effective-range expansion (4.50), and is extensively studied in Ref. [80]. In the presence of a bound state at $E = 0$, the present framework thus provides information about the scattering phase shift that is found to behave as

$$\delta_0^\infty \overset{k\to0}{\sim} \frac{\pi}{2} - \frac{r_{\mathrm{eff}}^\infty}{2}k + \mathcal{O}(k^2)\,. \tag{4.58}$$

We find that the s-wave phase shift starts at $\pi/2$, which is well-known from scattering theory for actual short-range potentials (cf. Refs. [28, 29]) and actually modifies Levinson's Theorem. The first-order term of the expansion in the wave number k is just given by the value of the effective range r_{eff}^∞ (4.54) in the limit $a \to \infty$.

The considerations of this section have been quite general so far ($\alpha > 3$ or $\alpha > 5$ for the discussion of the scattering length or the effective range, respectively). It is a known fact, that the scattering phase shift is an odd function of the wave number k only for truly short-range potentials that fall off faster than any power of the distance asymptotically. In the case of scattering by potentials with inverse-power tails $V_\alpha(r)$ with $\alpha > 2$, that is discussed here, the expansion of the phase shift in odd orders of the wavenumber k breaks down at $\mathcal{O}(k^m)$, with $m = \alpha - 2$ (see Ref. [36]). For the cases $\alpha \leq 5$, the effective-range expansion (4.49) up to $\mathcal{O}(k^3)$, will be modified by "anomalous", i.e., logarithmic or even-order terms. These can also be identified in the low-energy expansions of the tail functions.

In the following sections, we focus on the cases of tail potentials $V_\alpha(r)$ with integer values of α in the range $3 \leq \alpha \leq 6$. These are the most prominent cases for typical interactions between two compound particles, such as for atom-atom, atom-ion or atom-molecule interactions (cf. Appendix A) and will exhibit "anomalous" terms in the effective-range expansion. Some of the results presented are partially published in Ref. [60].

4.3.2 Induced dipolar interactions ($\alpha = 6$)

We study the elastic scattering from a potential that has an attractive tail proportional to $-1/r^6$. This case is very prominent, since it occurs, e.g., in the interaction of two ground-state atoms (see Appendix A). Its understanding is crucial in the field of ultracold atomic physics especially for the creation and manipulation of atomic Bose-Einstein condensates [24, 26, 81].

In this section, we present — for the reference potential $V_6(r) = -C_6/r^6$ — results for the tail functions for scattering, that are valid from the extreme quantum regime ($E \ll \mathcal{E}_6$) very close to the dissociation threshold to the semiclassical regime at moderately high energies ($E \gg \mathcal{E}_6$). Their low-energy behavior is studied in order to obtain an improved effective-range expansion of the scattering phase shift, which is valid in the limit of low collision energies.

Tail functions

In the following, the tail functions $A_\mathrm{s}/A_\mathrm{c}$, ϕ_s, ϕ_c and, for reasons of completeness, also the phase ξ_t are explicitly given for the case of a $-1/r^6$ reference potential. Corresponding analytical expansions are presented, where possible. The phase ξ_t can explicitly be given just by evaluating Eqs. (4.31) and (4.32) with $\alpha = 6$

$$\xi_\mathrm{t}^{\alpha=6} = -\frac{7}{8}\pi + \frac{1}{2}\eta_6 (k\beta_6)^{2/3}\,, \tag{4.59}$$

with the coefficient η_6 as given by Eq. (4.32) and in Table 4.5. The characteristic length scale of the potential tail is $\beta_6 = (2\mu C_6/\hbar^2)^{1/4}$. Expression (4.59) is valid for all collision energies.

The tail functions $A_\mathrm{s}/A_\mathrm{c}$, ϕ_s and ϕ_c can not be obtained analytically for all energies but are obtained from numerical calculations. The left-hand side of Figure 4.5 shows the ratio of the amplitudes $A_\mathrm{s}/A_\mathrm{c}$ (solid line) as obtained from numerically solving the radial Schrödinger equation (4.3) with the tail potential $V_6(r) = -C_6/r^6$ alone. The dotted line visualizes the low-energy behavior to first order, according to Eq. (4.37), while the

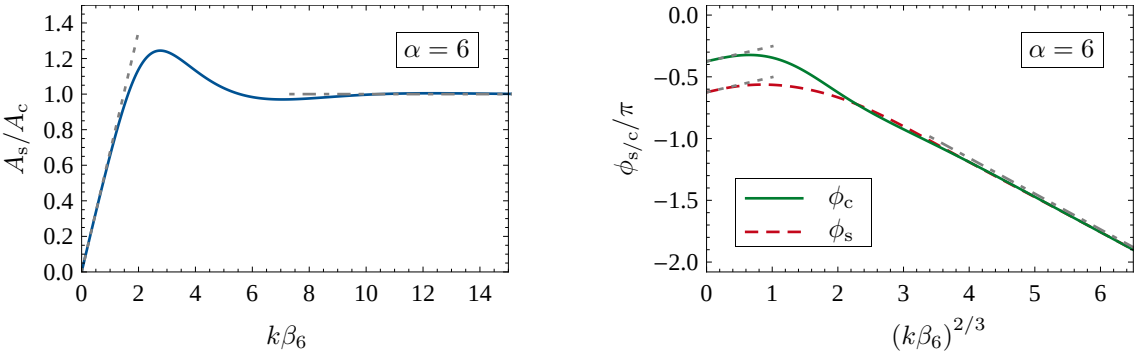

Figure 4.5: The graph on the left-hand side shows the universal behavior of the ratio of amplitudes A_s/A_c for an inverse-power tail (4.1) with $\alpha = 6$ as a solid line, plotted against the product $(k\beta_6)$ together with its low-energy behavior (dotted line) to first order in k [see Eq. (4.37)] and its high-energy behavior (dot-dashed line) given in Eq. (3.85). The graph on the right-hand side shows the universal behavior of the tail-dependent phases ϕ_s and ϕ_c for the same potential tail, but plotted against $(k\beta_6)^{2/3}$. The dotted lines and the dot-dashed line show the low-energy behavior to lowest order (4.43) and the high-energy behavior (4.33) respectively.

dot-dashed line represents the high energy limit, i.e., unity (3.85). We find that the exact numerical values follow the low-energy expansion almost up to $k\beta_6 \lesssim 1$. For higher energies ($k\beta_6 \gtrsim 8$), the ratio of amplitudes oscillates around its high-energy limit (dot-dashed line) with decreasing amplitude, so that A_s/A_c deviates from unity on scales smaller than 10^{-3} for energies corresponding to $k\beta_6 \gtrsim 15$, beyond the range plotted in Figure 4.5.

The corresponding low-energy behavior up to higher orders in the wave number k can, as demonstrated before, be given by the expansion of the absolute value of the amplitude $\mathcal{K}_{\text{refl}}^{\alpha=6}$ of quantum reflection from the attractive singular potential $V_6(r) = -C_6/r^6$

$$\frac{A_s}{A_c} = |\mathcal{K}_{\text{refl}}^{\alpha=6}| \overset{k\to 0}{\sim} \frac{1}{2}\frac{\Gamma(3/4)}{\Gamma(5/4)}(k\beta_6) - \frac{\pi}{15\sqrt{2}}(k\beta_6)^4 + \mathcal{O}(k^5)\,, \tag{4.60}$$

which is, of course, a special case of the expansion (4.38) presented in the previous section. The expansion (4.60) contains all terms up to and including $\mathcal{O}(k^4)$. This is verified in Figure 4.6(a), where the difference between the exact values of A_s/A_c and their low energy-behavior (4.60) divided by $(k\beta_6)^4$ is plotted against $k\beta_6$. From the observation that this quantity tends to zero in the limit of $k\beta_6 \to 0$, we can conclude that all terms up to and including the term $\mathcal{O}(k^4)$ entering the asymptotic expansion (4.60) are correct (see Appendix C) and the subsequent term is at least $\mathcal{O}(k^5)$.

The corresponding phases are shown in the right panel of Figure 4.5. The behavior of both the phase ϕ_c (solid line) and the phase ϕ_s (dashed line) is plotted against $(k\beta_6)^{2/3}$, which is the leading energy dependence at both low and high collision energies (dotted lines and dot-dashed line respectively). The common high energy-asymptote of both phases is just given by $-\tau_6(k\beta_6^{2/3})$ according to Eq. (4.33).

In the limit of low energies, the phase ϕ_c can, according to Eq. (4.43), be given by

$$\phi_c(k) \overset{k\to 0}{\sim} -\frac{3\pi}{8} + \frac{1}{2}\eta_6(k\beta_6)^{2/3} - \frac{1}{3}(k\beta_6)^2 + \mathcal{O}(k^4)\,. \tag{4.61}$$

From the graph shown in Figure 4.6(b) we can deduce that this expansion is not only correct up to $\mathcal{O}(k^2)$, as suggested by Eq. (4.43), but correctly gives all terms up to and

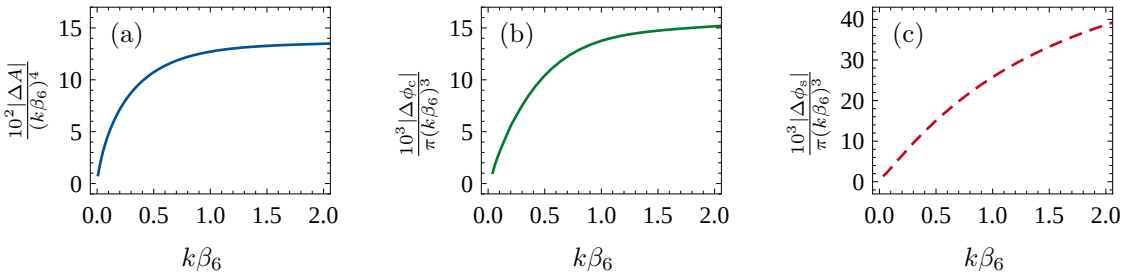

Figure 4.6: For a $-1/r^6$ tail, the difference between numerically obtained results for (a) the ratio of amplitudes A_s/A_c, (b) the phase ϕ_c and (c) the phase ϕ_s and the corresponding low-energy expansions [cf. Eqs. (4.60), (4.61) and (4.64)] are divided by the highest-order contribution to the analytical expansion and plotted against $(k\beta_6)$. The circumstance that all plotted quantities tend to zero in the limit $k\beta_6 \to 0$ shows the correctness of all analytically obtained terms in the corresponding expansion.

including $\mathcal{O}(k^3)$. The subsequent term in Eq. (4.61) that is not known analytically is thus $\mathcal{O}(k^4)$. Obviously, this is not a general feature of the phase ϕ_c but holds for the particular case of the reference potential $V_6(r)$ [Eq. (4.1)], for which there is no term $\mathcal{O}(k^3)$ in the asymptotic expansion (4.61) of the phase ϕ_c.

Since we have determined the low-energy behavior of the phase ϕ_c including all terms up to $\mathcal{O}(k^3)$, we can also determine the phase ϕ_s up to the same order. Since both phases are in general connected via

$$\phi_s = \phi_c + \arg\left(\frac{1-R}{1+R}\right) = \phi_c + \frac{\pi}{2} - \arg\left(\mathcal{K}_{\text{refl}}\right) , \tag{4.62}$$

according to Eq. (4.44), their difference can be evaluated by making use of the expressions (4.46) and (4.47) for $\alpha = 6$. This yields

$$\phi_s - \phi_c = \arg\left(\frac{1-R}{1+R}\right) \overset{k\to 0}{\sim} -\frac{\pi}{4} - \frac{\sqrt{2}\pi}{15}\frac{\Gamma(1/4)}{\Gamma(-1/4)}(k\beta_6)^3 + \mathcal{O}(k^4) . \tag{4.63}$$

With this expression and the expansion (4.61) of the phase ϕ_c given above, we can give an extended expansion for ϕ_s beyond the order of the energy

$$\phi_s(k) \overset{k\to 0}{\sim} -\frac{5\pi}{8} + \frac{1}{2}\eta_6(k\beta_6)^{2/3} - \frac{1}{3}(k\beta_6)^2 - \frac{\sqrt{2}\pi}{15}\frac{\Gamma(1/4)}{\Gamma(-1/4)}(k\beta_6)^3 + \mathcal{O}(k^4) . \tag{4.64}$$

The expansion of ϕ_s has a nonvanishing term $\mathcal{O}(k^3)$. The correctness of this term is again tested (see Appendix C) in Figure 4.6(c), where the ratio plotted tends to zero in the limit of small $k\beta_6$. This gives rise to the assumption that both ϕ_c and ϕ_s have been obtained correctly up to and including $\mathcal{O}(k^3)$ via the expansions (4.61) and (4.64).

Scattering phase shift

From the ratio of amplitudes A_s/A_c and the phases ϕ_s and ϕ_c that have been obtained for the case of an inverse-power tail $V_6(r)$ and are presented in Figure 4.5, we can deduce the s-wave scattering phase shift δ_0 by making use of Eq. (3.30) for any given value of the

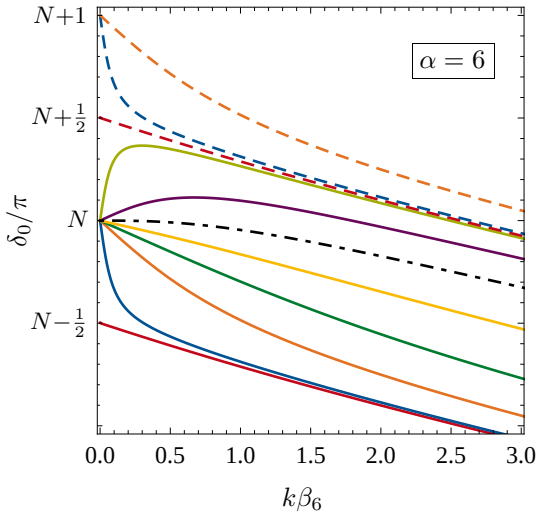

Figure 4.7: This figure shows the s-wave phase shift δ_0 as obtained via Eq. (3.30) for an inverse-power tail (4.1) with $\alpha = 6$, using ξ_t from Eq. (4.59) and the other tail functions as visualized in Figure 4.5. The solid lines show the phase shift for different values of the threshold quantum number's remainder $\Delta_{th} = \{0, 0.01, 0.1, 0.25, 0.5, 0.9, 0.99\}$. The dot-dashed line gives the phase shift for the special value of $\Delta_{th} = 3/4$, for which the scattering length from Eq. (4.66) is exactly zero. The three upper dashed lines again correspond to the phase shift for values of the remainder $\Delta_{th} = \{0, 0.01, 0.1\}$, but for the case that the number of bound states is increased by one.

threshold quantum number's remainder Δ_{th}. The results are shown in Figure 4.7, where possible further short-range corrections that could enter Eq. (3.30) in terms of $\gamma(E)$ [cf. Eq. (3.8)] are neglected.[5]

The results of Figure 4.7 illustrate how, on the one hand, a smooth variation of the remainder Δ_{th} in the range [0,1) causes smooth shifts of the s-wave phase shift at higher energies according to Eq. (4.35) where the value of Δ_{th} is manifest as a constant offset, while on the other hand, at very low collision energies, the phase shift δ_0 depends very sensitively on the remainder Δ_{th}. Small variations can lead to a significant change of the scattering properties. This violent behavior is reflected by the corresponding low-energy expansion of the s-wave phase shift

$$\begin{aligned}\tan\delta_0 \overset{k\to 0}{\sim} &-\frac{1}{2\sqrt{2}}\frac{\Gamma(3/4)}{\Gamma(5/4)}\left[1+\cot(\Delta_{th}\pi)\right](k\beta_6)\\ &-\frac{1}{6\sqrt{2}}\frac{\Gamma(3/4)}{\Gamma(5/4)}\frac{1}{\sin^2(\Delta_{th}\pi)}\left[1-3\pi\lambda_{sr}^2\right](k\beta_6)^3\\ &+\frac{\pi}{15}(k\beta_6)^4+\mathcal{O}(k^5)\,.\end{aligned} \tag{4.65}$$

[5]For typical interatomic potentials, these corrections scale with the depth of the interaction potential that is usually orders of magnitude larger than $\mathcal{E}_\alpha$. Therefore, deviations from the phase shift obtained for the case $\gamma(E) \equiv 0$ are most likely to be too small to be visualized on the scales of Figure 4.7.

This expansion has been obtained by inserting the low-energy expansions of both the phases ϕ_c and ϕ_s [Eqs. (4.61) and (4.64)] and the ratio of the amplitudes A_s/A_c [Eq. (4.60)] into the formula (3.30) that then yields the s-wave phase shift in the presence of a $-1/r^6$ potential tail. Further short-range corrections are incorporated according to Eq. (3.10). They first enter the expansion (4.65) in the term $\mathcal{O}(k^3)$ and are parametrized via $\lambda_{sr}^2 = \gamma_{sr}\mathcal{E}_6$. The quantity $\lambda_{sr} = \beta_{sr}/\beta_6$ can be considered a measure for the length scales on which the full potential deviates from the singular form $-C_6/r^6$ of its tail (see Section 4.3.1).

While the expansion (4.65) is already of appealing simplicity, one might consider it more appropriate to express this result in terms of the well-known scattering parameters, i.e., the scattering length a and the effective range r_{eff} as introduced in Eq. (4.50). In order to do so, the present expansion (4.65) is compared to the effective-range expansion (4.49). The leading-order term in k gives the scattering length that, in the present case of a $-1/r^6$ tail, is

$$a = \frac{1}{2\sqrt{2}} \frac{\Gamma(3/4)}{\Gamma(5/4)} \left[1 + \cot(\Delta_{th}\pi)\right] \beta_6 \,, \tag{4.66}$$

which is obviously a special case of Eq. (4.51). From this expression we can immediately see that the scattering length is positive in 3/4 of all possible values of the remainder Δ_{th} for interaction potentials with $-1/r^6$ tails (see also Ref. [40]). The effective range can now be given in terms of the scattering length

$$\begin{aligned} r_{eff} &= \frac{\sqrt{2}}{3} \left[\frac{\Gamma(1/4)}{\Gamma(3/4)} - 2\sqrt{2}\frac{\beta_6}{a} + 4\frac{\Gamma(3/4)}{\Gamma(1/4)}\frac{\beta_6^2}{a^2} \right] \left[1 - 3\pi\, \lambda_{sr}^2\right] \beta_6 \\ &= \frac{1}{3} \left[\frac{\Gamma(1/4)}{\Gamma(3/4)} \right]^2 \left[1 - 2\frac{\bar{a}}{a} + 2\left(\frac{\bar{a}}{a}\right)^2 \right] \left[1 - 3\pi\lambda_{sr}^2\right] \bar{a} \end{aligned} \tag{4.67}$$

In the *tail-dominated* limit $|\beta_{sr}| \ll \beta_6$ or $\lambda_{sr} \to 0$ this exact result tends to the universal result that was obtained in Ref. [44].

A further result that is worth discussing is the occurrence of a term proportional to k^4 in the extended effective-range expansion (4.65) which is an "anomalous" term of even order in the wavenumber k; it is a consequence of the nonanalyticity of the scattering matrix. The existence of this term was originally predicted by Hinckelmann and Spruch [82] using the Gell-Mann–Goldberger decomposition procedure together with the distorted wave Born approximation (see, e.g., Refs. [4, 29]). This result is confirmed by the present studies.

When there is a bound state exactly at the dissociation threshold, the scattering length is divergent ($a \to \infty$) and we find the low-energy expansion by inserting the corresponding remainder $\Delta_{th}^{\infty} = 0$ into Eq. (3.30) with the low-energy expressions (4.60), (4.61), and (4.64) for the tail functions for $-1/r^6$ potentials. This yields

$$\delta_0^{\infty} \overset{k\to 0}{\sim} \frac{\pi}{2} - \frac{\sqrt{2}}{6}\frac{\Gamma(1/4)}{\Gamma(3/4)} \left[1 - 3\pi\lambda_{sr}^2\right] (k\beta_6) + \mathcal{O}(k^2) \,, \tag{4.68}$$

which is just the particular case of Eq. (4.58) with $\alpha = 6$, since the effective-range expansion (4.50) holds for potentials with $-1/r^6$ tails (at least up to $\mathcal{O}(k^2)$). It is depicted in Figure 4.7 by the lowest solid line as well as by the lowest dashed line (red lines), that have been obtained via Eq. (3.30) for integer values of the threshold quantum number n_{th}.

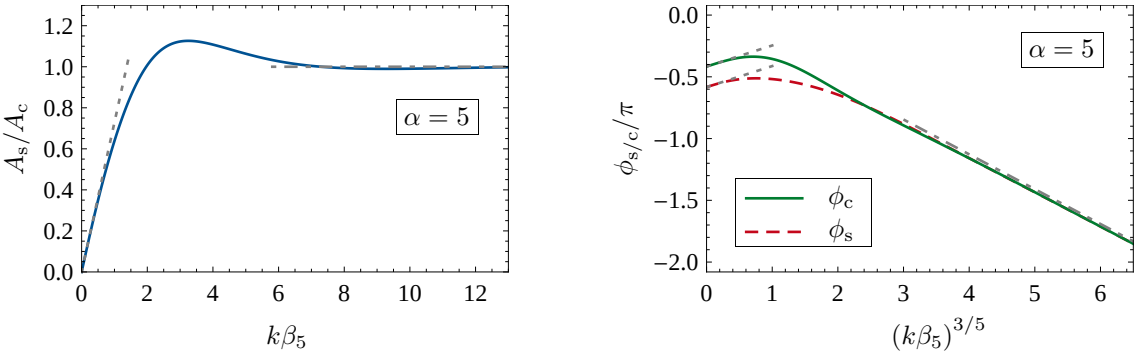

Figure 4.8: The graph on the left-hand side shows the universal behavior of the ratio of amplitudes A_s/A_c for an inverse-power tail (4.1) with $\alpha = 5$ as a solid line, plotted against the product $(k\beta_5)$ together with its low-energy behavior (dotted line) to first order in k [see Eq. (4.37)] and its high-energy behavior (dot-dashed line) given in Eq. (3.85). The graph on the right-hand side shows the universal behavior of the tail-dependent phases ϕ_s and ϕ_c for the same potential tail, but plotted against $(k\beta_5)^{3/5}$. The dotted lines and the dot-dashed line show the low-energy behavior (4.43) and high-energy behavior (4.33) respectively.

4.3.3 Quadrupole-quadrupole interactions ($\alpha = 5$)

An asymptotic $1/r^5$ behavior occurs in leading order of the interaction potential between two quadrupoles. This interaction potential will most certainly not be spherically symmetric. However, in the interaction between two atoms in certain internal states, a spherically symmetric form of the $1/r^5$ interaction can occur (cf. Appendix A). The strength coefficient C_5 of this interaction can, in principle, be either positive or negative. In the present work we only consider the case of an asymptotically attractive interaction potential.

From the theoretical point of view the case of an attractive inverse-power potential $V_5(r)$ [Eq. (4.1)] is of particular interest, since it constitutes the highest integer power α for which a finite effective-range term r_{eff} as defined via Eq. (4.49) does not exist. From the work Levy and Keller [36] it is known that an "anomalous" logarithmic term of the order $\mathcal{O}(k^3)$ occurs in the expansion of $\tan\delta_0$, which replaces the finite effective-range term that exists of all powers $\alpha > 5$.

Tail functions

In the case of an attractive $-1/r^5$ interaction at large distances, we can again evaluate the phase ξ_t analytically by solving the corresponding WKB integrals (3.9), that contain the explicit form of the potential tail $V_5(r)$, or by just evaluating Eqs. (4.31) and (4.32) with $\alpha = 5$. This yields

$$\xi_t^{\alpha=5} = -\frac{11}{12}\pi + \frac{2}{3}\eta_5(k\beta_5)^{3/5}\,, \tag{4.69}$$

where the characteristic length of the tail potential $V_5(r)$ is given by $\beta_5 = (2\mu C_5/\hbar^2)^{1/3}$. A numerical value for η_5 is found in Table 4.5.

Figure 4.8 shows the ratio of the amplitudes A_s/A_c (left panel) and the phases ϕ_c (right panel, solid line) and ϕ_s (right panel, dashed line) as obtained by numerically solving the Schrödinger equation (4.3) with the reference potential $V_5(r)$. The ratio A_s/A_c of the

amplitudes is plotted against the dimensionless product $k\beta_5$ in the range from zero to $k\beta_5 \approx 13$. While in its high-energy limit ($k\beta_5 \gtrsim 12$) it approaches unity (dot-dashed line), its low-energy behavior is given by

$$\begin{aligned}\frac{A_\mathrm{s}}{A_\mathrm{c}} = |\mathcal{K}_\mathrm{refl}^{\alpha=5}| \overset{k\to 0}{\sim} & \frac{\Gamma(2/3)}{3^{2/3}\Gamma(4/3)}(k\beta_5) - \frac{1}{6}(k\beta_5)^3 \ln(k\beta_5) \\ & + \frac{1}{72}\left(13 - 20\gamma_\mathrm{E} - 6\sqrt{3}\pi - 12\ln 2 + \ln 9\right)(k\beta_5)^3 \\ & + \frac{2\pi^2}{3^{7/6}\Gamma(1/3)^2}(k\beta_5)^4 + \mathcal{O}(k^5)\,, \end{aligned} \tag{4.70}$$

where the real number $\gamma_\mathrm{E} \simeq 0.577216$ is Euler's constant[6]. This expansion is, very similar to the case of $\alpha > 5$, obtained by making use of the relation (3.47) and the corresponding expression for $\mathcal{K}_\mathrm{refl}^{\alpha=5}$ from Ref. [78]. The expansion (4.70) starts linearly in the wavenumber k, as expected from Eq. (4.37). However, in strict contrast to the cases with $\alpha > 5$ (cf. Secs. 4.3.1 and 4.3.2), it exhibits an "anomalous" logarithmic term that is $\mathcal{O}(k^3)$, in accordance with Ref. [36]. Figure 4.9(a) shows the absolute value of the difference between the expansion (4.70) and the numerical values as shown in the left panel of Figure 4.8 divided by the $(k\beta_5)^4$, which is the highest order obtained in Eq. (4.70). We can see that this ratio tends to zero in the limit $k\beta_5 \to 0$ which ensures that all terms of the expansion (4.70), including the "anomalous" logarithmic contribution, have been obtained correctly (cf. Appendix C).

The right panel of Figure 4.8 shows the exact values of the phases ϕ_c (solid line) and ϕ_s (dashed line) plotted against $(k\beta_5)^{3/5}$, which is the leading-order energy dependence both at low and at high energies. Both phases approach their common high-energy behavior $-\tau_5(k\beta_5)^{3/5}$ as given by Eq. (4.33) with a numerical value for the coefficient τ_5 given in Table 4.5. The dotted lines illustrate the leading-order term at low energies both for ϕ_s and ϕ_c, according to Eq. (4.43) with η_5 as given by Eq. 4.32 or explicitly in Table 4.5. An expansion for the phase ϕ_c is obtained from the corresponding effective-range expansion (Section 3.3.3). The effective area $h_\mathrm{c}^{\alpha=5}$ takes a finite value (cf. Table 4.6) and we can explicitly state

$$\phi_\mathrm{c} \overset{k\to 0}{\sim} -\frac{5}{12}\pi + \frac{2}{3}\eta_5(k\beta_5)^{3/5} - \frac{\sqrt{\pi}}{3}\left(\frac{2}{3}\right)^{1/3}\Gamma(7/6)(k\beta_5)^2 + \mathcal{O}(k^4)\,. \tag{4.71}$$

From the ratio plotted in Figure 4.9(b) we find that this expansion is not only correct up to $\mathcal{O}(k^2)$, but that furthermore no term $\mathcal{O}(k^3)$ exists. The subsequent term of the expansion (4.73) is $\mathcal{O}(k^4)$.

For the phase ϕ_s the effective-range expansion of Section 3.3.3 does not yield a finite coefficient h_s for the term of order k^2. We can, however, obtain an expansion of ϕ_s beyond its leading order term via the same formalism that has been applied to the case of $\alpha = 6$, i.e., by making use of the relation (4.62) that connects the phases ϕ_s and ϕ_c via the amplitude R for quantum reflection by the singular attractive tail potential $V_5(r) = -C_5/r^5$. In the limit of low energies, the difference of the two phases can thus be

[6]Euler's constant ist also referred to as *Euler-Mascheroni constant* and can be defined via the relation $\gamma_\mathrm{E} = \lim_{n\to\infty}\left[\sum_{k=1}^{n}\frac{1}{k} - \ln(n)\right]$.

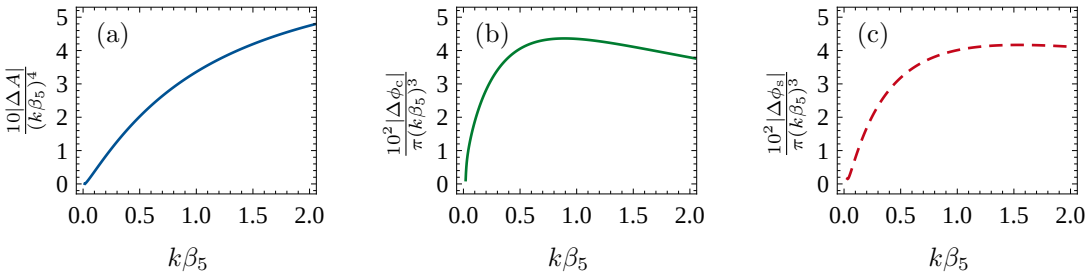

Figure 4.9: For a $-1/r^5$ tail, the difference between numerically obtained results for (a) the ratio of amplitudes $A_\mathrm{s}/A_\mathrm{c}$, (b) the phase ϕ_c and (c) the phase ϕ_s and the corresponding low-energy expansions [cf. Eqs. (4.70), (4.71) and (4.73)] are divided by the highest-order contribution to the analytical expansion and plotted against $(k\beta_5)$. The circumstance that all plotted quantities tend to zero in the limit $k\beta_5 \to 0$ shows the correctness of all analytically obtained terms in the corresponding expansion.

given by

$$\phi_\mathrm{s} - \phi_\mathrm{c} = \arg\left(\frac{1-R}{1+R}\right) \overset{k\to 0}{\sim} -\frac{\pi}{6} + \frac{3^{5/3}}{4\pi}\Gamma(4/3)^2 \ln(k\beta_5)(k\beta_5)^2 + \frac{3^{2/3}}{4\pi}\Gamma(4/3)^2\left(5\gamma_\mathrm{E} - \frac{13}{4} + \ln\frac{8}{\sqrt{3}} + \frac{\pi}{2\sqrt{3}}\right)(k\beta_5)^2 + \mathcal{O}(k^4) \tag{4.72}$$

according to Ref. [78]. The present expansion (4.72) exhibits an "anomalous" logarithmic term of the order k^2. Adding Eq. (4.72) to the expansion of ϕ_c yields

$$\phi_\mathrm{s} \overset{k\to 0}{\sim} -\frac{7}{12}\pi + \frac{2}{3}\eta_5(k\beta_5)^{3/5} - \frac{\sqrt{\pi}}{3}\left(\frac{2}{3}\right)^{1/3}\Gamma(7/6)(k\beta_5)^2 + \frac{3^{2/3}}{4\pi}\Gamma(4/3)^2\left(5\gamma_\mathrm{E} - \frac{13}{4} + \ln\frac{8}{\sqrt{3}} + \frac{\pi}{2\sqrt{3}} + 3\ln(k\beta_5)\right)(k\beta_5)^2 + \mathcal{O}(k^4)\,. \tag{4.73}$$

Since the expansion (4.72) of the difference of the phases does not include a term of the order $\mathcal{O}(k^3)$, the expansion (4.73) of ϕ_s is also correct up to $\mathcal{O}(k^3)$. This is confirmed by Figure 4.9(c), where the ratio that is plotted tends to zero in the limit $k\beta_5 \to 0$. Even though the effective-range formalism of Section 4.3.1 fails for ϕ_s in the reference potential $V_5(r)$, Eq. (4.73) gives an expansion for the phase ϕ_s up to and including the order of k^3.

Scattering phase shift

The scattering phase shift that occurs in scattering by a potential that has an attractive tail proportional to $-1/r^5$ is plotted in Figure 4.10 as obtained from Eq. (3.30) for different values of the threshold quantum number's remainder Δ_th. The solid lines correspond to the specific values $\Delta_\mathrm{th} = \{0, 0.01, 0.1, 1/3, 0.5, 0.9, 0.99\}$, while the dashed lines correspond to the lowest three solid lines but for a total number of bound states increased by one — in accordance with Levinson's theorem. The dot-dashed line marks the phase shift for the special case of $\Delta_\mathrm{th} = 2/3$, for which the scattering length is exactly zero [cf. Eq. (4.53)]. The lowest solid and the lowest dashed line both mark the case of a bound state exactly

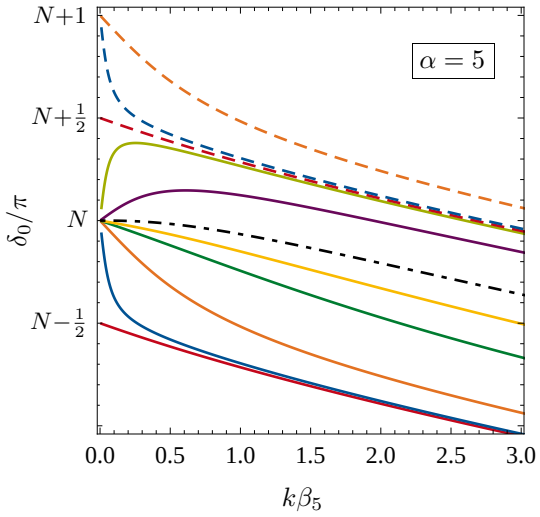

Figure 4.10: This figure shows the s-wave phase shift δ_0 as obtained via Eq. (3.30) for an inverse-power tail (4.1) with $\alpha = 5$, using ξ_t from Eq. (4.69) and the other tail functions as visualized in Figure 4.8. The solid lines show the phase shift for different values of the threshold quantum number's remainder $\Delta_{\text{th}} = \{0, 0.01, 0.1, 1/3, 0.5, 0.9, 0.99\}$. The dot-dashed line gives the phase shift for the special value of $\Delta_{\text{th}} = 2/3$, for which the scattering length from Eq. (4.75) is exactly zero. The three upper dashed lines again correspond to the phase shift for values of the remainder $\Delta_{\text{th}} = \{0, 0.01, 0.1\}$, but for the case that the number of bound states is increased by one.

at the dissociation threshold, in which the scattering length diverges and the scattering phase shift starts not at an integer multiple of π but at $\pi/2$.

For the general case of a nonzero value of the remainder Δ_{th}, the formula (3.30) with the tail functions as obtained with the tail potential $V_5(r)$ in Section 4.3.3 yields the low-energy limit of the scattering phase shift

$$\begin{aligned}\tan\delta_0 \overset{k\to 0}{\sim} & -ak + \frac{1}{3}(k\beta_5)^3 \ln(k\beta_5) \\ & - \frac{1}{2}\left[\tilde{F}_5 - \tilde{G}_5\frac{\beta_5}{a} + \tilde{H}_5\left(\frac{\beta_5}{a}\right)^2\right]\left(\frac{a}{\beta_5}\right)^2 (k\beta_5)^3 \\ & - \frac{\pi}{3}\frac{a}{\beta_5}(k\beta_5)^4 + \mathcal{O}(k^5)\,, \end{aligned} \tag{4.74}$$

where we have already carried out the replacement of the remainder Δ_{th} with the scattering length, that is, according to Eq. (4.51) for the case of scattering by a potential with a $-1/r^5$ tail, given by

$$a = \frac{1}{3^{2/3}}\frac{\Gamma(2/3)}{\Gamma(4/3)}\left[\frac{1}{2} + \frac{\sqrt{3}}{2}\cot(\Delta_{\text{th}}\pi)\right]\beta_5\,. \tag{4.75}$$

The expansion (4.74) of the scattering phase shift for an inverse-power potential tail (4.1) with $\alpha = 5$ exhibits an "anomalous" term that replaces the effective-range r_{eff} which takes a finite value for all inverse-power potential tails with $\alpha > 5$, but does not exist in this particular case.

The coefficients $\tilde{F}_5$, $\tilde{G}_5$, and $\tilde{H}_5$ that enter the expansion (4.74) of the scattering phase shift are given by

$$\begin{aligned}
\tilde{F}_5 &= \frac{9}{3^{1/6}\pi}\Gamma(4/3)^4 - \frac{2}{3^{1/3}}\Gamma(1/3)^2\,\lambda_{\rm sr}^2\,,\\
\tilde{G}_5 &= \frac{4}{3^{1/3}}\Gamma(4/3)^2 - \frac{4\pi}{\sqrt{3}}\,\lambda_{\rm sr}^2\,,\\
\tilde{H}_5 &= \frac{1}{18}\left[13 - 20\gamma_{\rm E} + 2\sqrt{3}\,\pi - 12\ln 2 + 2\ln 3\right] - 2\times 3^{1/3}\Gamma(2/3)^2\,\lambda_{\rm sr}^2\,,
\end{aligned}$$

They explicitly depend on the lowest-order short-range correction via $\lambda_{\rm sr}^2 = \gamma_{\rm sr}\mathcal{E}_5$, that accounts for short-range effects beyond what is accounted for by the threshold quantum number's remainder $\Delta_{\rm th}$. The fourth order term in the expansion (4.74) is universal in the sense that it depends only on the scattering length but on no further short-range parameters.

In the limit $\lambda_{\rm sr} = \beta_{\rm sr}/\beta_5 \to 0$, that might be referred to as the universal or tail-dominated limit, the expansion (4.74) of the scattering phase shift can be written as

$$\begin{aligned}
\tan\delta_0 \overset{k\to 0}{\sim} &-ak + \frac{1}{3}(k\beta_5)^3\ln(k\beta_5)\\
&- \frac{1}{2}\left[1.51684 - 2.21158\frac{\beta_5}{a} + 0.345441\left(\frac{\beta_5}{a}\right)^2\right]\left(\frac{a}{\beta_5}\right)^2(k\beta_5)^3\\
&- \frac{\pi}{3}\frac{a}{\beta_5}(k\beta_5)^4 + \mathcal{O}(k^5)\,,
\end{aligned} \tag{4.76}$$

and is — up to $\mathcal{O}(k^4)$ — determined by the scattering length alone. The coefficients $\tilde{F}_5$, $\tilde{G}_5$, and $\tilde{H}_5$ have been replaced by their exact numerical values for $\lambda_{\rm sr} = 0$. This limit might be sufficient to reproduce the low-energy scattering parameters in many realistic situations.

We now look at the particular case of in which a bound state exists at the dissociation threshold ($\Delta_{\rm th} = \Delta_{\rm th}^{\infty} = 0$) and the scattering length goes to infinity ($a \to \infty$). Since this special case is not a limiting case of the expansion (4.74), the formula (3.30) for the scattering phase shift needs to be expanded separately for $\Delta_{\rm th}^{\infty} = 0$, which yields

$$\delta_0^{\infty} \overset{k\to 0}{\sim} \frac{\pi}{2} - \frac{\tilde{F}_5}{2}(k\beta_5) + \mathcal{O}(k^2)\,. \tag{4.77}$$

This linear behavior can be found in Figure 4.10 where the phase shift is plotted against the product $(k\beta_5)$ for integer values of the threshold quantum number $n_{\rm th}$ (lowest solid line and lowest dashed line).

Notice, that an expansion for the scattering phase shift equivalent to Eq. (4.74) or Eq. (4.77) for potentials with inverse-power tails with $\alpha = 5$ has never been given in the existing literature so far. This might be due to the inflated interest in the cases of $-1/r^6$ and $-1/r^4$ tail potentials that are the most common long-range interactions in atomic physics. However, there is a growing interest in the isotropic, attractive $-1/r^5$ interaction, since it is a candidate for exotic photoassociation experiments [83]. Whether or not such speculations are justified, a comprehensive study of low-energy scattering phenomena certainly requires the understanding of $-1/r^5$ interactions at low energies as well.

4.3.4 Polarization interactions ($\alpha = 4$)

The case of an interaction via a potential with an inverse-power tail (4.1) with $\alpha = 4$ is rather common, since it occurs whenever a charged particle interacts with a neutral compound particle that has a nonvanishing dipole polarizability. The strength coefficient C_4 can simply be expressed in terms of the static dipole polarizability α_d of the neutral partner $C_4 = \alpha_\mathrm{d}/2$. When the neutral partner is in its ground state, the interaction is attractive at large distances. In atom-electron interactions this attraction can lead to bound states, i.e., negatively charged ions. Atom-ion collisions are, however, more suitable for the present treatment, since the high masses (compared to the electron mass) of the particles involved promote the existence of an inner WKB region in the full interaction potential.

The scattering phase shift for potentials with a tail that is $-C_4/r^4$, has been a subject of numerous studies by several authors (see Ref. [84] and references therein). Considering the low-energy scattering properties for this class of potentials, the groundbreaking works of O'Malley, Spruch, and Rosenberg [34, 35] need to be mentioned. These works are based on the exact solution for $-1/r^4$ potentials that can be given in terms of Matthieu functions [48]. O'Malley *et al.* were the first to present a *modified* effective-range expansion for the scattering phase shift δ_0 that contains the "anomalous" terms that are characteristic for the polarization interaction [Eq. (4.1) with $\alpha = 4$].

Tail functions

As in the previous cases, we can evaluate the phase ξ_t as given in Eq. (4.31) with $\alpha = 4$ in a straightforward fashion. This yields

$$\xi_\mathrm{t}^{\alpha=4} = -\pi + \eta_4 (k\beta_4)^{1/2}\,, \tag{4.78}$$

with the coefficient η_4 given in Eq. (4.32) and in Table 4.5 in numerical form. The characteristic length associated with the tail potential $V_4(r)$ is $\beta_4 = \sqrt{2\mu C_4}/\hbar$; for the case of a polarization induced interaction [cf. Eq. (A.6)] it is given by $\beta_4 = \sqrt{\alpha_\mathrm{d}\mu}/\hbar$. While expression (4.78) is valid over the whole range of energies considered, the further tail functions, i.e., $A_\mathrm{s}/A_\mathrm{c}$, ϕ_s, and ϕ_c can not be given analytically for all energies, but are obtained by solving the radial Schrödinger equation (4.3) with the reference potential $V_4(r)$ and the corresponding boundary conditions (3.27).

Exact values of the tail functions are depicted in Figure 4.11. The left panel shows the ratio $A_\mathrm{s}/A_\mathrm{c}$ plotted against the dimensionless product $k\beta_4$, together with its lowest-order term at low-energies (dotted line) as given by Eq. (4.37) and its high-energy limit, i.e., unity (dot-dashed line) [cf. Eq. (3.85)].

From the expression for the amplitude $\mathcal{K}_\mathrm{refl}^{\alpha=4}$ in Ref. [78], an expansion of the ratio of amplitudes $A_\mathrm{s}/A_\mathrm{c}$ in orders of the wave number k can be obtained [cf. Eq. (3.47)]. This yields

$$\begin{aligned}\frac{A_\mathrm{s}}{A_\mathrm{c}} = |\mathcal{K}_\mathrm{refl}^{\alpha=4}| \overset{k\to 0}{\sim} (k\beta_4) + \frac{4}{3}(k\beta_4)^3 \ln(k\beta_4) \\ + \left[\frac{8}{3}(\gamma_\mathrm{E} + \ln 2) + \frac{1}{2}\left(\frac{\pi}{3}\right)^2 - \frac{28}{9}\right](k\beta_4)^3 + \mathcal{O}(k^4)\,.\end{aligned} \tag{4.79}$$

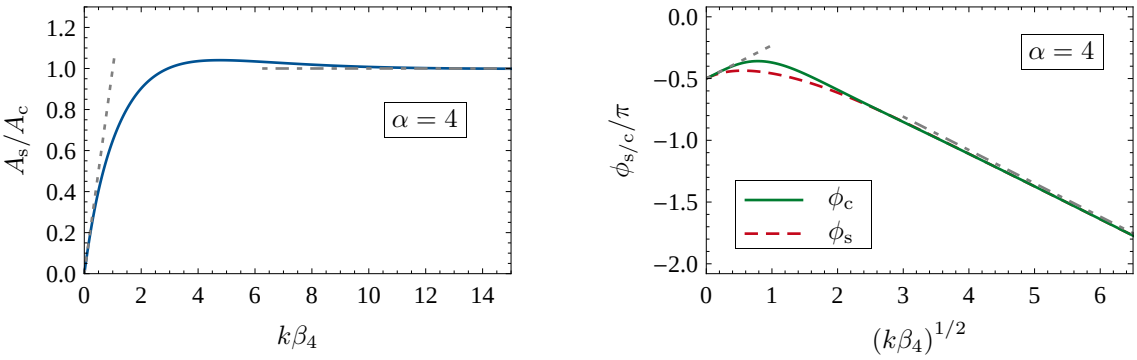

Figure 4.11: The graph on the left-hand side shows the universal behavior of the ratio of amplitudes A_s/A_c for an inverse-power tail (4.1) with $\alpha = 4$ as a solid line, plotted against the product $(k\beta_4)$ together with its low-energy behavior (dotted line) to first order in k [see Eq. (4.37)] and its high-energy behavior (dot-dashed line) given by Eq. (3.85). The graph on the right-hand side shows the universal behavior of the tail-dependent phases ϕ_s and ϕ_c for the same potential tail, but plotted against $(k\beta_4)^{1/2}$. The dotted lines and the dot-dashed line show the low-energy behavior (4.43) and high-energy behavior (4.33) respectively.

In this expansion an "anomalous" term can be identified, i.e., the logarithmic term which is $\mathcal{O}(k^3)$. Its implications on the scattering properties will be explained in the following section. Figure 4.12(a) shows the difference of the expansion (4.79) to the exact values for A_s/A_c divided by $(k\beta_4)^2$. In the limit $k\beta_4 \to 0$, this quantity tends to zero, which shows that all terms of the expansion (4.79) have been obtained correctly (see Appendix C).

The right panel of Figure 4.11 shows the phases ϕ_s and ϕ_c plotted against $(k\beta_4)^{1/2}$, which is the leading-order energy dependence both at low and at high energies. This is visualized by the dotted line that represents the common low-energy behavior according to Eq. (4.43) and the dot-dashed line that represents the common high-energy behavior of both phases according to Eq. (4.33).

The effective-range expansion for the phases from Section 3.3.3 yields an expansion of the phase ϕ_c that is correct up to and including the term $\mathcal{O}(k^2)$,

$$\phi_c \overset{k\to 0}{\sim} -\frac{\pi}{2} + \eta_4 (k\beta_4)^{1/2} - \frac{\pi}{3}(k\beta_4)^2 + \mathcal{O}(k^3)\,. \tag{4.80}$$

The comparison to the exact values that have been obtained numerically is visualized in Figure 4.12(b) and confirms the correctness of the expansion (4.80) up to the order of k^2. The effective-range expansion that yields Eq. (4.80) for ϕ_c breaks down for the phase ϕ_s for any inverse power-potential $V_\alpha(r)$ with $\alpha \leq 5$ in general, and thus also for the case of $\alpha = 4$ in particular. As already performed for the case of an inverse-power potential with $\alpha = 5$, we can find an expansion for the difference of the two phases ϕ_s and ϕ_c that are connected via Eq. (4.62). Their difference can be expressed via the amplitude R for quantum reflection by the singular inverse-power potential $V_4(r)$ as described by Eq. (3.31). With the identity (3.33) and the expansion of $\mathcal{K}_{\text{refl}}^{\alpha=4}$ taken from Ref. [78] this expansion yields

$$\phi_s - \phi_c = \arg\left(\frac{1-R}{1+R}\right) \overset{k\to 0}{\sim} -\frac{\pi}{3}(k\beta_4) + \frac{2\pi}{3}(k\beta_4)^2 + \mathcal{O}(k^3)\,. \tag{4.81}$$

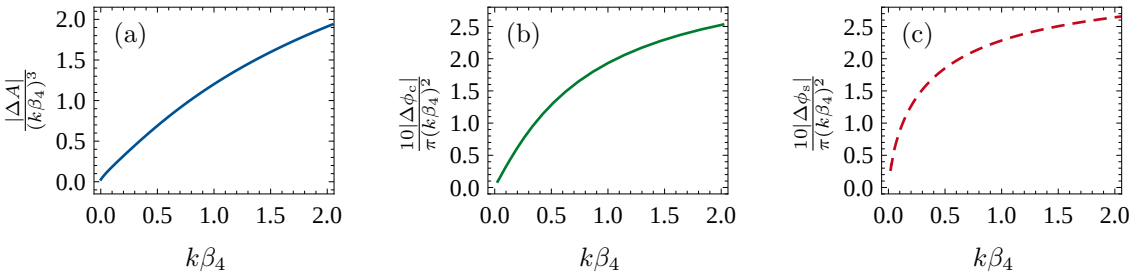

Figure 4.12: For a $-1/r^4$ tail, the difference between numerically obtained results for (a) the ratio of amplitudes A_s/A_c, (b) the phase ϕ_c and (c) the phase ϕ_s and the corresponding low-energy expansions [cf. Eqs. (4.79), (4.80) and (4.82)] are divided by the highest-order contribution to the analytical expansion and plotted against $(k\beta_4)$. The circumstance that all plotted quantities tend to zero in the limit $k\beta_4 \to 0$ shows the correctness of all analytically obtained terms in the corresponding expansion.

As already seen from Figure 4.11, the threshold values at $E = 0$ are the same for both phases. The expansion (4.81) thus contains no zeroth-order term in the wave number k. From the expansion (4.80) of the phase ϕ_c and the expansion of the difference $\phi_s - \phi_c$ [Eq. (4.81)] the expansion

$$\phi_s \overset{k\to 0}{\sim} -\frac{\pi}{2} + \eta_4(k\beta_4)^{1/2} - \frac{\pi}{3}(k\beta_4) + \frac{\pi}{3}(k\beta_4)^2 + \mathcal{O}(k^3)\,. \tag{4.82}$$

can be deduced for the phase ϕ_s. Its zeroth-order term is given by $-\pi/2$ which is, as mentioned before, the same as for the phase ϕ_c. The anomalous term of first order in k that enters the expansion (4.81) of the phase difference is carried over to the phase ϕ_s. From Figure 4.12(c) we may conclude that all terms up to $\mathcal{O}(k^2)$ entering Eq. (4.82) are given correctly; the quantity plotted tends to zero in the limit of low energies $(k\beta_4 \to 0)$ as required for the correct expansions (see Appendix C).

Scattering phase shift

The phase shift obtained in scattering by a potential with a $-1/r^4$ tail is depicted in Figure 4.13. Its shows the energy-dependent s-wave phase shift for different values of the threshold quantum number's remainder Δ_{th} as obtained via Eq. (3.30) with the tail functions of Section 4.3.4. The plot shows the phase shift for remainders of $\Delta_{th} = \{0, 0.01, 0.1, 1/4, 3/4, 0.9, 0.99\}$ for the total number of bound states N as solid lines. For the three lowest values of the remainder, the corresponding upper dashed lines show the phase shift for the case of one more bound state, in accordance with Levinson's theorem. The dot-dashed line marks the special case of a vanishing scattering length at a remainder of $\Delta_{th}^{(0)} = 1/2$, according to Eq. (4.53). The circumstance that this particular value is $1/2$ indicates that the probability for finding either a positive scattering length is exactly $1/2$, assuming the remainder is uniformly distributed on the interval $[0, 1)$. This is a unique feature of scattering by potentials interaction with $-1/r^4$ tails.

In order to obtain a low-energy expansion of the phase shift, the expansions of the tail functions A_s/A_c [Eq. (4.79)], ϕ_c [Eq. (4.80)], and ϕ_s [Eq. (4.82)] are inserted into Eq. (3.30). Together with a nonzero value of the remainder Δ_{th} and the small short-range correction $\gamma(E)$ according to Eq. (3.8) this immediately yields

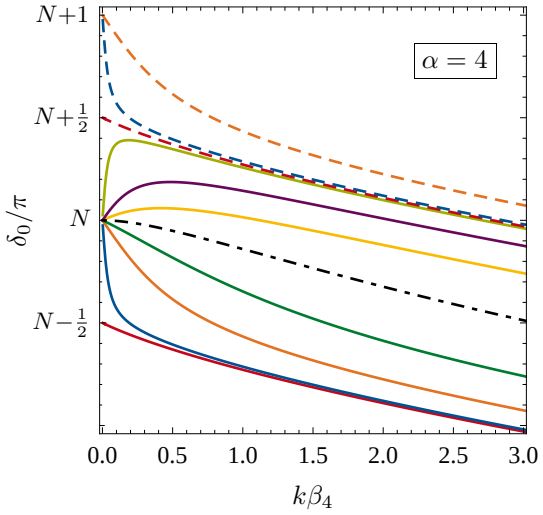

Figure 4.13: This figure shows the s-wave phase shift δ_0 as obtained via Eq. (3.30) for an inverse-power tail (4.1) with $\alpha = 4$, using ξ_t from Eq. (4.78) and the other tail functions as visualized in Figure 4.11. The solid lines show the phase shift for different values of the threshold quantum number's remainder $\Delta_{th} = \{0, 0.01, 0.1, 1/4, 3/4, 0.9, 0.99\}$. The dot-dashed line gives the phase shift for the special value of $\Delta_{th} = 1/2$, for which the scattering length from Eq. (4.84) is exactly zero. The three upper dashed lines again correspond to the phase shift for values of the remainder $\Delta_{th} = \{0, 0.01, 0.1\}$, but for the case that the number of bound states is increased by one.

$$\begin{aligned}\tan\delta_0 \overset{k\to 0}{\sim} & -ak - \frac{\pi}{3}(k\beta_4)^2 - \frac{4}{3}\frac{a}{\beta_4}(k\beta_4)^3\ln(k\beta_4) \\ & - \frac{4}{3}\left(2\gamma_E + 2\ln 2 - \frac{7}{3}\right)\frac{a}{\beta_4}(k\beta_4)^3 + \frac{\pi}{3}\left(\frac{a}{\beta_4}\right)^2(k\beta_4)^3 \\ & + \lambda_{sr}^2\left[1 + \left(\frac{a}{\beta_4}\right)^2\right]\pi(k\beta_4)^3 + \mathcal{O}(k^4)\,, \end{aligned} \tag{4.83}$$

where the remainder has already been expressed in terms of the scattering length, which is, according to Eq. (3.59) for $\alpha = 4$ with the values $\bar{a}_4 = 0$ and $b_4 = \beta_4$, given by

$$a = \frac{\beta_4}{\tan(\Delta_{th}\pi)}\,. \tag{4.84}$$

The expression (4.83) is formally equivalent to the famous expression derived in [34, 35], and it establishes a connection to the threshold quantum number n_{th} via Eq. (4.84). Furthermore, it exposes the universal character of the expression (4.83) for the phase shift; in the limit $\lambda_{sr}^2 = \gamma_{sr}\mathcal{E}_4 \to 0$ it depends only on the scattering length.

It is already argued in Refs. [34, 35] that the expansion of $\tan\delta_0$ is more elegant than the expansion of $k\cot\delta_0$. In addition, it is better suited for further application, e.g., in the context of effective interactions (see [85]) and pseudopotentials [86, 87] that have already been applied to the particular case of $-1/r^4$ interactions [88].

When the scattering length diverges ($a \to \infty$) in the case that there is a bound state at $E = 0$, we find, from expanding Eq. (3.30) with the tail functions for $-1/r^4$ tails and $\Delta_{\mathrm{th}} = \Delta_{\mathrm{th}}^{\infty} = 0$, an expression for the leading-order energy dependence of the phase shift at low-energies

$$\delta_0^{\infty} \overset{k\to 0}{\sim} \frac{\pi}{2} - \left[\frac{\pi}{3} - \pi\lambda_{\mathrm{sr}}^2\right](k\beta_4) + \mathcal{O}(k^2)\,. \tag{4.85}$$

As usual for the case of a bound state exactly at the dissociation threshold, the phase shift starts at $\pi/2$ and the lowest-order energy dependence is $\mathcal{O}(k)$. The lowest solid line and the lowest dashed line in Figure 4.13 show the scattering phase shift at integer values of the threshold quantum number n_{th}. Both lines start at a half-integer value of π and exhibit the linear behavior (4.85) in the limit of low-energies.

4.3.5 Dipole-dipole Interactions ($\alpha = 3$)

Attractive potential tails proportional to $-1/r^3$ are quite common in atomic physics. It is the leading radial dependence of the interaction energy between two permanent dipoles and also occurs in a spherically symmetric form as a resonant dipole-dipole interaction [7, 89]. In the latter case an atom in a given internal state interacts with an atom of the same species in a different internal state. If a dipole transition between the two internal states is allowed, the dipole-dipole interaction operator can give a nonvanishing contribution to the interaction energy, already in first order (see Appendix A).

The tail potential $V_3(r) = -C_3/r^3$ constitutes the lowest-integer order of inverse-power potentials (4.1) to which the formalism derived in Chapter 3 is applicable. Although it is subject to that formalism, its low-energy collision properties are very different from those of potentials with inverse-power tails (4.1) with $\alpha > 3$; a scattering length that describes the scattering process in the limit of very low collision energies does not exist for the case of a long-range $1/r^3$ interaction. That is why, in contrast to the interactions previously discussed, scattering from potentials with attractive $-1/r^3$ tails is, to the present day, only poorly understood.

An analytical threshold law describing the low-energy scattering for the repulsive case of $1/r^3$ interactions including all terms that are $\mathcal{O}(k)$ was given by del Giudice and Galzenati in 1965 [79] and was rederived by Gao in 1999 [90]. The attractive case, however, is more complicated due to the additional influence of the short-range part of the interaction potential that deviates from the $-1/r^3$ behavior; this case has not been studied to a satisfactory extend so far.

In their comprehensive work [36] on scattering from long-range potentials, Levy and Keller also study the case of attractive $1/r^3$ interactions. They predict the low-energy behavior of the phase shift to be given by

$$\tan\delta_0 \overset{k\to 0}{\sim} -(k\beta_3)\ln(k\beta_3) + \mathcal{O}(k)\,, \tag{4.86}$$

with the characteristic length of the inverse-cube tail given by $\beta_3 = 2\mu C_3/\hbar^2$. The expansion (4.86) still constitutes the established form of a threshold law for elastic scattering from inverse-cube potentials in today's literature [4, 27, 84]. It is correct in the limit of very low energies but neglects further terms of first order in the wave number k. In particular, the expansion (4.86) does not contain any information about the influence of the short-range potential on the low-energy scattering process. Further approaches [91, 92] to

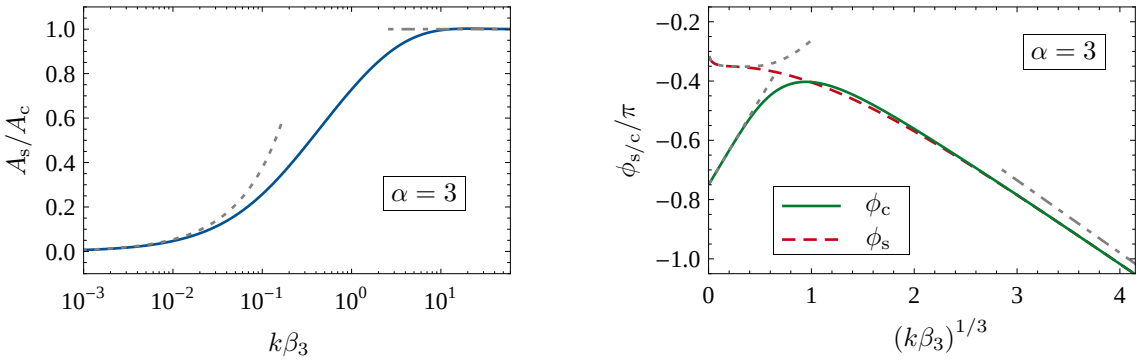

Figure 4.14: The graph on the left-hand side shows the universal behavior of the ratio of amplitudes A_s/A_c for an inverse-power tail (4.1) with $\alpha = 3$ as a solid line, plotted against the product $(k\beta_3)$ on a logarithmic scale together with its low-energy behavior (dotted line) to first order in k as given by Eq. (4.88) and its high-energy behavior (dot-dashed line) given in Eq. (3.85). The graph on the right-hand side shows the universal behavior of the tail-dependent phases ϕ_s and ϕ_c for the same potential tail, but plotted against $(k\beta_3)^{1/3}$. The dotted lines and the dot-dashed line show behaviors of the phases at low energies (4.89) and (4.91) and high-energy behavior (4.33) respectively.

low-energy scattering in the presence of attractive inverse-cube interactions make use of the Gell-Mann – Goldberger two-potential formula and the distorted wave Born approximation (as established in Ref. [82]).

Tail functions

Although it is a very particular case, the $-1/r^3$ interaction is still fulfills the preconditions for the applicability of the formalism developed in Chapter 3. Therefore the tail functions are obtained in a similar fashion as for the cases for which a scattering length exists ($\alpha > 3$). The phase ξ_t is given in Eq. (4.31) and can be evaluated for the case $\alpha = 3$. This yields

$$\xi_t^{\alpha=3} = -\frac{\pi}{4} + 2\eta_3 (k\beta_3)^{1/3}\,, \tag{4.87}$$

with η_3 given analytically by Eq. (4.32) and numerically in Table 4.5. The phase ξ_t exhibits the typical semiclassical energy dependence $(k\beta_3)^{1/3}$ for $1/r^3$ tail potentials. The expression (4.87) is valid over the whole energy range considered.

The further tail functions are depicted in Figure 4.14. The left panel shows the ratio A_s/A_c of the amplitudes of the fundamental solutions (3.29) in an attractive inverse-cube potential. It is plotted against the dimensionless product $(k\beta_3)$ on a logarithmic scale in order to adequately resolve the low-energy limit, which is visualized as the dotted line in the left panel of Figure 4.14. Due to the nonexistence of a mean scattering length $\bar{a}$ for inverse-cube potentials, the low-energy expansion of A_s/A_c can no longer be given by Eq. (4.37). It can, however, equivalently be obtained from the expansion of $\mathcal{K}_{\text{refl}}^{\alpha=3}$ as given in Ref. [78], which yields

$$\frac{A_s}{A_c} = |\mathcal{K}_{\text{refl}}^{\alpha=3}| \overset{k\to 0}{\sim} \pi \sqrt{1 + \left(\frac{\frac{3}{2} - 3\gamma - \ln(2k\beta_3)}{\pi}\right)^2}\,(k\beta_3) + \mathcal{O}(k^2)\,. \tag{4.88}$$

From the left panel of Figure 4.14 it can be seen that this expansion gives the correct low-energy behavior of the ratio of amplitudes. It is, however, only a good approximation to $A_\mathrm{s}/A_\mathrm{c}$ at very low energies $k\beta_3 \lesssim 10^{-2}$.

The right panel of Figure 4.14 shows the phases ϕ_c (solid line) and ϕ_s (dashed line) plotted against the dimensionless quantity $(k\beta_3)^{1/3}$. The dot-dashed line gives the common high-energy asymptote of both phases that is given by $-\tau_3(k\beta_3)^{1/3}$ according to Eq. (4.33). The dotted lines give the analytic low-energy expansions of the respective phases. The phase ϕ_c can — according to Eq. (3.56) — be expanded at least to the order of the wave number k, since the function $w_0(r)$ (4.10), which is approached by the fundamental solution $u^{(c)}(r)$ (3.53), is well defined for an inverse-power potential (4.1) with $\alpha = 3$

$$\phi_\mathrm{c} \overset{k\to 0}{\sim} -\frac{3\pi}{4} + 2\eta_3(k\beta_3)^{1/3} + \mathcal{O}(k^2)\,. \tag{4.89}$$

This expansion perfectly fits the exact values of ϕ_c as plotted in the right panel of Figure 4.14.

The near-threshold expansion of the phase ϕ_s can not be obtained via a similar procedure, due to the lack of an appropriate zero-energy solution $w_1(r)$ (3.49) that, as discussed in Section 4.1 does not exist for the reference potential $V_3(r)$. Similar to the cases previously discussed, the low-energy behavior of the phase ϕ_s can be obtained from the phase ϕ_c together with an expansion of the phase difference according to Eq. (4.62). This difference is expressed via the amplitude R of quantum reflection by the tail potential $V_3(r) = -C_3/r^3$. This yields

$$\phi_\mathrm{s} - \phi_\mathrm{c} = \arg\left(\frac{1-R}{1+R}\right) \overset{k\to 0}{\sim} \arctan\left(\frac{\frac{3}{2} - 3\gamma - \ln(2k\beta_3)}{\pi}\right) + \mathcal{O}(k^1)\,, \tag{4.90}$$

including all known orders of $\mathcal{K}_\mathrm{refl}^{\alpha=3}$ in the expansion. Therefore, we can not predict the behavior of the phase ϕ_s beyond zeroth order in the wave number k. Its energy dependence below the $\mathcal{O}(k^1)$ is given by

$$\phi_\mathrm{s} \overset{k\to 0}{\sim} -\frac{3\pi}{4} + \arctan\left(\frac{\frac{3}{2} - 3\gamma - \ln(2k\beta_3)}{\pi}\right) + 2\eta_3(k\beta_3)^{1/3} + \mathcal{O}(k^1)\,. \tag{4.91}$$

From the numerical results plotted in the right panel of Figure 4.14 we can confirm that this expansion gives the correct low-energy behavior of the exact values of the phase ϕ_s. Its limiting value $\phi_\mathrm{s}(0) = -\pi/4$ is approached logarithmically, which is hard to resolve in the right panel of Figure 4.14.

The validity of expansions of the tail functions is, in the case of inverse-power potentials (4.1) with $\alpha = 3$, restricted to low orders of the wave number k. This is due to the occurrence of "anomalous" terms already in the leading order of the expansion (cf. Eq. (4.90). Therefore, the correctness of the expansions according to the scheme presented in Appendix C is not illustrated separately; its validity has, however, been verified for the expansions presented in this section.

Scattering phase shift

Possible phase shifts due to scattering from a potential with an attractive inverse-cube tail are visualized in Figure 4.15. The results plotted are obtained by evaluating the

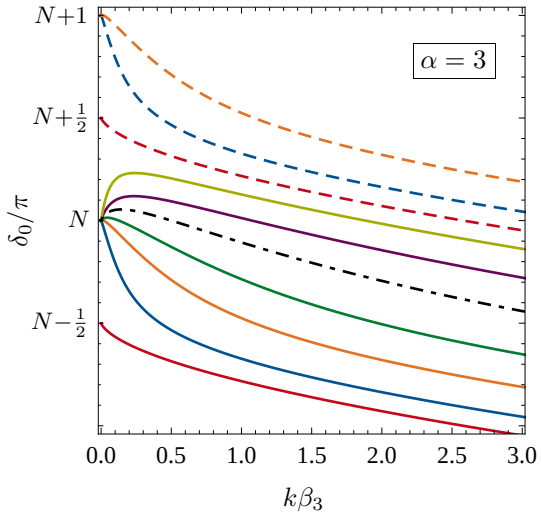

Figure 4.15: This figure shows the s-wave phase shift δ_0 as obtained via Eq. (3.30) for an inverse-power tail (4.1) with $\alpha = 3$, using ξ_t from Eq. (4.87) and the other tail functions as visualized in Figure 4.11. The solid lines show the phase shift for different values of the threshold quantum number's remainder $\Delta_\mathrm{th} = \{0, 0.1, 1/4, 2/5, 3/4, 0.9\}$. The dot-dashed line gives the phase shift for the special value of $\Delta_\mathrm{th} = 0.591127$, for which the phase shift starts like $-(k\beta_3)\ln(k\beta_3) + \mathcal{O}(k^2)$. The three upper dashed lines again correspond to the phase shift for values of the remainder $\Delta_\mathrm{th} = \{0, 0.1, 1/4\}$, but for the case that the number of bound states is increased by one.

expression (3.30) for the scattering phase shift δ_0 with the tail functions for the reference potential $V_3(r)$ that are given above (see Figure 4.14). The solid lines show the phase shift for different values of the remainder $\Delta_\mathrm{th} = \{0, 0.1, 1/4, 2/5, 3/4, 0.9\}$, representing the influence of different short-range potentials. The dashed lines correspond to the lowest three solid lines but for a total number of bound states that is increased by one.

The low-energy expansion of the phase shift is obtained by inserting the expansions (4.88), (4.89), and (4.91) for the tail functions of the reference potential $V_3(r)$ into the formula (3.30) for the scattering phase shift. This yields

$$\tan\delta_0 \overset{k\to 0}{\sim} -\left[\ln(k\beta_3) + \frac{\pi}{\tan(\Delta_\mathrm{th}\pi)}\right](k\beta_3) + \left(\frac{3}{2} - 3\gamma_\mathrm{E} - \ln 2\right)(k\beta_3) + \mathcal{O}(k^2)\,, \qquad (4.92)$$

which contains all terms of $\mathcal{O}(k)$. While the threshold laws that have been discussed in the previous sections essentially depended on the scattering length, we can clearly see from Eq. (4.92) that a finite scattering length does not exist in the presence of a $-1/r^3$ potential tail, which is due to the logarithmic term already incorporated in the well-known expression (4.86). This term causes the divergence of the elastic scattering cross section (cf. Eq. (2.25)) in the limit of low-energies. The expansion (4.92) depends on the short-range form of the full interaction potential via the threshold quantum number's remainder Δ_th that is manifest in the first-order term in k. These terms contribute to the zero-energy cross section and must, therefore, not be neglected.

Corresponding formulae were derived by Shakeshaft [91] (1972) and Ganas [92] (1973). Their derivation is based on the two-potential formula as used by Hinckelmann and Spruch [82]. As pointed out in the latter work, it contains a particular weakness; it requires the knowledge of the scattering properties of an unphysical, truncated potential. That is why formula (4.92) for the low-energy phase shift in the presence of $-1/r^3$ interactions is more insightful. It relies on a single parameter, that has an inherent physical meaning and incorporates the influence of the short-range potential to the low-energy scattering properties.

When there is a bound state exactly at the dissociation threshold ($\Delta_{\text{th}} = \Delta_{\text{th}}^{\infty} = 0$), the phase shift starts at $\pi/2$, as required. The leading-order dependence on the wave number k can not be given explicitly, since the term $\mathcal{O}(k^2)$ is not known in the expansion (4.89) of the phase ϕ_{c}. For an inverse-cube tail potential, the question of the phase shift's behavior in the case of a bound state at $E = 0$ was already addressed in Ref. [93], but a comprehensive answer is not given there.

4.4 Summary of results

The inverse-power potentials $V_\alpha(r) = -C_\alpha/r^\alpha$ with $\alpha > 2$ have been identified to be ideal candidates for the reference potentials of the formalism derived in Chapter 3; by definition they are more singular than $-1/r^2$ at the origin and vanish faster than $-1/r^2$ asymptotically. This makes them ideal candidates for a treatment within the framework of the phase-corrected WKB theory (see Section 2.2). The distinct regions of WKB validity have been identified and the analytical zero-energy solutions have been presented.

The properties of the quantization function $F_\alpha(E)$ (3.16) for the general case of the inverse-power reference potentials $V_\alpha(r) = -C_\alpha/r^\alpha$ with $\alpha > 2$ have been studied both in the regime of high energies, where the semiclassical picture holds, and in the immediate near-threshold regime, where purely quantum mechanical effects play a predominant role. For an inverse-cube potential tail, an explicit analytical expression (4.27) for the tail part $F_{\alpha=3}$ of the quantization function has been presented. It is based on a highly accurate approximation of the outer reflection phase $\phi_{\text{out}}(E)$ accounting for analytical limiting expansions. Such high accuracy was not achieved in the cases $\alpha = 6$ [13, 41] and $\alpha = 4$ [42] that have previously been studied.

The expression for the scattering phase shift have also been analyzed; low- and high-energy expansions have been presented for the tail-related functions $A_{\text{s}}/A_{\text{c}}$, ϕ_{s} and ϕ_{c} that were obtained by explicitly solving the Schrödinger equation with the inverse-power reference potential. For the particular integer cases $3 \leq \alpha \leq 6$ these tail functions have been presented and the scattering phase shift for potentials with the corresponding tails have been derived. For each of the tail potentials considered the phase shift has been illustrated as a function of the energy for different values of the threshold quantum number's noninteger remainder $\Delta_{\text{th}} \in [0, 1)$. For all of these cases, low-energy expansions of the tail functions have been given, from which modified effective-range expansions for the s-wave phase shift has been derived. These exhibit characteristic terms for each power α, that can not be reproduced with any other potential tail. In particular, a comprehensive threshold law for elastic scattering by potentials with attractive inverse-cube tails has been presented for the first time. We have also studied the modifications of the low-energy expansions of

the phase shift for the special case when there is a bound state exactly at the dissociation threshold ($\Delta_{\mathrm{th}} = 0$).

Chapter 5

Application to specific systems

The formalism for the description of quantization and scattering, that has been developed in the preceding chapters is now applied to specific problems. We first study the applicability of the quantization function (4.27) that has been derived in Section 4.2.2 for inverse-cube tail potentials. It is applied to homonuclear long-range molecules. In the subsequent section, the applicability of our approach is demonstrated for two model Lennard-Jones potentials, studying both quantization and scattering. In particular, the threshold law (4.92) for scattering from potentials with $-1/r^3$ tails is verified. Section 5.2.3 deals with the theory's applicability to potential tails that are not well described by a single inverse-power term. The scattering phase shift for a model potential with a mixed tail consisting of two inverse-power terms is analyzed from this point of view.

5.1 Vibrational bound states in long-range molecules

In this section we study the application of the quantization function (4.27) for inverse-cube tails to homo-nuclear alkali dimers forming pure long-range molecules [94]. Typical internuclear distances are much larger there than those for usual chemical binding potentials. The asymptotic behavior of such a potential well can often be described by the resonant dipole-dipole interaction [89]. In these cases the potential tail is proportional to $-1/r^3$ at large distances (see Appendix A).

Nowadays it has become possible to determine the energy eigenvalues of the vibrational states with the method of *photoassociation spectroscopy* (see e.g. Ref. [74, 75, 95]). Using this method, it is possible to locate the bound states in very broad energy regions. Nevertheless the high density of states in such a long-range potential still makes the measurement of bound states very close to the threshold difficult. A discussion of these results has already been published in Ref. [71].

5.1.1 Determination of the potential tail's dispersion coefficient

One aim of photoassociation spectroscopy experiments is the determination of accurate strength coefficients C_3 from the bound-state spectra that are obtained. Given the energy eigenvalues and the strength coefficient C_3, the reduced outer classical turning point

corresponding to each energy eigenvalue reads

$$s_n = (\kappa_n \beta_3)^{1/3} = \frac{\sqrt{2\mu}}{\hbar} C_3^{1/3} \left(-E_n\right)^{1/6} . \tag{5.1}$$

This relates the strength coefficient C_3 to the energy spectrum via the quantization function (4.27) for inverse-cube tails.

Recent analyses are still predominantly done utilizing the LeRoy-Bernstein function (4.15), despite its wrong near-threshold behavior. The reason is the simple linear relation between n and the reduced outer classical turning point s_n in the corresponding quantization rule. The results obtained for C_3 via the LeRoy-Bernstein function (4.15) are close to those obtained using the correct quantization function (4.27), as long as the vibrational levels used are not too close to threshold, since the difference between $F_{\alpha=3}(E)$ and $F_{\alpha=3}^{\mathrm{NDE}}(E)$ is only a constant offset at large binding energies [see Eq. (4.22)].

The higher the energy difference to the threshold is, the more important are the effects due to the short-range part of the binding potential that can only be treated phenomenologically, so that quantization functions based on the potential tail alone can only be considered an approximation. Using the correct quantization function (4.27) these problems far from threshold will be the same as with the LeRoy-Bernstein function (4.15), the accuracy of the correct quantization function (4.27) however increases towards threshold. The best determination of the strength coefficient is measuring vibrational levels as close to the dissociation threshold as possible and then using the correct quantization function (4.27).

5.1.2 Extrapolation and number of bound states

The fitting procedure, to determine the strength coefficient C_3 of the inverse-cube potential tail, yields the remainder Δ_{th} of the threshold quantum number n_{th}. Its integer part $\lfloor n_{\mathrm{th}} \rfloor$ depends on the counting of the bound states; it can only be determined correctly if the correct quantum numbers, as obtained by counting from $n = 0$ for the ground state, are assigned to the vibrational levels measured. The range of energy that is accessible in a single experiment usually does not encompass the whole spectrum; the ground state is thus not detected in most experiments. If a certain range of the spectrum is known, the relation

$$n(E_n) = n_{\mathrm{th}} - F_{\alpha=3}(E_n) + \gamma_{\mathrm{sr}} E_n \tag{5.2}$$

[cf. Eqs. (3.14) and (3.15)] can be used to extrapolate the spectrum towards lower binding energies, all the way up to the dissociation threshold.

In recent works [75–77], effective quantum numbers $\tilde{n} = \lfloor n_{\mathrm{th}} \rfloor - n$ counting from 0 at the highest-lying state to $\lfloor n_{\mathrm{th}} \rfloor$ for the ground state are assigned to the levels observed. Each observed energy level can then be associated to its correct effective quantum number $\tilde{n}$ without knowing either n or $\lfloor n_{\mathrm{th}} \rfloor$, but only their difference.

In case that the observed levels lie far enough from threshold, both the LeRoy-Bernstein function (4.15) and the correct quantization function (4.27) yield essentially the same coefficient C_3, but the remainder obtained from the LeRoy-Bernstein function (4.15) will be offset by 1/2 relative to the correct remainder.

If the correct remainder in an interaction potential with a $-1/r^3$ tail is $\Delta_{\mathrm{th}} > 1/2$, i.e. in half of all possible cases, then naive extrapolation via the LeRoy-Bernstein formula will

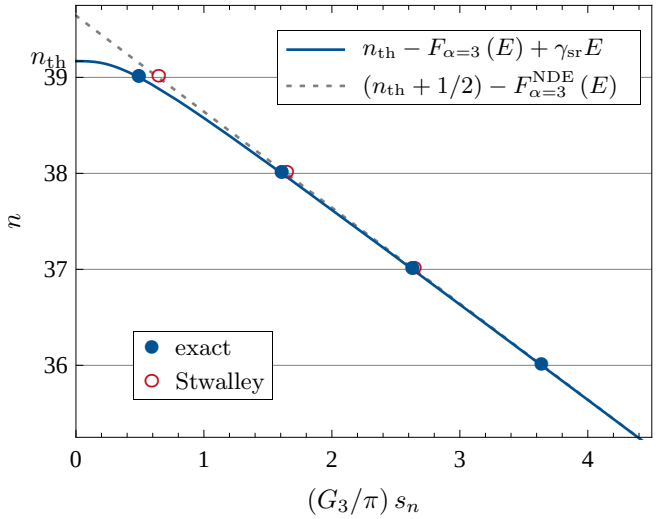

Figure 5.1: Vibrational quantum number n versus the reduced outer classical turning point s_n (5.1) for bound-state energies in the long-range 0_g^- configuration of Na_2. Both the exact values (filled circles) and the values extrapolated by Stwalley via the LeRoy-Bernstein formula (empty circles) are shown. The solid line determines the positions of the exact eigenenergies and is based on the correct quantization function (4.27), whereas the dotted line indicates the energies that would have been expected using the LeRoy-Bernstein function (4.15). It is clearly visible that the quantization function (4.27) gives the correct results.

predict a spurious bound state near the threshold, which leads to a wrong assignment of the downward quantum numbers to the bound states and an overestimation (by one) of the total number of bound states in the near threshold region.

As an example, we discuss a work of William Stwalley [94] that deals with pure long-range sodium dimers near the $Na(3P_{3/2})$+$Na(3S_{1/2})$ dissociation asymptote. The bound-state spectrum was calculated numerically based on the adiabatic potentials of Ref. [94, 96] for both the 0_g^- and the 1_u symmetry by using the conventional Bohr-Sommerfeld quantization rule. Since the numerical determination of the highest-lying bound states was not possible then, the spectrum was extrapolated to the threshold using the semiclassical LeRoy-Bernstein quantization function (4.15), as derived in Refs. [14, 15].

Based on the energies calculated by Stwalley [94] for the 0_g^- configuration up to $n = 36$, Gao [97] extrapolated the spectrum to the threshold using a pure quantum approach derived from exact wave functions for the inverse-cube potential tail, without any reference to WKB wave functions. In order to check the accuracy of the various extrapolation procedures, we have calculated the exact bound-state energies for the potential from Ref. [96] by solving the Schrödinger equation numerically. Exact values for the highest six vibrational levels are given in Table 5.1 and Table 5.2

We can use relation (5.2) to extract values for the strength coefficient C_3, the threshold quantum number $n_{\rm th}$ and the leading-order coefficient $\gamma_{\rm sr}$ of the short-range contribution to the exact quantization function. By fitting Eq. (5.2) to the three bound-state energies E_n with $n = 34, 35$ and 36, for the 0_g^- configuration (see Table 5.1), we obtain $C_3 = 6.39\,$a.u. which reproduces the strength of the tail in the adiabatic potential curve [94, 96] exactly. The threshold quantum number is found to be $n_{\rm th} = 39.1690$ which is

n	exact	Stwalley [94]
34	1.81083×10^{-5}	1.8262×10^{-5}
35	5.60556×10^{-6}	5.6648×10^{-6}
36	1.29912×10^{-6}	1.3175×10^{-6}

Table 5.1: Exact vibrational energy eigenvalues (in cm^{-1}) for the three bound states with $n = 34, 35$ and 36 in the pure long-range sodium dimer dissociating to $\mathrm{Na}(3P_{3/2})$+$\mathrm{Na}(3S_{1/2})$ with 0_g^- symmetry. These have been calculated by numerically solving the Schrödinger equation with the adiabatic potential from Ref. [94, 96]. The second column shows the values obtained by Stwalley [94] via conventional Bohr-Sommerfeld quantization.

about one half smaller than the value determined in [94], as expected, due to the offset of 1/2 in the LeRoy-Bernstein function compared to the correct quantization function. The leading-order coefficient of $\gamma(E)$ is obtained as $1/\gamma_{\mathrm{sr}} = -0.767404\,\mathrm{cm}^{-1}$; relating this to a characteristic length scale for the short-range effects via $|\gamma_{\mathrm{sr}}| = 2\mu\beta_{\mathrm{sr}}^2/\hbar^2$ gives $\beta_{\mathrm{sr}} \approx 2.62\,\mathrm{a.u.}$, which is very small compared to the characteristic length parameter of the potential tail, given by $\beta_3 = 2\mu C_3/\hbar^2 \approx 2.68 \times 10^5\,\mathrm{a.u.}$ in this case.

Having determined these three parameters, the energies of the remaining near-threshold bound states can be read off from the correct quantization condition at each point, where $n_{\mathrm{th}} - F_{\alpha=3}(E) + \gamma_{\mathrm{sr}}E$ equals $37, 38$ and 39. We compare these extrapolated values for the energies to the exact spectrum in Figure 5.1 and Table 5.2. The values extrapolated via the LeRoy-Bernstein formula deviate from the exact values more, the closer the energy is to threshold. The values obtained via Gao's quantum extrapolation and with our correct quantization function (4.27) are in better agreement with the exact values up to the threshold.

The energy eigenvalues for the highest three states extrapolated via (5.2) with the quantization function (4.27) agree within $10^{-16}\,\mathrm{cm}^{-1}$ to $10^{-14}\,\mathrm{cm}^{-1}$ with the exact eigenvalues obtained by solving the Schrödinger equation. The deviation of the values from [97] is somewhat larger, partly because Gao's extrapolation is based on Stwalley's energies that were calculated under the assumption, that the reflection phases equal $\pi/2$; this is almost correct for high binding energies but becomes less accurate towards the dissociation threshold. So the energy eigenvalues calculated in Ref. [94] differ a little from the exact eigenvalues, even for $n < 37$ (see Table 5.1).

In the case of 1_u symmetry in the same sodium system the threshold quantum number

n	Stwalley [94]	Gao [97]	this work	exact
37	1.9247×10^{-7}	1.8908×10^{-7}	1.85419×10^{-7}	1.85419×10^{-7}
38	1.1215×10^{-8}	1.0065×10^{-8}	9.74157×10^{-9}	9.74156×10^{-9}
39	4.1916×10^{-11}	9.2524×10^{-12}	8.00658×10^{-12}	8.00685×10^{-12}

Table 5.2: Vibrational energy eigenvalues (in cm^{-1}) for the highest three bound states in the pure long-range sodium dimer dissociating into $\mathrm{Na}(3P_{3/2})$+$\mathrm{Na}(3S_{1/2})$ with 0_g^- symmetry from different extrapolation methods compared to the exact values

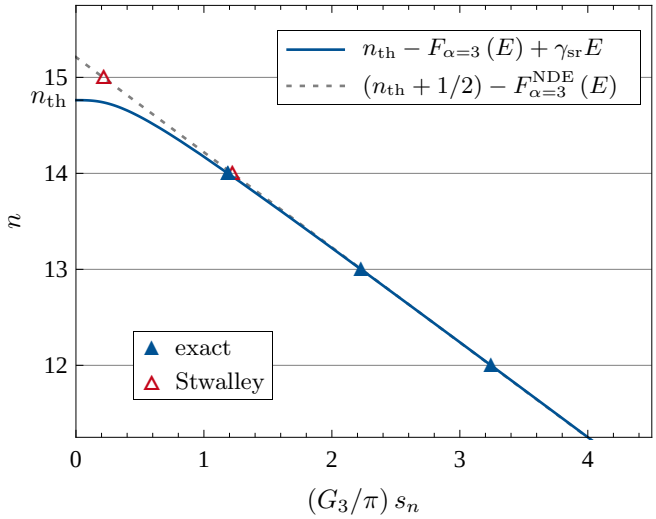

Figure 5.2: Same as in Figure 5.1 but for the long-range 1_u configuration. Here the extrapolation via the LeRoy-Bernstein formula wrongly indicates a spurious 16^{th} bound state ($n = 15$), whereas the use of the correct quantization function (4.27) shows, that this state does not exist.

obtained by extrapolation via the LeRoy-Bernstein formula is 15.22 in Ref. [94] and therefore a spurious 16^{th} bound state is predicted whereas the extrapolation with the correct quantization function (4.27) would have yielded $n_{\mathrm{th}} \approx 14.72$, which tells us that this state does not exist (see Figure 5.2). The total number of bound states therefore is 15, not 16 as stated. An analogous mistake occurs in Ref. [15], where corresponding results for the $B^1\Sigma_u^+$ state of H_2 are presented. In the latter case the threshold quantum number was found to be 43.26 ± 0.04, implying a 44^{th} bound state ($n = 43$), whereas using the correct quantization function would have yielded $n_{\mathrm{th}} \approx 42.76$ and therefore no bound state with $n = 43$ exists.

In case of an inverse-cube potential tail, the offset in the LeRoy-Bernstein formula leads to an overestimation of the threshold quantum number n_{th} by 1/2, and hence to the prediction of an additional spurious bound state in half of all possible cases. With the correct quantization function (4.27), n_{th} can be determined with high accuracy from a few bound-state energies. One way of avoiding the assignment of a nonexistent bound state with the LeRoy-Bernstein formula could be to simply subtract the offset 1/2 from the threshold quantum number obtained by linear extrapolation. This can only work with fair reliability, however, if the states used for the fit are far enough from threshold. On the other hand short-range effects destroy the linear dependence on s in this region. Closer to threshold short-range effects are less problematic but the picture of a constant offset is less accurate.

5.2 Application to model potentials

In order to verify the results of the previous chapters, we apply the formalism that has been developed in Chapter 3 to certain model potentials. Two Lennard-Jones potentials with different inverse-power tails are analyzed making use of the results of Chapter 4. We

also study the case of a model potential with a mixed tail consisting of two inverse-power terms. A separation of the influence of the potential tail is also achieved for this case.

5.2.1 (12|6) Lennard-Jones potential

The near-threshold quantization and the scattering properties of a (12|6) Lennard-Jones potential is analyzed. It is in general given by

$$V_{12|6}(r) = \mathcal{E}\left[\left(\frac{r_{\min}}{r}\right)^{12} - 2\left(\frac{r_{\min}}{r}\right)^{6}\right]. \tag{5.3}$$

This potential has its minimum at $r_{\min}$ with $V_{12|6}(r_{\min}) = -\mathcal{E}$. Due to its simple form it certainly constitutes one of the most common potentials for modelling interatomic interaction with $-C_6/r^6$ tails. The dispersion coefficient $C_6 = 2\mathcal{E}r_{\min}^6$ is expressed in terms of the rest position $r_{\min}$ and the well depth $\mathcal{E}$. The radial Schrödinger equation (2.6) for s waves with the (12|6) Lennard-Jones potential (5.3) can be rescaled by expressing all lengths in units of the rest position ($\rho = r/r_{\min}$)

$$\left[-\frac{d^2}{d\rho^2} + B_{12|6}\left(\frac{1}{\rho^{12}} - \frac{2}{\rho^6} - \frac{E}{\mathcal{E}}\right)\right] u_0(\rho)\,, \tag{5.4}$$

where the dimensionless Lennard-Jones strength parameter $B_{12|6} = 2\mu\mathcal{E}r_{\min}^2/\hbar^2$ is introduced. It can clearly be seen that the form of the solutions $u_0(\rho)$ of Eq. (5.4) only depends on the strength parameter $B_{12|6}$ and the energy in units of the well depth. In particular, it does not depend on the rest position $r_{\min}$ and the well depth $\mathcal{E}$ independently. The characteristic length scale of the $-1/r^6$ tail of the interaction potential can then be expressed via

$$\beta_6 = (2B_{12|6})^{1/4} r_{\min}\,. \tag{5.5}$$

For our analysis, we consider a strength parameter of $B_{12|6} = 10^4$. The number of bound states in a (12|6) Lennard-Jones potential can be estimated by approximating the threshold quantum number n_{th} via the generalized Bohr-Sommerfeld quantization rule (2.45) at the threshold energy $E = 0$ [cf. Eq. (3.4)] under the assumption that the inner reflection phase $\phi_{\text{in}}(0)$ is $\pi/2$ and the outer reflection phase $\phi_{\text{out}}(0)$ is $3\pi/4$ according to Eq. (4.19) with $\alpha = 6$. This yields

$$n_{\text{th}} \approx \frac{1}{\pi\hbar}\int_{\sigma}^{\infty}\sqrt{-2\mu V_{12|6}(r)}\,dr - \frac{5}{8} = \frac{\Gamma\left(\frac{4}{3}\right)}{2^{7/6}\sqrt{\pi}\,\Gamma\left(\frac{11}{6}\right)}\sqrt{B_{12|6}} - \frac{5}{8}\,, \tag{5.6}$$

with the zero of the potential at the distance $\sigma = 2^{-1/6} r_{\min}$. For the choice $B_{12|6} = 10^4$, this approximation yields $n_{\text{th}} \approx 23.2330$. We can thus conclude that a total number of 24 bound states exists in the (12|6) Lennard-Jones potential (5.3) with $B_{12|6} = 10^4$ and that the noninteger remainder takes a value of $\Delta_{\text{th}} \approx 0.2330$. This value is certainly not exact but might offer a good estimate.

The eigenenergies of the 24 bound states were already calculated in Ref. [98] and the highest five energy levels are given in units of the potential depth $\mathcal{E}$ in Table 5.3. In order to relate these energies to the scales of the potential tail they are converted to units of

n	$-E_n/\mathcal{E}$	$-E_n/\mathcal{E}_6$
19	0.006657024344	9414.454112
20	0.003047136244	4309.301403
21	0.001052747695	1488.810068
22	0.000198340301	280.495544
23	0.000002696883	3.813969

Table 5.3: Scaled energy eigenvalues of the highest five vibrational s-wave bound states in a (12|6) Lennard-Jones potential (5.9) with a strength parameter of $B_{12|6} = 10^4$. The energies are given both in units of the potential well depth $\mathcal{E}$ and in units of the characteristic energy scale $\mathcal{E}_6$ of the potential tail.

the characteristic energy scale $\mathcal{E}_6$ of the potential tail. For general (12|6) Lennard-Jones potentials (5.3) the potential depth is related to this energy scale via $\mathcal{E} = \sqrt{2}B_{12|6}^{3/2}\mathcal{E}_6$. For the particular case of $B_{12|6} = 10^4$, this yields $\mathcal{E} = \sqrt{2} \times 10^6\mathcal{E}_6$. The values obtained for the eigenenergies are also given in Table 5.3.

From the bound-state energies listed in Table 5.3, a discrete set of values for the short-range parametrization can be deduced via the relation

$$n_{\mathrm{th}} + \gamma(E_n) = n + F_{\alpha=6}(E_n)\,, \tag{5.7}$$

that is just a reformulation of the quantization condition (3.14) in the presence of $-1/r^6$ potential tails. The tail part $F_{\alpha=6}(E)$ of the quantization function can be derived by using its definition (4.18) and explicitly evaluating the outer reflection phase numerically. An explicit analytical form for the tail part of the quantization function for $-1/r^6$ tails has been given in Ref. [13]. The results for the short-range parametrization $n_{\mathrm{th}} + \gamma(E)$ as obtained from the highest five levels (Table 5.3) via Eq. (5.7) are depicted as dots in the left half (negative energies) of Figure 5.3.

For positive energies the quantity $n_{\mathrm{th}} + \gamma(E)$ (solid line in Figure 5.3) can be extracted from the scattering phase shift δ_0 for s waves. The parametrization (3.30) of the phase shift can be inverted to yield an expression for the short-range parameters

$$n_{\mathrm{th}} + \gamma(E) = -\frac{1}{\pi}\arctan\left(\frac{A_{\mathrm{s}}/A_{\mathrm{c}}\sin(\phi_{\mathrm{s}} - \xi_{\mathrm{t}}) - \tan\delta_0\cos(\phi_{\mathrm{c}} - \xi_{\mathrm{t}})}{A_{\mathrm{s}}/A_{\mathrm{c}}\cos(\phi_{\mathrm{s}} - \xi_{\mathrm{t}}) + \tan\delta_0\sin(\phi_{\mathrm{c}} - \xi_{\mathrm{t}})}\right). \tag{5.8}$$

The tail functions that are used are those that have already been presented in Section 4.3.2.

It can clearly be seen from Figure 5.3 that the discrete values for $n_{\mathrm{th}} + \gamma(E)$ calculated via Eq. (5.7) and the continuous values obtained from Eq. (5.8) merge smoothly at the threshold energy $E = 0$. We can thus conclude that our definition of the tail potential $-1/r^6$ is sufficient for providing a clean separation of tail effects from the short-range effects, so that their parametrization $n_{\mathrm{th}} + \gamma(E)$ is insensitive to the actual position of the dissociation threshold. The smooth behavior can be approximated by the linear relation $n_{\mathrm{th}} + \gamma_{\mathrm{sr}}E$, which is shown in Figure 5.3 as the dashed line. From a fit to the values of $n_{\mathrm{th}} + \gamma(E)$ closest to the threshold energy, we find that the exact value of the threshold quantum number's remainder is $\Delta_{\mathrm{th}} = 0.232732$. This result deviates from the semiclassical estimate

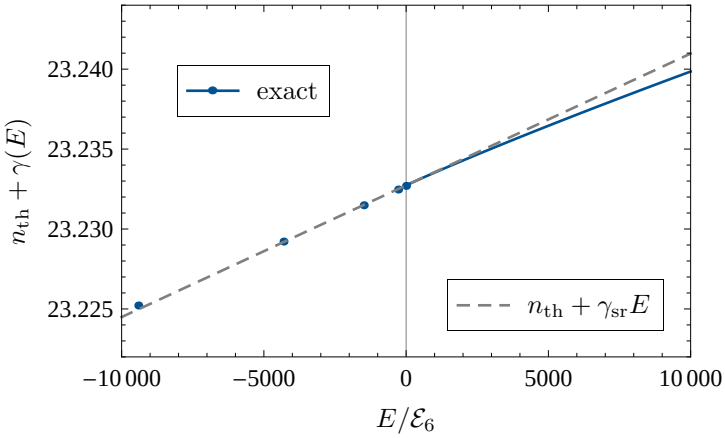

Figure 5.3: Short-range parametrization $n_{\mathrm{th}} + \gamma(E)$ for a (12|6) Lennard-Jones potential (5.3) with a strength parameter of $B_{12|6} = 10^4$. The dots give the results of Eq. (5.7) with the bound-state energies from Table 5.3. The solid line gives the results obtained from Eq. (5.8) with the exact values of the s-wave phase shift and the scattering tail functions from Section 4.3.2. The dashed line shows the leading-order energy dependence $n_{\mathrm{th}} + \gamma_{\mathrm{sr}} E$ with $n_{\mathrm{th}} = 23.2327$ and $\gamma_{\mathrm{sr}} \mathcal{E}_6 = 8.24 \times 10^{-7}$

via Eq. (5.6) by only 2.7×10^{-4}. With this remainder the scattering length of the potential (5.3) with $B_{12|6} = 10^4$ can be obtained via Eq. (4.66). Together with the relation (5.5), this yields $a = 12.0213\, r_{\mathrm{min}}$. The short-range parameter γ_{sr} is very small in case that the energy is expressed in units of the characteristic energy scale $\mathcal{E}_6$ of the potential tail $\gamma_{\mathrm{sr}} \mathcal{E}_6 = \lambda_{\mathrm{sr}}^2 = 8.24 \times 10^{-7}$, which is small as already argued in Section 3.1. Expressing the energy in terms of the $\mathcal{E}$ gives $\gamma_{\mathrm{sr}} = 1.1657/\mathcal{E}$. With these values, Eq. (4.67) yields $r_{\mathrm{eff}} = 8.31752\, r_{\mathrm{min}}$ for the effective range.

In Ref. [13], slightly different numbers are obtained for n_{th} and γ_{sr}. This deviation is due to the fact that in Ref. [13] the quantity $n_{\mathrm{th}} + \gamma(E)$ was extrapolated towards the threshold from bound-state energies that obviously leave a certain gap, which corresponds to the binding energy of the least bound state, to $E = 0$. From the phase shift, which is a continuous quantity, the threshold quantum number n_{th} can be explicitly calculated via Eq. (5.8) to arbitrary precision without any extrapolation.

5.2.2 (6|3) Lennard-Jones potential

We want to demonstrate the applicability of our formalism also for the case of an inverse-cube tail. A model potential with a $-1/r^3$ tail can simply be constructed using the well-known Lennard-Jones form. The potential

$$V_{6|3}(r) = \mathcal{E} \left[\left(\frac{r_{\mathrm{min}}}{r} \right)^6 - 2 \left(\frac{r_{\mathrm{min}}}{r} \right)^3 \right], \tag{5.9}$$

will in the following be referred to as the (6|3) Lennard-Jones potential. As in the case of a (12|6) Lennard-Jones potential, the distance r_{min} is the position of the potential minimum, and $V_{6|3}(r_{\mathrm{min}}) = -\mathcal{E}$ is its minimum energy. The zero of this potential is given by $\sigma = 2^{-1/3} r_{\mathrm{min}}$. The total number of bound states can again be estimated by evaluating the modified WKB expression (3.4) for the threshold quantum number n_{th}

n	$-E_n/\mathcal{E}$	n	$-E_n/\mathcal{E}$	n	$-E_n/\mathcal{E}$
0	0.890841	8	0.085204	16	0.00128430
1	0.701602	9	0.0580083	17	0.000565823
2	0.545472	10	0.0383812	18	0.000218672
3	0.418174	11	0.0245816	19	0.0000705157
4	0.315713	12	0.0151634	20	0.0000174078
5	0.234396	13	0.00895200	21	2.77767×10^{-6}
6	0.170850	14	0.00501655	22	1.88535×10^{-7}
7	0.122024	15	0.00263932	23	8.19184×10^{-10}

Table 5.4: Scaled energy eigenvalues of the 24 vibrational s-wave bound states in a (6|3) Lennard-Jones potential (5.9) with a strength parameter of $B_{6|3} = 700$.

from the generalized Bohr-Sommerfeld quantization rule (2.45)

$$n_{\mathrm{th}} \approx \frac{1}{\pi\hbar}\int_{\sigma}^{\infty}\sqrt{-2\mu V_{6|3}(r)}\,dr - 1 = \frac{2^{2/3}}{\sqrt{\pi}}\frac{\Gamma(7/6)}{\Gamma(5/3)}\sqrt{B_{6|3}} - 1\,, \tag{5.10}$$

where the outer reflection phase is given by its threshold value $\phi_{\mathrm{out}}(0) = 3\pi/2$ (see Eq. (4.19)) and the inner reflection phase is assumed to be given by its conventional semiclassical value $\phi_{\mathrm{in}}(0) = \pi/2$. As in the previous case of a (12|6) Lennard-Jones potential, the radial Schrödinger equation depends only on the strength parameter $B_{6|3} = 2\mu\mathcal{E}r_{\mathrm{min}}^2/\hbar^2$ and the energy in units of the well depth $\mathcal{E}$.

For our analysis we choose a strength parameter of $B_{6|3} = 700$. Estimating the number of bound states via Eq. (5.10) yields $n_{\mathrm{th}} \approx 23.3507$, i.e., the potential supports 24 bound states and the threshold quantum number's remainder is $\Delta_{\mathrm{th}} \approx 0.3507$.

The dispersion coefficient of the inverse-power tail potential is $C_3 = 2\mathcal{E}r_{\mathrm{min}}^3$. The corresponding characteristic length scale β_3 can be expressed in terms of $B_{6|3}$ and r_{min},

$$\beta_3 = 2B_{6|3}r_{\mathrm{min}}\,. \tag{5.11}$$

Thus we find that the energy $\mathcal{E}_3$ is connected to the well depth via $\mathcal{E} = 4B_{6|3}^3\mathcal{E}_3$. For the particular case of $B_{6|3} = 700$, this means $\mathcal{E} = 1.327 \times 10^9\mathcal{E}_3$.

The exact bound-state solutions of the Schrödinger equation with the potential (5.9) and the corresponding eigenenergies have been calculated for $B_{6|3} = 700$ and are listed in Table 5.4. They have already been published in Ref. [71]. Knowing these bound-state energies, the short-range parametrization can be obtained for energies below the dissociation threshold $E = 0$. Since $n_{\mathrm{th}} + \gamma(E)$ is expected to be a smooth function of the energy and insensitive to the actual position of the threshold, it can be linearly extrapolated to above-threshold energies. The scattering properties such as the phase shift and the cross section for elastic scattering can be derived.

The exact energy eigenvalues are analyzed using the quantization function $F_{\alpha=3}(E)$ (4.27) for inverse-cube tails. The threshold quantum number and the behavior of the short-range correction are determined via the relation

$$n_{\mathrm{th}} + \gamma(E_n) = n + F_{\alpha=3}(E_n)\,, \tag{5.12}$$

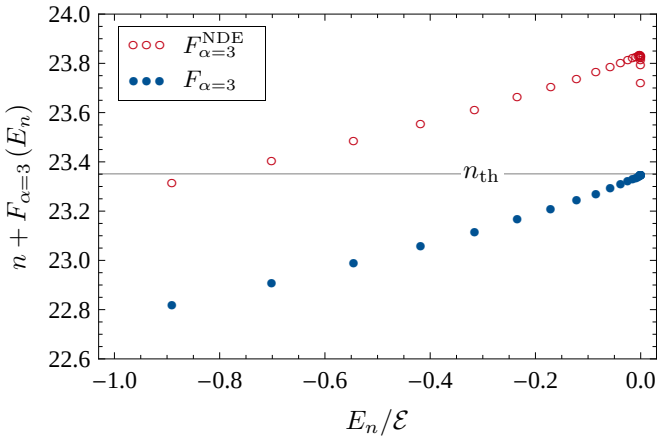

Figure 5.4: The right-hand side of Eq. (5.12) is plotted pointwise against bound-state enegies E_n in units of the depth $\mathcal{E}$ of the (6|3) Lennard-Jones potential (5.9) (filled circles). The corresponding results obtained via the LeRoy-Bernstein function (4.15) instead of the correct quantization function (4.27) are shown as empty circles.

in analogy to Eq. (5.7). The results are depicted in Figure 5.4 which shows a plot of $n_{\mathrm{th}}+\gamma(E_n)$ against the scaled bound-state energies $-E_n/\mathcal{E}$ (filled dots). In order to expose the advantages of the correct quantization function over the LeRoy-Bernstein function, the results obtained with the purely semiclassical quantization function (3.18) are also shown in Figure 5.4 as hollow dots. We find that theses results are shifted from the exact values by approximately 1/2 for high binding energies [cf. Eq. (4.29)]. For low binding energies, we find that the exact values smoothly approach the exact value of the threshold quantum number as $E_n \to 0$, while the semiclassical values do not show satisfactory convergence properties.

To extrapolate the short-range parameters across the dissociation threshold to positive energies, the parameters n_{th} and γ_{sr} in Eq. (5.12) are determined by fitting a straight line to the dots presented in Figure 5.4 using only the highest-lying states. For this procedure, the high accuracy of the outer reflection phase in Eq. (4.26) becomes important since the difference of the values $n+F_{\alpha=3}(E_n)$ for the highest two bound states is only 2.76725×10^{-7}. The uncertainty of the quantization function (4.27) should be noticeably smaller than this difference, as is the case in the present work (see Figure 4.3). From the data shown in Figure 5.4 the threshold quantum number is extracted as $n_{\mathrm{th}} = 23.3512$, which agrees to within 5×10^{-4} with the value $n_{\mathrm{th}} \approx 23.3507$ obtained from Eq. (5.10). The leading-order coefficient γ_{sr} of the short-range correction $\gamma(E)$ to the quantization function is found to be $\gamma_{\mathrm{sr}} = 1.47417/\mathcal{E}$. This coefficient can be related to a length scale β_{sr} for the short range effects by $\gamma_{\mathrm{sr}} = 2\mu\beta_{\mathrm{sr}}^2/\hbar^2$. This gives $\beta_{\mathrm{sr}} \approx 0.05\, r_{\mathrm{min}}$ which is very small compared to characteristic length parameter of the potential tail, $\beta_3 = 1400\, r_{\mathrm{min}}$ (see Eq. (5.11)). Relating the short-range correction to the energy scale $\mathcal{E}_3$ yields $\gamma_{\mathrm{sr}} = 1.11\times10^{-9}/\mathcal{E}_3$.

With these values, we can predict the low-energy scattering properties of the (6|3) Lennard-Jones potential (5.9) with the strength parameter $B_{6|3} = 700$. Figure 5.5 shows the results for s-wave cross section σ_0 (dotted line) as obtained via Eq. (2.25) with the phase shift obtained from Eq. (3.30) and the values for n_{th} and γ_{sr} as determined from the bound-state spectrum. These results are compared to the exact values for the cross section,

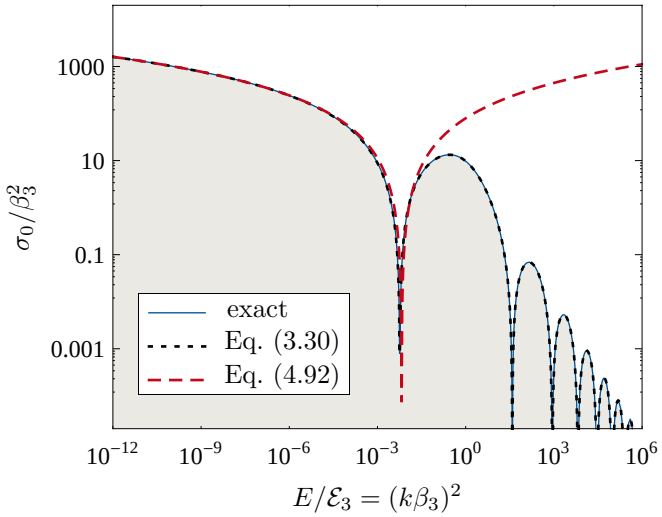

Figure 5.5: The s-wave scattering cross section for the (6|3) Lennard-Jones potential (5.9) with $B_{6|3} = 700$ is plotted in units of β_3^2 against the energy in units of $\mathcal{E}_3$ on a doubly logarithmic scale. The exact values (solid line) are obtained by solving the Schrödinger equation numerically. They are accurately reproduced by the dotted line which illustrates the results obtained via Eq. (3.30) with the correct values for n_{th} and γ_{sr}. The corresponding low-energy expansion (dashed line) is obtained from the threshold law (4.92) for inverse-cube tails.

which are obtained by solving the radial Schrödinger equation (2.6) numerically (solid line). We find that the values for the cross section σ_0 are practically indistinguishable. The values for the s wave phase shift agree to within 10^{-5} over the whole energy range considered. Figure 5.5 also gives the low-energy expansion of the cross section (dashed line) as obtained via the low-energy expansion (4.92) of the phase shift for potentials with inverse-cube tails using the value $\Delta_{\text{th}} = 0.3512$. It is found that this expression gives the correct low-energy behavior of the cross section and might offer an estimate of its actual value up to the energies $\sim 10^{-2}\mathcal{E}_3$. The correctness of the threshold law (4.92) for inverse-cube tails is hereby verified.

5.2.3 Model potential with a mixed tail

The potential tail may contain nonnegligible contributions in addition to its leading $1/r^\alpha$ term, and these contributions can affect the long-range behavior of the wave function in a significant way, even very close to threshold. To show how the definition of the potential tail needs to be modified in case of such a potential tail, we study the scattering by a potential that has a tail that can be expressed as the sum of two inverse-power terms. This application of the formalism developed in Chapter 3 has been published in Ref. [60].

As an example, consider a potential tail consisting of two inverse-power terms

$$V_{\text{tail}}(r) = -\frac{C_4}{r^4} - \frac{C_6}{r^6} = -\frac{\hbar^2}{2\mu}\left[\frac{(\beta_4)^2}{r^4} + \frac{(\beta_6)^4}{r^6}\right] . \tag{5.13}$$

as typically occur in the interaction of an neutral compound particle with a compound particle that has nonzero net charge, e.g., the interaction of an atom with an ion. The

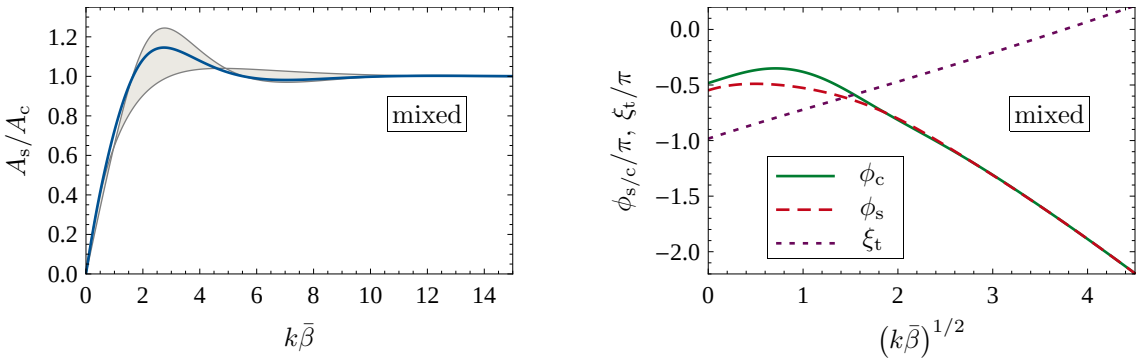

Figure 5.6: The ratio A_s/A_c of the amplitudes defined in Eqs. (3.29) for the mixed tail (5.13) with $\beta_4 = \beta_6 \equiv \bar{\beta}$. The shaded area is bounded by the corresponding results for the single-power tails that are already shown in Figs. 4.5 and 4.11 respectively. The corresponding phases ϕ_s and ϕ_c for the mixed tail (5.13) with $\beta_4 = \beta_6 \equiv \bar{\beta}$. The short-dashed line shows the phase ξ_t defined by Eq. (3.9).

theory described in Chapter 3 is easily applied to such mixed tails. The tail functions depend on the relative weights of the two terms in (5.13), as given, e.g., by $\lambda = (\beta_4/\beta_6)^2$. The zero-energy solutions $w_0(r)$ and $w_1(r)$ for the mixed tail potential (5.13) can be given in terms of hypergeometric functions for arbitrary values of λ (see Ref. [99]). The low-energy behavior of the tail functions can thus be given analytically [54, 100]. The ratio of the amplitudes is

$$\frac{A_s}{A_c} \overset{k\to 0}{\sim} 2 \left| \frac{\Gamma\left(\frac{3}{4} - \frac{1}{4}i\lambda\right)}{\Gamma\left(\frac{1}{4} - \frac{1}{4}i\lambda\right)} \right| (k\beta_6)\,, \tag{5.14}$$

and the threshold values of the phases are given by

$$\begin{aligned}
\phi_s(0) &= -\frac{5\pi}{8} - \frac{\lambda}{4}\left(1 - \ln\left(\frac{\lambda}{4}\right)\right) + \arg\Gamma\left(\frac{1}{4} - \frac{i\lambda}{4}\right)\,, \\
\phi_c(0) &= -\frac{3\pi}{8} - \frac{\lambda}{4}\left(1 - \ln\left(\frac{\lambda}{4}\right)\right) + \arg\Gamma\left(\frac{3}{4} - \frac{i\lambda}{4}\right)\,, \\
\xi_t(0) &= -\frac{7\pi}{8} - \frac{\lambda}{4}\left(1 - \ln\left(\frac{\lambda}{4}\right)\right) + \arg\Gamma\left(\frac{3}{4} - \frac{i\lambda}{4}\right)\,,
\end{aligned} \tag{5.15}$$

all depending on the relative weight λ of the two terms of the mixed tail potential (5.13). To construct a specific example, we choose the two characteristic lengths to be identical, $\beta_4 = \beta_6 \equiv \bar{\beta}$, so the mean scattering length and the threshold length are

$$\bar{a} = 0.187041\,\bar{\beta}\,, \quad b = 0.899758\,\bar{\beta}\,. \tag{5.16}$$

Therefore the ratio of amplitudes then is

$$A_s/A_c \overset{k\to 0}{\sim} 0.918994\,(k\bar{\beta}) \tag{5.17}$$

at low energies. The left panel of Figure 5.6 shows the ratio A_s/A_c of the amplitudes as function of $k\bar{\beta}$, together with the results for the single-power tails $V_6(r)$ and $V_4(r)$ that are already shown in Figures. 4.5 and 4.11 respectively. As expected, we find that the ratio of

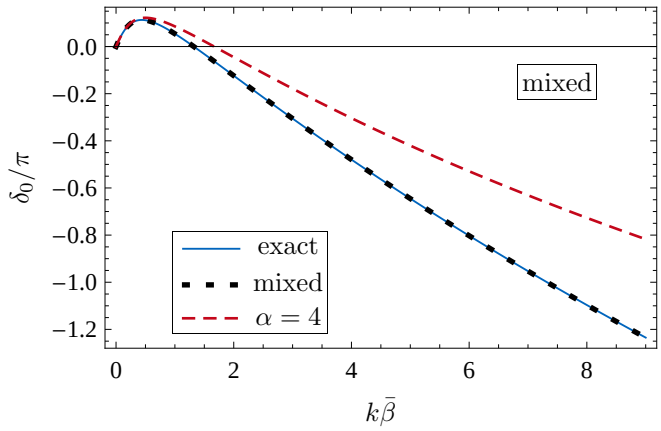

Figure 5.7: s-wave phase shift δ_0 as function of $k\bar{\beta}$ for the model potential (5.19). The exact values (solid line) are reproduced within $3 \times 10^{-6}\pi$ by the formula (3.30) with the tail functions for the mixed tail (5.13), see Figure 5.6. In contrast, using the tail functions of the single-power $1/r^4$ case (dashed line) is insufficient beyond the immediate near-threshold regime.

amplitude $A_\mathrm{s}/A_\mathrm{c}$ essentially lies between the values of its single-power counterparts. For higher energies it is closer to the values for a pure $-1/r^6$ reference potential.

The phases ϕ_s, ϕ_c that are obtained by solving the radial Schrödinger equation (2.6) are plotted in the right panel Figure 5.6 as functions of $(k\bar{\beta})^{1/2}$ together with the phase ξ_t defined by Eq. (3.9). They start at the values

$$\begin{aligned} \phi_\mathrm{s}(0) &= -\,0.547875\,\pi\,, \\ \phi_\mathrm{c}(0) &= -\,0.482634\,\pi\,, \\ \xi_\mathrm{t}(0) &= -\,0.982634\,\pi\,. \end{aligned} \tag{5.18}$$

according to Eqs. (5.15). For a single-power $1/r^4$ potential tail, this plot would be a straight line in the semiclassical region, $(k\bar{\beta})^{1/2} \gtrsim 2$. An explicit analytical expression for ξ_t is not available for the mixed tail (5.13).

We now apply the theory to the potential

$$V(r) = \frac{\hbar^2}{2\mu}\left[\frac{(\beta_\mathrm{rep})^{10}}{r^{12}} - \frac{\bar{\beta}^4}{r^6} - \frac{\bar{\beta}^2}{r^4}\right] \tag{5.19}$$

with $\beta_\mathrm{rep} = \bar{\beta}/7$. The threshold quantum number is estimated via (2.45) with the threshold value of the outer reflection phase for the tail potential (5.13) given in Ref. [99] as $n_\mathrm{th} \approx 87.865788$, so the potential supports 88 bound states. The scattering length is numerically determined as $a = -1.817681\,\bar{\beta}$, so the correct value of the remainder, which follows with (5.16) from Eq. (3.60) is $\Delta_\mathrm{th} = 0.865714$. Figure 5.7 shows the exact phase shift (solid line) together with the prediction of Eq. (3.30) (short-dashed line). The agreement is better than $3 \times 10^{-6}\pi$ in the range covered by this figure.

If we were to take $V_\mathrm{tail}(r)$ to be given by the leading single-power term $V_4 = -C_4/r^4$ only, then $\bar{a}$ would vanish and b would be equal to $\bar{\beta}$. This would imply choosing $\Delta_\mathrm{th} = 0.839903$, in order to reproduce the exact scattering length which is a property of the full potential (5.19) via Eq. (3.60). However, with this choice of Δ_th, the single-power

treatment can reproduce only the immediate near-threshold behaviour of the exact phase shift. This is shown by the long-dashed line in Figure 5.7, which is the corresponding prediction of Eq. (3.30) based on tail functions for $1/r^4$ potentials as given in Section 4.3.4. It does not reproduce the exact values at high energies; significant deviations become noticeable already at very small energies ($k\bar{\beta} \approx 0.5$).

We can conclude, that using only the leading-order inverse power term $-C_4/r^4$ is not sufficient to properly describe the scattering properties of the potential (5.19). However, including the next-to-leading order term in the definition of $V_{\text{tail}}(r)$ [see Eq. (5.13)], a clean separation between tail and short-range effects is achieved also for this case.

5.3 Summary of results

The quantization function $F_{\alpha=3}(E)$ (4.27) for inverse-cube tails has been applied to highly excited states in homonuclear dimers forming long-range molecules, in order to achieve a separation of the influence of the long-range tail potential on the bound-state spectrum from effects due to the short-range part of the potential. Its performance has been compared to that of the semiclassical LeRoy-Bernstein function (4.15). The correct quantization function (4.27) has been used to extrapolate a known stretch of the spectrum towards higher energies all the way to the dissociation threshold. Short-range effects have been included via Eq. (5.12), and the determination of n_{th} is all the more accurate, the closer the states used for the extrapolation are to threshold. This is in contrast to the LeRoy-Bernstein formula which has the wrong energy dependence near threshold.

For a (12|6) Lennard Jones model potential the bound-state spectrum and the scattering phase shift have been calculated numerically. The use of the quantization function $F_{\alpha=6}(E)$ [13] and the tail functions $A_{\text{s}}/A_{\text{c}}$, ϕ_{s}, ϕ_{c}, and ξ_{t} as obtained with the single inverse-power reference potential $V_6(r) = -C_6/r^6$ (see Section 4.3.2) provides a good separation of the tail effects and the short-range correction $\gamma(E)$ to n_{th} is found to be a smooth function that is not sensitive to the actual position of the threshold energy.

The threshold quantum number n_{th} of a given (6|3) Lennard-Jones potential has explicitly been determined from its the bound state spectrum. With this result the scattering properties have been obtained from the knowledge of the bound-state spectrum by extrapolating the leading-order term of $n_{\text{th}} + \gamma(E)$ to positive energies. This procedure is found to be very accurate. The corresponding results obtained for the scattering cross section are in excellent agreement with the exact values. The correct value of the threshold quantum number's remainder Δ_{th} provides the correct threshold law according to Eq. (4.92).

In many realistic cases a single-power tail might not be sufficient to even reproduce the correct low-energy behavior of the scattering phase shift. For the case of a mixed tail potential (5.13) the performance of the tail functions obtained from the mixed reference potential has been compared to that of the tail functions for a pure $-1/r^4$ tail as given in Section 4.3.4. It is found that the exact phase shift which is accurately reproduced by the tail functions of the mixed reference potential differs significantly from the single-power estimate even at very low energies.

Chapter 6

Conclusions and Outlook

In the present thesis, a theoretical framework is presented that offers a clean and transparent separation of the short-range physics from the influence of the long-range potential tail in near-threshold quantization and scattering phenomena in the presence of tail potentials that are more singular than $-1/r^2$ at the origin and vanish faster than $1/r^2$ asymptotically. For two-body interaction potentials that occur in the field of atomic physics, the long-range tail of the interaction potential can be calculated explicitly, e.g., by using perturbation theory, while the short-range part of the potential remains unknown in general.

The separation of short-range effects from the influence of the tail potential is achieved by constructing a short-range wave function (Section 3.1) that serves as a boundary condition for the tail potential. With this boundary condition, the wave function in the presence of the full interaction potential $V(r)$ is reproduced using only the tail potential $V_{\text{tail}}(r)$ as reference. The short-range wave function is analytically accessible via the framework of the modified WKB approximation, which is presented in Section 2.2. The short-range parametrization includes the noninteger remainder Δ_{th} of the threshold quantum number n_{th} that is a property of the full interaction potential. The parametrization is essentially insensitive to the actual position of the threshold energy. It thus promotes the understanding of the interdependence of scattering properties and bound-state spectra in potentials with singular attractive tails.

The concept of the quantization function that has originally been developed in Refs. [13, 41, 43] is revisited (Section 3.2) in order to keep the presentation self contained. In fact, the derivation of the quantization function using the actual form of a short-range solution (3.8), as performed in the present work, is even more insightful concerning the separation of short-range effects from the influence of the tail potential.

A formulation for the scattering properties in the presence of singular attractive tail potentials has been developed in Section 3.3. A formula for the scattering phase shift [Eq. (3.30)] is presented, which depends only on the properties of the tail potential and the threshold quantum number's noninteger remainder Δ_{th}. Further short-range corrections might be included by replacing the remainder by the short-range parametrization $\Delta_{\text{th}} + \gamma(E)$, where $\gamma(E)$ is a smooth function of the energy that scales with the potential depth and vanishes at the dissociation threshold.

The tail potentials that are considered in the present work support neither purely elastic scattering processes nor the existence of bound states. They do, however, support the process of quantum reflection, i.e., the nonclassical reflection at an attractive potential

without any actual barrier. We explicitly related the tail functions $A_\mathrm{s}/A_\mathrm{c}$, ϕ_s and ϕ_c for elastic scattering that enter Eq. (3.30) to the physically tangible properties of the tail potential, i.e., the amplitude R for quantum reflection by and the amplitude T for transmission through the anticlassical region at rather large distances in the tail potential.

For arbitrary reference potentials that fall off faster than $1/r^2$ and are more singular than $-1/r^2$ at the origin, limiting expansions for the tail functions $A_\mathrm{s}/A_\mathrm{c}$, ϕ_s and ϕ_c, which enter the formula (3.30) for the scattering phase shift are presented. The high-energy behavior obtained from the semiclassical WKB approximation that becomes increasingly accurate in the limit of high energies. The low-energy expansions are determined by the properties of the zero-energy solutions in the tail potential; the correct threshold laws for elastic scattering are obtained.

Inverse-power potentials $V_\alpha(r) = -C_\alpha/r^\alpha$ with $\alpha > 2$ are identified to be appropriate reference potentials for the formalism developed in Chapter 3; their properties are studied in Chapter 4. It is found that all relevant properties of these potentials do not depend on the energy and the strength of the potential independently, but only on the energy in units of the characteristic energy scale $\mathcal{E}_\alpha$ of the inverse-power reference potential. The tail functions for the description of elastic scattering thus show a universal energy dependence for each power α.

For the case of below-threshold energies the quantization function is studied in the limit of high and low binding energies. The difference to the purely semiclassical LeRoy-Bernstein quantization rule is explicitly pointed out in order to show that the quantization function established in Section 3.2 reproduces the correct progression of bound states in the immediate near-threshold regime. For the case of inverse-cube tail potentials, a highly accurate analytical form of the quantization function is presented that can readily be used for the description of bound-state spectra as obtained experimentally, e.g., from photoassociation spectroscopy.

For interaction potentials with arbitrary inverse-power tails with $\alpha \geq 6$, the exact effective-range expansions of the scattering phase shift is explicitly given; the influence of the tail potential enters only in terms of the known low-energy expansions of the tail functions $A_\mathrm{s}/A_\mathrm{c}$, ϕ_s and ϕ_c that can explicitly be evaluated for inverse-power reference potentials with $\alpha \geq 6$. For the integer orders $3 \leq \alpha \leq 6$, the tail functions are given explicitly as obtained from solving the Schrödinger equation with the corresponding reference potential. For these cases, analytical modified effective-range expansions are presented that contain anomalous terms, which are characteristic for each power α and do not occur in the presence of a different tail potential.

A scattering length exists for all interaction potentials with attractive tails that fall off faster than $-1/r^3$. For the particular case of asymptotic inverse-cube interactions an anomalous terms occurs already in leading order and a finite scattering length does not exist. For this case, an exact threshold law (4.92) for elastic scattering is obtained from within our theoretical framework; a corresponding formula can not be found in the existing literature so far.

In Chapter 5 the framework that has been developed in the preceding chapters is applied to physically relevant situations. Its applicability is tested for different interaction potentials. With the help of the quantization function for inverse-cube tail potential, the near-threshold bound-state spectra of homonuclear dimers are studied. The deficiency of the purely semiclassical LeRoy-Bernstein formula becomes apparent; it fails to describe

the progression of weakly bound states, while the correct form (3.16) of the quantization function remains valid all the way to the dissociation threshold.

For model Lennard-Jones potentials, which have inverse-power tails, the interdependence of the bound-state levels and the scattering cross section is demonstrated. For s waves, the short-range parametrization is derived from the exact bound-state spectrum and the exact cross section for elastic scattering by making use of the tail functions that are derived and presented in Chapter 4 for inverse-power tail potentials. For a (6|3) Lennard-Jones potential, the threshold law (4.92) for elastic scattering by attractive inverse-cube potential tails is verified by comparison to exact numerical values.

For a model potential with a mixed tail that is the superposition of a $-1/r^4$ and a $-1/r^6$ term, results are presented in Section 5.2.3. The tail functions are calculated from the particular form of the potential tail; universal scaling laws as for the case of an pure inverse-power tail do not exist. However, the separation of the influence of the tail potential from short-range effects is also achieved for this case. The comparison with exact numerical data for the scattering phase shift shows that the consideration of the leading $-1/r^4$ term alone does not provide an appropriate choice of the tail potential; the exact scattering phase shift differs significantly from the pure inverse-power case.

The applicability of the theoretical framework developed in the preceding chapters is thus successfully demonstrated; the appropriate choice of the reference potential provides insight into the short-range physics, which, together with the influence of the tail potential, determines the scattering properties and bound state spectra of a given two-body system.

Further prospects

The present work restricts itself to the treatment of s-wave interaction, in order to provide a comprehensive study within the limits of a doctoral thesis. However, the applicability of the theoretical framework presented is by no means restricted to the case of zero angular momentum. In rotational states the effective radial potential contains a centrifugal term [cf. Eq. (2.7)]. Including this additional term in the reference potential, it still matches the preconditions that are formulated in Chapter 3. For each partial wave, the result of Chapter 3 can be adapted. For deep potentials with inverse-power tails $V_\alpha(r) = -C_\alpha/r^\alpha$ with $\alpha > 2$, Lemeshko and Friedrich [101, 102] have derived a relation

$$n_{\mathrm{th}}(l) \approx n_{\mathrm{th}}(l=0) - \frac{l}{\alpha - 2} \tag{6.1}$$

that connects the threshold quantum number for s waves with those for higher angular momenta, in order to analyze the progression of weakly bound rotational states. The inclusion of higher angular momenta thus does not necessarily require the consideration of further short-range parameters, at least not for low collision energies where only few partial waves contribute to the elastic cross section. The tail functions are modified in such a way that the parametrization (3.30) remains valid and typical features such as shape resonances can be reproduced.

Furthermore, the applicability of the theory is not restricted to inverse-power tails as considered in Chapter 4 or tail potentials that are certain superpositions of inverse-power term as in Section 5.2.3. As long as there is an appropriate reference potential that is more singular than $1/r^2$ and falls off faster than $1/r^2$ at large distances, the separation of

short-range effects from the influence of the tail potential can be achieved. The range of applicability can, without any loss of generality, be extended to tails including even more inverse power-terms as might be appropriate for the full description of the interaction of two ground state atoms (see Appendix A) or to the case of more complicated structures of the tail potential. The present formalism has already been successfully applied to the description of the Strontium dimer Sr_2 [103] including all terms of the dispersion forces up to and including the induced quadrupole-quadrupole interaction and considering nonzero angular momenta.

The interaction of atoms and molecules with each other and with ionic partners can, in general, not be assumed to be solely determined by single-channel physics. Typical interatomic interactions are modified by multichannel phenomena. In elastic scattering of two compound particles, Feshbach resonances might occur, which modify the observed bound-state spectra and scattering cross sections (see, e.g., Ref. [4]). This is due to the prolonged lifetime of the scattering complex when closed-channel bound states become accessible. In a recent study [104] based on the results of the present thesis, it is shown how, under given circumstances, the existence of a Feshbach resonance essentially modifies the short-range parametrization in the following fashion

$$\Delta_{\mathrm{th}} \to \Delta_{\mathrm{th}} - \frac{1}{\pi} \arctan\left(\frac{\bar{\Gamma}/2}{E - E_{\mathrm{R}}}\right) , \tag{6.2}$$

where $\bar{\Gamma}$ is the resonance width, which is independent of the energy, and E_{R} is the actual resonance position. With the parametrization (6.2), the multichannel problem can effectively be reduced to a single-channel problem with adapted boundary conditions. Analyzing experimental data, as in the spirit of Section 5.2, then reveals the specific resonant features in the short-range parameterization (6.2). This offers insight into the interdependence of multichannel spectra and scattering phenomena. Previous works, such as Refs. [76, 105, 106], that analyze the modification of bound-state spectra in the presence of channel coupling could largely benefit from this formulation, as the scattering cross sections for a collision complex in a very particular internal state can in principle be predicted from the progression of bound state energies.

Appendix A

Interatomic Potentials

This appendix discusses the typical long-range tails $V_{\text{tail}}(r)$ of the interaction potentials between two atoms, and also for the case of interaction of an atom with a charged particle such as an ion.

Atom-atom interactions

The electrostatic potential of a charge distribution at a distance much larger than the extension of the charge distribution itself can be divided into contributions stemming from different multipole moments [10]. The interaction energy between two charge distributions can be given in terms of combinations of these multipole terms. For a quantum mechanical description of these interaction terms, the coordinates relative to the center of mass coordinates are just replaced by the corresponding position operators.

Therefore, the interaction between two neutral atoms A and B can — at large internuclear separations r — be described by the interaction operator

$$\hat{W} = \hat{W}_{\text{dd}} + \hat{W}_{\text{dq}} + \hat{W}_{\text{qd}} + \hat{W}_{\text{qq}} + \dots \tag{A.1}$$

where each term is indexed by the order of the interacting multipoles.[1] The resulting forces are typically referred to as *van der Waals forces* or *dispersion forces*. The interaction of the 2^{n_A}-pole moment of particle A with the 2^{n_B}-pole moment of particle B contributes to the total asymptotic interaction energy with a term proportional to r^{-n}, with $n = n_A + n_B + 1$; induced polarizations contribute with a r^{-2n} term, as they are obtained from second-order perturbation theory with the interaction operator (A.1). Since the neutral atoms posses no net charge, the lowest order contribution in (A.1) is the dipole-dipole interaction operator

$$\hat{W}_{\text{dd}} = \frac{1}{r^3}\left(\hat{x}_{\text{A}}\hat{x}_{\text{B}} + \hat{y}_{\text{A}}\hat{y}_{\text{B}} - 2\hat{z}_{\text{A}}\hat{z}_{\text{B}}\right) \tag{A.2}$$

acting on both the elements of $\mathcal{H}_{\text{A}}$ and $\mathcal{H}_{\text{B}}$, which are the Hilbert spaces containing the atomic states of atom A and B, respectively. The strength coefficient of the interaction can be calculated via perturbation theory in a straightforward fashion [12].

[1] d=dipole, q=quadrupole, and so forth.

Two atoms in spherically symmetric ground states, such as alkali metal atoms, neither posses permanent dipole nor quadrupole moments. Therefore the lowest-order contribution to the interaction energy originates from the second-order perturbation with the dipole-dipole operator and gives

$$V_{\text{tail}}(r) = -\frac{C_6}{r^6}\,, \tag{A.3}$$

for sufficiently large internuclear separations. The interaction strength C_6 is referred to as the *dispersion coefficient*. The induced dipole-dipole interaction is always attractive, since a second-order correction to the ground state is always negative [53]. In this case, the next-to-leading terms are $-C_8/r^8$ from the induced dipole-quadrupole interaction and $-C_{10}/r^{10}$ from the induced quadrupole-quadrupole interaction [107].

The situation changes when both interacting atoms have a nonvanishing orbital angular momentum and total angular momentum. The expectation value of the dipole moment vanishes in every pure atomic state [53], but for certain atomic states ($L \neq 0$, $J \neq 0, 1/2$) the expectation value of the quadrupole moment is nonzero. In these cases, we obtain

$$V_{\text{tail}}(r) = \pm\frac{C_5}{r^5}\,. \tag{A.4}$$

This interaction can either be attractive or repulsive, depending on the particular internal states of the interacting atoms.

The special case of the interaction of two identical atoms in different internal states has a certain peculiarity: each state of the system has an additional double degeneracy due to the possibility of exchanging the atoms' internal states. For atoms in different states that are connected via a nonvanishing probability of a dipole transition, there will be nonzero off-diagonal matrix elements already from first-order corrections due to the dipole-dipole interaction (cf. [12, 107])

$$V_{\text{tail}}(r) = \pm\frac{C_3}{r^3}\,. \tag{A.5}$$

This type of interaction is referred to as the *resonant dipole-dipole interaction* [89]. It can either be attractive or repulsive.

In general, all of the atom-atom interactions might be modified due to retardation effects (see Refs. [9, 108, 109]). These effects are not considered in this work.

Atom-ion interaction

When interacting with an ion or a point charge, the atom is instantaneously exposed to the Coulomb field caused by the partner's charge $\phi_{\text{Coulomb}}(r) \propto -1/r$. The lowest possible order of multipole interactions might occur, when the atom is in an internal state so that it possesses a nonvanishing expectation value of the quadrupole moment, as discussed in the context of Eq. (A.4). In this rather exotic case the atom-ion interaction could in principle be $\propto 1/r^3$.

For more common cases, i.e., when the atom is in its ground state, the leading order term will be due to the second-order contribution from the perturbation with the charge-dipole interaction term that itself is $\propto 1/r^2$. The asymptotic interaction energy can then

be given as

$$V_{\mathrm{tail}}(r) = -\frac{C_4}{r^4} = -\frac{\alpha_{\mathrm{d}}}{2\,r^4}\,, \tag{A.6}$$

with α_{d} being the static dipole polarizability (see, e.g., Refs. [53, 110]). For ground-state atoms this interaction is always attractive. The long-range interaction potential between an atom and an electron is also of the form (A.6). This long-range attraction can in principle enable the formation of negatively charged ions [53].

Appendix B

The Transmission Amplitude

While not essentially a primary subject of the present work, the low-energy expansion of the transmission coefficient in the process of quantum reflection by attractive singular potentials is given for the reason of self-consistence.

This quantum reflection process can in general be characterized by the stationary wave function

$$\frac{T}{\sqrt{p(r)}}\exp\left(-\frac{i}{\hbar}\int_{r_E}^{r}p(r')dr'\right)\longleftrightarrow\frac{1}{\sqrt{\hbar k}}\left[\exp(-ikr)+R_r\exp(ikr)\right] \tag{B.1}$$

(see, e.g., Refs. [67, 78]). This notation means that the solution of the Schrödinger equation that behaves as an inward traveling wave in the inner region is split up into an inward traveling wave plus a reflected wave in the outer asymptotic region. The subscript r refers to the *right* (i.e. outer) side from which the wave is incident in the first place.

Chosing a suitable linear combination of the solution (B.1) and its complex conjugate, we can also find the solution that correctly describes the process of *near-side quantum reflection* [68], i.e., an outward traveling wave being reflected by the potential.

$$\frac{1}{\sqrt{p_0(r)}}\left[\exp\left(\frac{i}{\hbar}\int_{r_E}^{r}p(r')dr'\right)+R_l\exp\left(-\frac{i}{\hbar}\int_{r_E}^{r}p(r')dr'\right)\right]\longleftrightarrow\frac{T}{\sqrt{\hbar k}}\exp(ikr)\,. \tag{B.2}$$

From this expression it follows for the reflection amplitude

$$R_l=-\left|R_r\right|\mathrm{e}^{-i\phi_{R_r}}\mathrm{e}^{2i\phi_T}\,, \tag{B.3}$$

which shows, that the very general relationships

$$T_r=T_l\equiv T\,,\qquad R_l=-R_r^*\frac{T}{T^*}\,, \tag{B.4}$$

connecting the left-side transmission and reflection to the corresponding right-side quantities [54, 69] is well fulfilled.

For singular potential tails, the near-threshold behavior of the transmission amplitude can be determined by comparing

$$\frac{\sqrt{\hbar k}}{\sqrt{p_0(r)}}\frac{1}{T}\exp\left(\frac{i}{\hbar}\int_{r_E}^{r}p_E(r')dr'\right)+\begin{pmatrix}\text{inward-traveling}\\ \text{WKB wave}\end{pmatrix}\longleftrightarrow\exp(ikr)\,. \tag{B.5}$$

to an appropriate linear combination of the zero-energy solutions introduced in (3.19) and (3.20).

At low energies the asymptotic form can be written as

$$\mathrm{e}^{ikr} \overset{kr\to 0}{\sim} 1 + ikr + \mathcal{O}(k^2) = w_0(r) + ikw_1(r) + \mathcal{O}(k^2)\,. \tag{B.6}$$

In the limit $r \to 0$ the wave function satisfying the boundary condition (B.5) reads

$$\frac{1}{\sqrt{p_0(r)}}\left\{D_0 \cos\left(\frac{1}{\hbar}\int_\infty^r p_0(r')dr' + \frac{\phi_0}{2}\right) + ikD_1 \cos\left(\frac{1}{\hbar}\int_\infty^r p_0(r')dr' + \frac{\phi_1}{2}\right)\right\}, \tag{B.7}$$

which can be split up into an outward- and an inward-traveling part

$$\frac{1}{\sqrt{p_0(r)}}\frac{D_0\mathrm{e}^{i\phi_0/2} + ikD_1\mathrm{e}^{i\phi_1/2}}{2}\exp\left(\frac{i}{\hbar}\int_\infty^r p_0(r')dr'\right) + \begin{pmatrix}\text{inward-traveling}\\ \text{WKB wave}\end{pmatrix}. \tag{B.8}$$

Comparing only the outward-traveling part of Eqs. (B.5) and (B.8) gives an expression for the transmission amplitude

$$T \overset{k\to 0}{\sim} \frac{2\sqrt{\hbar k}}{D_0\mathrm{e}^{i\phi_0/2} + ikD_1\mathrm{e}^{i\phi_1/2}}\exp\left[\frac{i}{\hbar}\lim_{r\to 0}\left(\int_{r_E}^r p_E(r')dr' - \int_\infty^r p_0(r')dr'\right)\right] + \mathcal{O}(k^2)\,, \tag{B.9}$$

which can — to order k — be rephrased as

$$T \overset{k\to 0}{\sim} 2\frac{\sqrt{\hbar k}}{D_0}(1 - i\bar{a}k - bk) \exp\left[i\left(-\frac{\phi_0}{2} + \frac{1}{\hbar}\int_0^{r_E}\left[p_0(r) - p_E(r)\right]dr + \frac{1}{\hbar}\int_{r_E}^\infty p_0(r)dr\right)\right] + \mathcal{O}(k^2)\,. \tag{B.10}$$

With $T = |T|\,\mathrm{e}^{i\phi_T}$ we can write

$$|T| \overset{k\to 0}{\sim} 2\frac{\sqrt{\hbar k}}{D_0}\left[1 - bk + \mathcal{O}(k^2)\right], \tag{B.11}$$

$$\phi_T \overset{k\to 0}{\sim} -\frac{\phi_0}{2} + \frac{1}{\hbar}\int_0^{r_E}\left[p_0(r) - p_E(r)\right]dr + \frac{1}{\hbar}\int_{r_E}^\infty p_0(r)dr - \bar{a}k + \mathcal{O}(k^2) \tag{B.12}$$

for the modulus and the phase of the transmission amplitude.

Note that, with the well-known relation $|R| \overset{k\to 0}{\sim} 1 - 2bk + \mathcal{O}(k^2)$ [78] the conservation rule for the flux density (3.36) gives the identity

$$D_0 = \sqrt{\hbar/b} \tag{B.13}$$

and therefore

$$|T| \overset{k\to 0}{\sim} 2\sqrt{bk}\left[1 - bk + \mathcal{O}(k^2)\right]. \tag{B.14}$$

Furthermore, it has to be mentioned that the result for phase of the transmission amplitude (B.12), that is correctly derived here, is not identical to the result obtained in Ref. [68], since the matching to the given zero-energy solutions was performed wrong in that work.

Appendix C

Verification of asymptotic expansions

In the present work and especially in Chapter 4 asymptotic expansions of given quantities play a major role. A tool that is used to verify the correctness of the expansions obtained by analytical means is introduced and explained in the following.

Consider a function $f(x)$. This function can be written in the form

$$f(x) = \sum_{n=0}^{\infty} f_n x^{p_n} \,, \tag{C.1}$$

where $\{p_n\}$ is a strictly monotonic increasing sequence of positive rational numbers. The function $f(x)$ can be written as an asymptotic expansion

$$f(x) \overset{x\to 0}{\sim} \underbrace{\sum_{n=0}^{N} f_n x^{p_n}}_{=f_N(x)} + \mathcal{O}(x^{p_{N+1}}) \,, \tag{C.2}$$

which defines the function $f_N(x)$ that includes the leading order terms of $f(x)$ up to and including the term $\mathcal{O}(x^{p_N})$, where N is a given integer number. We can now define

$$\Delta f_N = f(x) - f_N(x) = \sum_{n=N+1}^{\infty} f_n x^{p_n} \tag{C.3}$$

which gives the remaining higher-order terms of $f(x)$ that have not been included into $f_N(x)$. The ratio

$$\frac{\Delta f_N}{x^{p_N}} = \sum_{n=N+1}^{\infty} f_n x^{(p_n - p_N)} \tag{C.4}$$

has a particular property, i.e., it tends to zero in the limit of small arguments x,

$$\lim_{x\to 0} \frac{\Delta f_N}{x^{p_N}} = 0 \,, \tag{C.5}$$

which is due to the fact that $p_n - p_N > 0 \; \forall n \geq N+1$. This property is self-evident, but can be made use of, in case that expansion coefficients f_n are not known in general.

If we now consider a function $g(x)$, we can state

$$\lim_{x \to 0} \frac{g(x) - f(x)}{x^{p_N}} = 0 \tag{C.6}$$

if and only if

$$g(x) \overset{x \to 0}{\sim} f_N(x) + \mathcal{O}(x^{p_{N+1}}) \,, \tag{C.7}$$

i.e., if and only if $g(x)$ is identical to $f(x)$ up on and including the term of the order $\mathcal{O}(x^{p_n})$.

Knowing the values of the function $f(x)$, but not its expansion coefficients, offers the opportunity to check whether a candidate function $g(x)$ reproduces the correct lower-order behavior of the function $f(x)$ up to and including the order $\mathcal{O}(x^{p_N})$.

Bibliography

[1] J. J. Balmer, Ann. Phys. (Leipzig) **261**, 80 (1885).

[2] E. Schrödinger, Ann. Phys. (Leipzig) **386**, 109 (1926).

[3] E. Rutherford, Philos. Mag. **21**, 669 (1911).

[4] H. Friedrich, *Theoretical atomic physics*, Springer, Berlin, 2006.

[5] M. J. Seaton, Rep. Prog. Phys. **46**, 167 (1983).

[6] C. Jungen, editor, *Molecular applications of quantum defect theory*, IOP, 1996.

[7] R. Eisenschitz and F. London, Z. Phys. **60**, 491 (1930).

[8] F. London, Z. Phys. **63**, 245 (1930).

[9] H. B. G. Casimir and D. Polder, Phys. Rev. **73**, 360 (1948).

[10] J. D. Jackson, *Classical electrodynamics*, Wiley, New York, 1966.

[11] T. F. Gallagher, *Rydberg atoms*, Cambridge Univ. Press, Cambridge, 1994.

[12] C. Cohen-Tannoudji, B. Diu, and F. Laloë, *Quantum mechanics*, Wiley, New York.

[13] P. Raab and H. Friedrich, Phys. Rev. A **78**, 022707 (2008).

[14] R. J. LeRoy and R. B. Bernstein, J. Chem. Phys. **52**, 3869 (1970).

[15] W. C. Stwalley, Chem. Phys. Lett. **6**, 241 (1970).

[16] M. H. Anderson, J. R. Ensher, M. R. Matthews, C. E. Wieman, and E. A. Cornell, Science **269**, 198 (1995).

[17] K. B. Davis, M.-O. Mewes, M. R. Andrews, N. J. van Druten, D. S. Durfee, D. M. Kurn, and W. Ketterle, Phys. Rev. Lett. **75**, 3969 (1995).

[18] M.-O. Mewes, M. R. Andrews, D. M. Kurn, D. S. Durfee, C. G. Townsend, and W. Ketterle, Phys. Rev. Lett. **78**, 582 (1997).

[19] I. Bloch, T. W. Hänsch, and T. Esslinger, Phys. Rev. Lett. **82**, 3008 (1999).

[20] M. Greiner, O. Mandel, T. Esslinger, T. W. Hänsch, and I. Bloch, Nature (London) **415**, 39 (2002).

[21] Y.-J. Lin, R. L. Compton, K. Jiménez-García, W. D. Phillips, J. V. Porto, and I. B. Spielman, Nat. Phys. **7**, 531 (2011).

[22] S. Ospelkaus, K.-K. Ni, D. Wang, M. H. G. de Miranda, B. Neyenhuis, G. Quéméner, P. S. Julienne, J. L. Bohn, D. S. Jin, and J. Ye, Science **327**, 853 (2010).

[23] K.-K. Ni, S. Ospelkaus, D. Wang, G. Quéméner, B. Neyenhuis, M. H. G. de Miranda, J. L. Bohn, J. Ye, and D. S. Jin, Nature (London) **464**, 1324 (2010).

[24] E. Tiesinga, A. J. Moerdijk, B. J. Verhaar, and H. T. C. Stoof, Phys. Rev. A **46**, R1167 (1992).

[25] E. Timmermans, P. Tommasini, M. Hussein, and A. Kerman, Phys. Rep. **315**, 199 (1999).

[26] C. Chin, R. Grimm, P. Julienne, and E. Tiesinga, Rev. Mod. Phys. **82**, 1225 (2010).

[27] P. G. Burke, *Potential scattering in atomic physics*, Plenum Press, 1977.

[28] J. R. Taylor, *Scattering theory: the quantum theory on nonrelativistic collisions*, Wiley, New York, 1972.

[29] R. G. Newton, *Scattering theory of waves and particles*, Springer, New York, 1982.

[30] E. Fermi and L. Marshall, Phys. Rev. **71**, 666 (1947).

[31] J. S. Schwinger, Phys. Rev. **72**, 742 (1947).

[32] J. M. Blatt and J. D. Jackson, Phys. Rev. **76**, 18 (1949).

[33] H. A. Bethe, Phys. Rev. **76**, 38 (1949).

[34] T. F. O'Malley, L. Spruch, and L. Rosenberg, J. Math. Phys. **2**, 491 (1961).

[35] T. F. O'Malley, L. Rosenberg, and L. Spruch, Phys. Rev. **125**, 1300 (1962).

[36] B. R. Levy and J. B. Keller, J. Math. Phys. **4**, 54 (1963).

[37] B. Gao, Phys. Rev. A **78**, 012702 (2008).

[38] Z. Idziaszek, T. Calarco, P. S. Julienne, and A. Simoni, Phys. Rev. A **79**, 010702 (2009).

[39] T. M. Hanna, E. Tiesinga, and P. S. Julienne, Phys. Rev. A **79**, 040701 (2009).

[40] G. F. Gribakin and V. V. Flambaum, Phys. Rev. A **48**, 546 (1993).

[41] H. Friedrich and P. Raab, Phys. Rev. A **77**, 012703 (2008).

[42] P. Raab and H. Friedrich, Phys. Rev. A **80**, 052705 (2009).

[43] P. Raab, *Die Quantisierungsfunktion für attraktive, singuläre Potentialschwänze*, Doctoral thesis, Technische Universität München, 2009.

[44] V. V. Flambaum, G. F. Gribakin, and C. Harabati, Phys. Rev. A **59**, 1998 (1999).

[45] P. G. Burke and C. J. Joachain, *Theory of electron atom collisions*, Plenum Press, New York.

[46] N. F. Mott and H. S. W. Massey, *The theory of atomic collisions*, Clarendon Pr., Oxford, 1950.

[47] B. H. Bransden, *Atomic collision theory*, Benjamin/Cummings, Reading, 1983.

[48] M. Abramowitz, editor, *Handbook of mathematical functions: With formulas, graphs, and mathematical tables*, Dover, New York, 1968.

[49] G. Wentzel, Z. Phys. **38**, 518 (1926).

[50] H. A. Kramers, Z. Phys. **39**, 828 (1926).

[51] L. Brillouin, C. R. Acad. Sci. **183** (1926).

[52] H. Jeffreys, Proc. Math. Soc. London **23**, 428 (1925).

[53] L. D. Landau and E. M. Lifschitz, *Quantenmechanik*, Akademie-Verlag, Berlin, 1979.

[54] H. Friedrich and J. Trost, Phys. Rep. **397**, 359 (2004).

[55] M. V. Berry and K. E. Mount, Rep. Prog. Phys. **35**, 315 (1972).

[56] N. Fröman and P. O. Fröman, *JWKB Approximation: contributions to the theory*, North-Holland, Amsterdam, 1965.

[57] H. Friedrich and J. Trost, Phys. Rev. Lett. **76**, 4869 (1996).

[58] J. Trost, *Nicht-ganzzahlige Maslov-Indizes — Die Reflexionsphase in der WKB-Wellenfunktion*, Doctoral thesis, Technische Universität München, 1996.

[59] J. Trost, C. Eltschka, and H. Friedrich, J. Phys. B **31**, 361 (1998).

[60] T.-O. Müller, A. Kaiser, and H. Friedrich, Phys. Rev. A **84**, 032701 (2011).

[61] T.-O. Müller, A. Kaiser, and H. Friedrich, Phys. Rev. A **84**, 054702 (2011).

[62] R. Côté, H. Friedrich, and J. Trost, Phys. Rev. A **56**, 1781 (1997).

[63] F. Shimizu, Phys. Rev. Lett. **86**, 987 (2001).

[64] V. Druzhinina and M. DeKieviet, Phys. Rev. Lett. **91**, 193202 (2003).

[65] H. Friedrich, G. Jacoby, and C. G. Meister, Phys. Rev. A **65**, 032902 (2002).

[66] H. Friedrich and A. Jurisch, Phys. Rev. Lett. **92**, 103202 (2004).

[67] F. Arnecke, H. Friedrich, and J. Madroñero, Phys. Rev. A **74**, 062702 (2006).

[68] E. Mesfin and H. Friedrich, Phys. Rev. A **74**, 032103 (2006).

[69] R. Côté, B. Segev, and M. G. Raizen, Phys. Rev. A **58**, 3999 (1998).

[70] F. Arnecke, *Das Schwellenverhalten von Streuphasen in singulären Potentialen*, Doctoral thesis, Technische Universität München, 2008.

[71] T.-O. Müller and H. Friedrich, Phys. Rev. A **83**, 022701 (2011).

[72] R. Côté, E. I. Dashevskaya, E. E. Nikitin, and J. Troe, Phys. Rev. A **69**, 012704 (2004).

[73] M. J. Moritz, C. Eltschka, and H. Friedrich, Phys. Rev. A **64**, 022101 (2001).

[74] A. Fioretti, D. Comparat, C. Drag, C. Amiot, O. Dulieu, F. Masnou-Seeuws, and P. Pillet, Eur. Phys. J. D **5**, 389 (1999).

[75] M. Pichler, H. Chen, and W. C. Stwalley, J. Chem. Phys. **121**, 6779 (2004).

[76] H. Jelassi, B. V. de Lesegno, and L. Pruvost, Phys. Rev. A **74**, 012510 (2006).

[77] J. Ma, L. Wang, Y. Zhao, T. Xiao, and S. Jia, J. Mol. Spectrosc. **255**, 106 (2009).

[78] F. Arnecke, J. Madroñero, and H. Friedrich, Phys. Rev. A **77**, 022711 (2008).

[79] E. del Giudice and E. Galzenati, Nuovo Cimento **38**, 443 (1965).

[80] B. Gao, Phys. Rev. A **62**, 050702(R) (2000).

[81] I. Bloch, J. Dalibard, and W. Zwerger, Rev. Mod. Phys. **80**, 885 (2008).

[82] O. Hinckelmann and L. Spruch, Phys. Rev. A **3**, 642 (1971).

[83] M. Lepers, O. Dulieu, and V. Kokoouline, Phys. Rev. A **82**, 042711 (2010).

[84] H. R. Sadeghpour, J. L. Bohn, M. J. Cavagnero, B. D. Esry, I. I. Fabrikant, J. H. Macek, and A. R. P. Rau, J. Phys. B **33**, R93 (2000).

[85] C. Cohen-Tannoudji and D. Guéry-Odelin, *Advances in atomic physics: an overview*, World Scientific, New Jersey, 2011.

[86] J. M. Blatt and V. F. Weisskopf, *Theoretical nuclear physics*, Wiley; Chapman & Hall, New York; London, 1952.

[87] K. Huang and C. N. Yang, Phys. Rev. **105**, 767 (1957).

[88] C. H. Greene, A. S. Dickinson, and H. R. Sadeghpour, Phys. Rev. Lett. **85**, 2458 (2000).

[89] G. W. King and J. H. van Vleck, Phys. Rev. **55**, 1165 (1939).

[90] B. Gao, Phys. Rev. A **59**, 2778 (1999).

[91] R. Shakeshaft, J. Phys. B **5**, L115 (1972).

[92] P. S. Ganas, Physica **68**, 164 (1973).

[93] M. Klaus, J. Math. Phys. **29**, 148 (1988).

[94] W. C. Stwalley, Y.-H. Uang, and G. Pichler, Phys. Rev. Lett. **41**, 1164 (1978).

[95] P. D. Lett, P. S. Julienne, and W. D. Phillips, Ann. Rev. Phys. Chem. **46**, 423 (1995).

[96] M. Movre and G. Pichler, J. Phys. B **10**, 2631 (1977).

[97] B. Gao, Phys. Rev. Lett. **83**, 4225 (1999).

[98] R. Paulsson, F. Karlsson, and R. J. L. Roy, J. Chem. Phys. **79**, 4346 (1983).

[99] C. Eltschka, *WKB im antiklassischen Grenzfall*, Doctoral thesis, Technische Universität München, 2001.

[100] C. Eltschka, M. J. Moritz, and H. Friedrich, J. Phys. B **33**, 4033 (2000).

[101] M. Lemeshko and B. Friedrich, Phys. Rev. A **79**, 050501 (2009).

[102] M. Lemeshko and B. Friedrich, J. At. Mol. Sci. **1**, 41 (2010).

[103] A. Kaiser, T.-O. Müller, and H. Friedrich, J. Chem. Phys. **135**, 214302 (2011).

[104] F. Schwarz, T.-O. Müller, and H. Friedrich, Phys. Rev. A **85**, 052703 (2012).

[105] H. Jelassi, B. V. de Lesegno, L. Pruvost, M. Pichler, and W. C. Stwalley, Phys. Rev. A **78**, 022503 (2008).

[106] L. Pruvost and H. Jelassi, J. Phys. B **43**, 125301 (2010).

[107] I. G. Kaplan, *Intermolecular interactions: physical picture, computational methods, model potentials*, Wiley, Chichester, 2006.

[108] W. J. Meath and J. O. Hirschfelder, J. Chem. Phys. **44**, 3210 (1966).

[109] M. Marinescu, J. F. Babb, and A. Dalgarno, Phys. Rev. A **50**, 3096 (1994).

[110] B. H. Bransden and C. J. Joachain, *Physics of atoms and molecules*, Prentice Hall, Harlow, 2003.

Acknowledgments

First I would like to thank Harald Friedrich for giving me the opportunity of joining his research group at Technische Universität München. It has always been a pleasure working with him and in the enriching atmosphere for which he provides. My work has strongly been influenced by his way of thinking about physics and life in general.

I am deeply indebted to all the group members of T30a, Martin Fink, Sebastian Schröter, Javier Madroñero, Johannes Eiglsperger, Moritz Schönwetter, and Patrick Raab with whom I had the pleasure of working in the field of theoretical atomic physics. I want to thank them for supporting my work in all of its stages.

Special credit also goes to Alexander Kaiser and Frauke Schwarz, who worked on this project as diploma students and considerably contributed to its success. I wish all the best for their future academic careers.

Last but not least I want to thank my family and friends who have supported and encouraged me during my physics studies both in Heidelberg and Munich. I am especially grateful to Vera with whom I have been sharing my life for quite some time now and who has always been a major support to me.